Characterization and application of methane cometabolism for methanol production in ammonia oxidizing bacteria

Yu-Chen Su

Submitted in partial fulfillment of the
requirements for the degree of
Doctor of Philosophy
in the Graduate School of Arts and Sciences

COLUMBIA UNIVERSITY

2017

Abstract

Characterization and application of methane cometabolism for methanol production in ammonia oxidizing bacteria

Yu-Chen Su

The requirement of external carbon for conventional biological nitrogen removal (BNR) process has stimulated research on more resource-efficient treatment technologies. Bioconversion of methane to methanol using ammonia oxidizing bacteria (AOB), a process relies on the activity of ammonia monooxygenase expressed by AOB, offers an alternative and sustainable carbon source as all the components (ammonia, AOB, and methane) are often available within the water resource recovery facilities. Though the concept of biomethanol production using AOB has been proposed decades ago, previous studies have been primarily focused on the kinetics of methane oxidation in axenic batch cultures. In this study, the overall objectives were to (1) develop a platform for biomethanol production using AOB in a continuous process and (2) investigate the mechanism of methane cometabolism in AOB under chemostat conditions. Pure culture AOB (*Nitrosmonas europaea* and *Nitrosomonas eutropha*) and mixed culture nitrifying consortia were cultivated in bioreactors and continuously exposed to methane to study the responses of nitrifying bacteria at reactor level (nitrification performance) and molecular level (genes and proteins expression).

The mixed culture experiments successfully demonstrated continuous biomethanol production with two types of bioreactor configurations. Acclimation of the mixed

culture nitrifying consortia to co-exposure and co-oxidation of ammonia and methane were shown at multiple levels (reactor performance, biomass concentrations, bacterial activities, and genes expression). Furthermore, the accumulation of nitrite and a more substantive impact on nitrite oxidizing bacteria growth (compared to AOB) indicated the possibility for partial nitrification (ammonia-N to nitrite-N) coupled with biomethanol production, thereby opening the prospect for even more resource-efficient concurrent carbon and nitrogen management and removal. On the other hand, experiments with axenic AOB culture showed that methane exposure negatively and reversibly affected ammonia oxidation and AOB growth. Proteomics and gene expression data from pure culture experiments suggested that AOB modulating their catabolic (energy synthesis) and anabolic (biomass synthesis) pathways in response to methane exposure. Moreover, *N. eutropha* experiments demonstrated the potential adaptation of AOB to methane supplementation. Comparative transcriptomic analysis of methane cometabolism in *N. europaea* and *N. eutropha* showed that AOB upregulated genes involved in ATP production while downregulated genes involved in NADH production, organic molecules synthesis and cell division.

In conclusion, this work provides insights for the process optimization for integrated AOB-mediated biomethanol production and (full- or partial-) nitrification processes as well as structured process modeling to facilitate such optimization and process scale-up and adoption. The whole transcriptomic analysis delineates a comprehensive and detailed view regarding methane cometabolism in AOB.

Table of Contents

List of Figures

List of Tables

List of Abbreviations

Adenosine triphosphate	ATP
Alcohol dehydrogenase	ADH
Ammonia monooxygenase	AMO
Ammonia oxidizing bacteria	AOB
Biological nitrogen removal	BNR
Calvin-Benson-Bassham cycle	CBB cycle
Chemical oxygen demand	COD
Coding sequence	CDS
Concentrations of ammonia, hydroxylaimine, nitrite, nitrate	S_{NH3}, S_{NH2OH}, S_{NO2}, S_{NO3}
Concentrations of methanol	S_{CH3OH}
Continuous stirred tank reactor	CSTR
Electron donor	ED
Electron transport chain	ETC
Formaldehyde dehydrogenase	FaDH
Formate dehydrogenase	FDH
Hydraulic retention time	HRT
Hydroxylamine oxidoreductase	HAO
Methane oxidizing bacteria	MOB
Methanol dehydrogenase	MDH
Next generation sequencing	NGS
Nicotinamide adenine dinucleotide hydride	NADH
Nitric oxide	NO
Nitric oxide reductase	NOR
Nitrite oxidizing bacteria	NOB
Nitrite reductase	NIR
Nitrous oxide	N_2O
Particulate methane monooxygenase	pMMO
Proton motive force	PMF
Quantitative polymerase chain reaction	qPCR
Ribulose biphosphate carboxylase/oxygenase	RubisCO
Simultaneous nitrification and denitrification	SND
Solids retention time	SRT
Soluble methane monooxygenase	sMMO
Specific oxygen uptake rate	sOUR
Wastewater treatment plant	WWTP
Water resource recovery facility	WRRF

Acknowledgements

First, I would like to express my deepest gratitude to my advisor, Dr. Kartik Chandran, for all his support and critical insights throughout the research. It was amazing to be able to observe and learn from one of the most brilliant scientists so closely. I would like to thank Dr. O. Roger Anderson, Dr. William Becker, Dr. Ngai Yin Yip, and Dr. Ponisseril Somasundaran for their advices as my dissertation committee members.

I would like to thank my lab colleagues, Eirene Pavlakis, Dr. Medini Annavajhala, Mee Rye Park, Ranran Hu, Shashwat Vajpeyi, Zheqin Li, Catherine Hoar for spending hours together in the lab and learning together. I would like to thank Dr. Huijie Lu, Dr. Daqian Jiang, Dr. Hongkeun Park, Dr. Sandeep Sathyamoorthy, Dr. Joon Ho Ahn, and Dr. Luis Arellano-Garcia for their helpful advices. I would like to thank Eileen Irizarry, Karen Del Aguila, and Elizabeth Allende for their help on our purchasing and all the miscellaneous questions.

Finally, I would like to thank my family and friends, either in New York or in Taiwan, for their supports. Especially I would like to thank my mother and brother, though I can never thank them enough, for their endless care and support.

CHAPTER 1 Introduction

1.1 Biological nitrogen removal

Biological nitrogen removal (BNR) has become the most common practice for nitrogen control in wastewater treatment sector since its emergence. Two-step BNR, which relies on autotrophic nitrification and heterotrophic denitrification, has been studied extensively and is among the most prevalent operational scheme. Nitrification is the oxidation of ammonia to nitrate by chemolithoautotrophic bacteria under predominantly aerobic conditions. Nitrification is conventionally considered to occur in two sequential oxidative stages: ammonia to nitrite (ammonia oxidation, nitritation) by ammonia oxidizing bacteria (AOB) or ammonia oxidizing archaea (AOA) and nitrite to nitrate (nitrite oxidation, nitratation) by nitrite oxidizing bacteria (NOB). Each nitrification step is mostly catalyzed by distinct microorganisms, which use ammonia or nitrite as electron donor and oxygen as electron acceptor, while carbon dioxide is used as the carbon source. Denitrification is a bioconversion process, which occurs preferentially under anoxic conditions during which oxidized nitrogen compounds (such as HNO_2 and HNO_3) are used as electron acceptors instead of oxygen. Organic or inorganic compounds such as ethanol, methanol, acetate, glycerin or even ammonia, Fe(III), reduced sulfur compounds could be used as the electron source for denitrifiers[1, 2].

1.2 Changing paradigm toward water resource recovery facilities (WRRFs)

Increasing population pressures to water bodies globally have elicited on one hand

more stringent effluent wastewater limits to address point-source pollution. To overcome in part the additional energy and material demand for enhanced wastewater treatment, new paradigms are being explored including that of recovering resources from wastewater streams, including energy and nutrients[3]. The successful application of these new paradigms could potentially transform WWTPs into water resource recovery facilities (WRRFs).

Anaerobic digestion is the most common approach for biological conversion of organic carbon streams relevant to WRRFs (such as biosolids) to renewable energy and biofuel, while also reducing the volume of biosolids and providing biological stabilization of microbial pathogens. Most WRRFs are now generating some degree of biogas as part of their biosolids management strategies[4]. Typically, however, the biogas is flared to avoid fugitive methane emissions. In a marked improvement to this practice, a growing number of co-generation facilities are being financed and constructed under the support of USEPA to actually use the biogas produced via anaerobic digestion for producing heat and power[4] .

1.3 Methane as carbon source for biological nitrogen removal

In addition to the above conventional end-uses of biogas, other potential applications also exist and could help WRRFs expand their treatment capacity or simply allow them to explore the production of other commercially attractive chemicals and fuels such as ethanol, biohydrogen, or polyhydroxyalkanoates[5]. Additionally, methane, as the main component of biogas, has been considered as carbon source for

denitrification[6-9]. The possibility of using methane *indirectly* as a *precursor* carbon source for denitrification[6, 7, 9-12] has been demonstrated with different groups of bacteria. Methanotrophs (methane-oxidizing bacteria, MOB), which metabolize methane as the sole energy and carbon source, were cultured together with denitrifying bacteria and fed with methane and nitrite/nitrate. As methane was oxidized by MOB, intermediates such as methanol, formate, citrate, acetate were released into the bulk liquid and served as potential carbon sources for denitrifiers[13].

1.4 Bacterial catalysts for methanol production

Biological production of methanol from methane using methanotrophic bacteria has been proposed decades ago[14]. The challenge of using methanotrophs for methanol production is that methanol is further converted into formaldehyde, formate and finally carbon dioxide. This could be a significant disadvantage if the purpose of the produced methanol or other metabolites is to serve as a carbon source for heterotrophic denitrifiers. Various inhibitors have been tested to halt the methanol oxidation process in methanotrophs[15]. However, the use of such inhibitors could be economically unfavorable and the inhibitors could be detrimental to other biological process as well, if the methanol is to be used *in-situ* for denitrification.

Table 1.1 Summary of studies evaluating biogenic methanol production in batch reactors using mixed nitrifying cultures or axenic cultures of ammonia oxidizing bacteria.

Description	Electron Source	Max S_{MeOH} [*2] $mgCODL^{-1}$	**Biomass Specific MeOH Prod. Rate** $mg\text{-}CH_3OH\text{-}COD^{-1}(mg\text{-}AOB\text{-}CODd)^{-1}$ Max	Average/Steady state	Note	Ref.
N. europaea cell suspension [*1]	NH_3	27.3	0.80	0.35	1 mM NH_3-N	16
	NH_3	28.7	0.52	0.42	10 mM NH_3-N	
N. europaea cell suspension [*1]	None	N/A	N/A	0.10		17
	NH_3	N/A	N/A	0.59	10 mM NH3-N	
N. europaea cell suspension [*1,3]	None	12.4	0.09	0.03	30 ^oC	18
	NH_3	21.2	0.10	0.06	30 ^oC, 0.1 mM NH_3-N pulse feed	
	NH_3	20.4	0.09	0.06	30 ^oC, 0.2 mM NH_3-N pulse feed	
Mixed liquor	NH_3	23.5 ± 0.5	0.21	0.06	NH_3 feed batch	19
	NH_2OH	27.5 ± 0.8	0.30	0.07	NH_2OH feed batch	
	NH_3 + NH_2OH	31.5 ± 1.2	0.22	0.07	Simultaneous NH_3 and NH_2OH feed batch	
	NH_3+ NH_2OH	40.7 ± 0.2	0.20	0.09	Alternate NH_3 and NH_2OH feed batch	
	NH_2OH	59.9 ± 1.1	0.82	0.39	Biomass replenishment	

[*1] Biomass concentration conversion factors: 1 mg dry wt =1.42 mg COD; 1 mg wet wt/mL = 344 mgCOD/L.

[*2] Methanol concentration conversion factor: 1 mM methanol = 48 $mgCODL^{-1}$ methanol.

[*3] Also tested NH_2OH-N as electron donor but NH_3-N was found more effective.

1.5 Co-oxidation of ammonia and methane in ammonia oxidizing bacteria

On the other hand, methanol production has also been reported by pure culture AOB[16-18] as well as nitrifying activated sludge[19] (Table 1). The results using mixed culture nitrifying activated sludge which was enriched in AOB have been especially promising in terms of high methanol production rates and high yields when compared with pure culture studies[19]. Furthermore, utilizing AOB in nitrifying activated sludge is advantageous since sterile operation required for pure culture applications is not required any longer and nitrifying biomass is abundantly available and easily accessible in WRRFs which perform nitrification or BNR.

Chemolithoautotrophic ammonia oxidizing bacteria (AOB) typically acquire energy from the oxidation of ammonia (NH_3) to nitrite (HNO_2), play a crucial role in the global nitrogen cycle in natural and engineered environments. During AOB catabolism, ammonia is first oxidized to hydroxylamine (NH_2OH) by ammonia monooxygenase (AMO) (eq 1), and NH_2OH is further oxidized to nitrite (NO_2^-) by hydroxylamine oxidoreductase (HAO) (eq 2). During NH_2OH oxidation, four electrons are released and transferred to a ubiquinone pool, where two electrons are channeled back to AMO for subsequent NH_3 oxidation and remaining electrons are channeled toward the electron transport chain to generate and sustain the proton motive force (Figure 2)[20]

$$NH_3 + O_2 + 2e^- \xrightarrow{AMO} NH_2OH + H_2O \quad (1)$$

$$NH_2OH + H_2O \xrightarrow{HAO} NO_2^- + 5H^+ + 4e^- \quad (2)$$

Ammonia monooxygenase (AMO), which shares many similar characteristics

with particulate methane monooxygenase (pMMO)[21], is the key enzyme that initiates AOB catabolism. Owing to a common evolutionary ancestor[21] AMO and pMMO share common substrates including NH_3, methane (CH_4), and various recalcitrant pollutants[22]. The similarities in the substrate pool for these two enzymes leads to the prospect of cometabolic biotransformation of non-energy yielding substrates. Additionally, in AOB, cometabolic transformation of other (non-NH_3) substrates by AMO requires concurrent ammonia oxidation since that the electrons consumed by AMO are released from the hydroxylamine (product of ammonia oxidation) oxidation.

$$CH_4 + O_2 + 2H^+ + 2e^- \xrightarrow{AMO} CH_3OH + H_2O \quad (3)$$

The competition between two substrates for AMO[23] result in competitive inhibition of the oxidation of primary substrate, NH_3-N, and could have further impacts at whole-cell level. For example, methane, as a competitive inhibitor for NH_3[24-26], hinders NH_3 oxidation and subsequent electron-release by downstream NH_2OH oxidation, potentially negatively impacting electron transport chain and energy metabolism in AOB.

The daughter products from the oxidation of alternative substrate could also lead to product inhibition. For example, it has been demonstrated that phenol, the daughter product of benzene and toluene oxidation by AOB, resulted in 50% inhibition level at a concentration of 8 μM[27] for *N. europaea* cultures. Similarly for methane co-metabolism by AOB, methanol has been shown to inhibit ammonia oxidation both in pure cultures of *N. europaea*[18, 25] and in mixed culture nitrifying biomass[19]. Unlike

MOB, no methanol, formaldehyde, or formate oxidizing enzymes are found in common AOB genomes (Table 2). However, previous studies have demonstrated the capacity of AOB to further metabolize methanol (albeit minimally) and have proposed mechanisms and possible participating enzymes (illustrated in Figure 1 and summarized in Table 2). For instance, although methanol dehydrogenase is absent in AOB, genes encoding alcohol dehydrogenase family proteins are found in *N. europaea* and *N. eutropha* genomes (Table 2), which could drive further methanol oxidation. Studies also proposed that *N. europaea* was capable of methanol oxidation through AMO[18, 28] and formaldehyde oxidation to formate[28], a far less inhibitory compound[29].

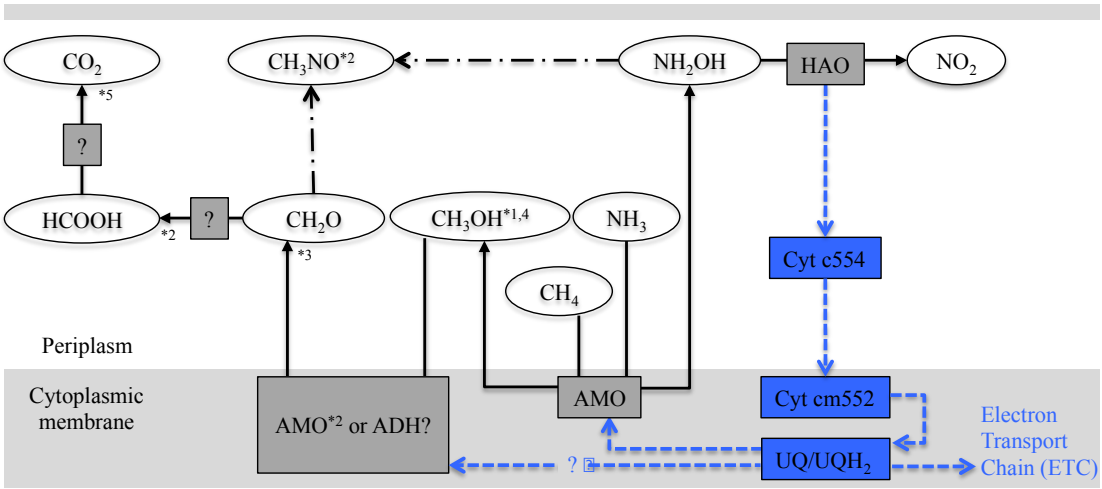

Figure 1.1. Postulated methane metabolism pathways in *N. europaea*. Open circles represent nitrogen and carbon species involved in methane metabolism. Blue blocks and arrows represent electron carriers and fluxes, respectively, during ammonia oxidation process. Black lines indicate the conversion between each nitrogen species and gray blocks represent enzymes participated (or postulated to be involved) in the oxidation/conversion steps. Hooper and Terry (1973)[29] *1, Voysey and Wood (1987)[28] *2, and Taher and Chandran (2013)[19] *4 showed that methanol specific inhibit ammonia oxidation but not hydroxylamine oxidation. Voysey and Wood (1987)[28] *2 proposed and demonstrated that methanol was oxidzied to formaldehyde by AMO and formaldehyde reacted with hydroxylamine to form formaldoxime (dashed lines), which was inhibitive to hydroxylamine oxidation. Wang et al (2010)[18] *3 demonstrated loss of methanol during batch incubation but the mechanism was unclear. Jones and Morita (1983)[24] *5 showed that $^{14}CH_4$ was converted to $^{14}CO_2$ and incorporated into biomass in *Nitrosococcus oceanus* but the mechanism remains unknown.

Table 1.2 Reactions and possible enzymes associated with methane metabolism in *N. europaea*, *N. eutropha* and *Methylococcus capsulatus Bath*.

Reactions and possible participated enzymes	***N. europaea***	***N. eutropha***	***M. capsulatus Bath*[1]**
$CH_4 \rightarrow CH_3OH$	AMO[2]	AMO	pMMO, sMMO
$CH_3OH \rightarrow CH_2O$	AMO[3,4], ADH? (NE0620, NE0742, NE0820, NE0907)	ADH? (Neut_1071, Neut_1385)	MDH
$CH_2O \rightarrow HCOOH$	N/A[3]	N/A	FaDH
$HCOOH \rightarrow CO_2$	N/A[5]	N/A	FDH

Abbreviations: ADH = alcohol dehydrogenase; MDH = methanol dehydrogenase; FaDH = formaldehyde dehydrogenase; FDH = formate dehydrogenase

[1] Model methanotroph which genome sequence is available [30] .

[2] Hyman and Wood [16]; Hyman, Murton and Arp [17]; Keener and Arp [23].

[3] Voysey and Wood [28]

[4] Wang, Tabata, Kamachi and Okura [18] demonstrated methanol loss but mechanism unknown.

[5] Jones and Morita [24] demonstrated a complete methane oxidation process (from CH_4 to CO_2) and also CH_4-C incorporated into biomass but mechanism unknown.

1.6 *Nitrosomonas europaea* and *Nitrosomonas eutropha* as model ammonia oxidizing bacteria and their methane metabolism capacity

To understand methane cometabolism in AOB at transcriptional, translational, and reactor levels, two of the most prevalent AOB detected in WRRFs were selected for further investigation. *N. europaea* is the single most studied AOB which exists in soil as well as natural and engineered aquatic environments such as wastewater treatment plants. It was first identified from soils and taxonomically labeled as such by Winogradsky in early 1904[31]. *N. eutropha* was isolated later from municipal sewage at Chicago in the 1970s[32]. The genomes of both *N. europaea* and *N. eutropha*, have been sequenced and afford significant information regarding their potential capabilities [33, 34], Both bacteria utilize ammonia as sole source for energy and fix carbon from CO_2 via Calvin-Benson-Bassham cycle. Genome analysis shows that *N. europaea* and *N. eutropha* share 14% of orthologous coding sequences (CDSs). Both species contain two copies of gene clusters encode functional AMO (*amoCAB*)[35] and three copies of HAO (*hao*) and associated cytochromes (*cycAB*)[34, 36] (Table 3) in a nearly identical arrangement. Despite their close phylogenetic relationship, genome surveys also indicate considerable differences between *N. europaea* and *N. eutropha*. For example, of the 2460 protein-encoding genes derived from the *N. europaea* genome sequence, 312 (13%) with unknown function were unique to *N. europaea*[33]. On the other hand, analysis of the *N. eutropha* genome sequence revealed that 19% of its protein coding CDSs was not found in other AOB genomes[34].

However, a detailed evaluation at the systems biology level of the capacity of

these two AOB to oxidize methane remains lacking. Herein, we aim to evaluate the impact of methane cometabolism by first looking at the genomes of *N. europaea* and *N. eutropha* for pathways involved in (1) nitrogen and energy metabolism and (2) anabolism, especially carbon fixation.

1.7 Nitrogen metabolism, electron transport chain (ETC), and energy metabolism in AOB

The extensive studies on *N. europaea* and *N. eutropha* forms the basis of our understanding on nitrogen metabolism, electron transport, and energy metabolism in AOB (Figure 2)[20, 37]. Analysis of genome sequences shows that genes encode proteins for extraction of electrons from ammonia (AMO, AHO, ubiquinone), primary electron flow (cytochrome c552, cytochrome bc_1, terminal oxidases, NADH-ubiquinone dehydrogenase), secondary electron flow (NIR, NOR, cytochrome c'-beta. cytochrome P460) and transcription regulators (NsrR, NnrS) are identified in both *N. europaea* and *N. eutropha* genomes (Table 1.3). There are both common features and distinctions in the overall carbon and nitrogen metabolism of *N. europaea* and *N. eutropha*. As with most AOB, during NH_3 oxidation four electron equivalents are released per mole of hydroxylamine oxidized and are transferred to UQ/UQH_2 pool through cytocrhome c554 (Cyt c_{554}) and membrane-bound cytochrome cm552 (Cyt cm_{552}). These electrons are either (1) returned to AMO for further ammonia oxidation (2) directed to NADH-quinone oxidoreductase for NADH regeneration or (3) moving toward downstream electron transport chain (ETC) for proton gradient generation.

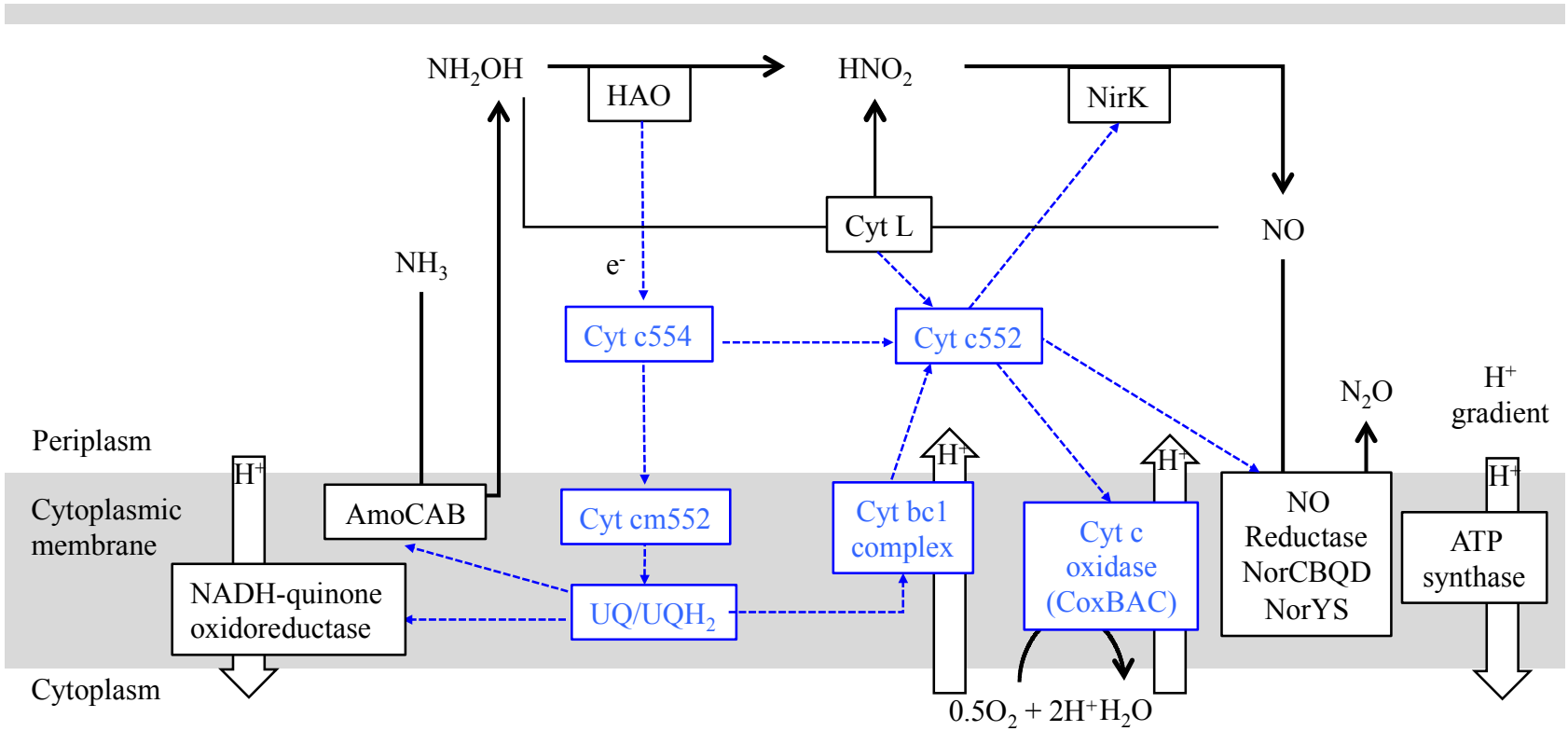

Figure 1.2. Nitrogen species transformation, electron flows, and associated enzymes in *N. europaea* (Adapted form Chandran et al (2011)[37] and Stein (2011)[38]). Blocks represent nitrogen species and enzymes, respectively, participated in the oxidation cascade. Blue lines and blue blocks indicate electron flows and electron carriers, respectively. White arrows indicate proton flows either increase proton gradient (H^+ is pumped from cytoplasm to periplasm) or energy synthesis with specialized enzymes driven by proton motive force (PMF, H^+ flow from periplasm to cytoplasm).

Table 1.3. Gene inventory with implications in ammonia oxidation, N-oxide metabolism and terminal oxidase in *N. europaea* and *N. eutropha* genome.

Enzyme and its associated partners	***N. europaea***	***N. eutropha***
Ammonia monooxygenase	*amoCAB*ED[1] (NE945-940, NE2064-2059) *amoC3* (NE1411)	*amoCAB-orf4,5* (Neut_2078-2074, Neut_2319-2315) *amoC3* (Neut_1520)
Hydroxylamine oxidoreductase	*haoAB-cycAB* (NE0962-0959, NE2339-2336) *haoAB-cycA* (NE2044-2042)	*haoAB-cycAB* (Neut_2335-2332, Neut_1793-1790) *haoAB-cycA* (Neut_1672-1670)
Nitrite reductase	*ncgBCA-nirK* (NE0927-0924)	ncgBCA-*nirK* (Neut_1406-1403)
Nitric oxide reductases (cNOR)	*norCBQD* (NE2003-2006)	*norCBQD* (Neut_0518-0521)
Cytochrome c'-beta	*cytS* (NE0824)	Neut_1345
Cytochrome P460	*cyp* or *cytL* (NE0011)	Neut_0132
Cytochrome c oxidase aa_3 (NO reductase, sNOR)	*senC* (NE0682) *norY* (NE0683), *norS* (NE0684)	*senC* (Neut_1876) *norY* (Neut_1875), *norS* (Neut_1874)
Nitrosocyanin	*ncyA* (NE0143)	Neut_2173
Nitrite-sensitive transcription repressor (nirK gene cluster regulator)	*nsrR* (NE0928)[2]	*nsrR* (Neut_1407)

Table 1.3 (continued). Gene inventory with implications in ammonia oxidation, N-oxide metabolism and terminal oxidase in *N. europaea* and *N. eutropha* genome.

Enzyme and its associated partners	***N. europaea***	***N. eutropha***
NO-responsive transcriptional regulator	*nnrS* (NE1722)[1,3]	Neut_1938[3]
Cytochrome c oxidase aa_3	*coxA* (NE1016), *coxB* (NE1017) *coxC* (NE1013), *ctaG* (NE1015)	Neut_2394, Neut_2395 Neut_2392, Neut_2393
Quinol oxidase bo_3	N/A	Neut_694-697
Cytochrome c oxidase cbb_3	N/A	Neut_1582-1585

[1] Kozlowski et al (2016)[39]. NE2059 was previously annotated as copper resistance protein C (*copC*) in Stein et al (2007)[34].
[2] Beaumont et al (2004)[40]. Assigned as NE0926 in Kozlowski et al (2016)[39]
[3] Both NE1722 [33] and Neut_1938 belong to Fur (ferric uptake regulator) family.

Electrons that are directed to ETC are channeled through the cytochrome bc_1 complex to cytochrome c552 and translocate proton across membrane. Cytochrome c oxidase accepts electrons from Cyt c552 and diverts the electrons toward oxygen. Four protons are abstracted from the cytoplasm during the reduction of O_2 and two protons are released into periplasm, which further increases the proton gradient. The proton motive force drives the synthesis of ATP by ATP synthase. Cyt c552 is also proposed to be the electron donor for nitrite reductase (NIR) and nitric oxide reductase (NOR) and it was hypothesized that the flux of electrons to NIR was related to oxygen level[20]. Only one type of terminal oxidase, cytochrome c oxidase aa3-type, and is found in *N. europaea*. However, *N. eutropha* genome harbors multiple terminal oxidases including aa3-type and cbb3-type cytochrome c oxidase, and bo3-type quinol oxidase (Table 3)[34], indicate a more complex and flexible electron transfer pathways for *N. eutropha*.

With the general maps of nitrogen metabolism and ETC in mind, we aim to understand the impacts of methane, as a substrate for AMO therefore serves as an additional electron sink, on AOB energy metabolism. The additional of $NaNO_2$ were presumably acted as not only a toxic compound but also an additional electron sinks since that the reduction of nitrite and detoxification of NO both required electrons (Figure 2). When exposing the ammonia substrate and additional $NaNO_2$, *amoA* and *norB* expression was not affected in *N. europaea* and *N. eutropha* batch cultures. On the other hand, *nirK* expression was upregulated in *N. europaea* but not in *N. eutropha* during incubation[41]. In addition, when AMO activity was inhibited by C_2H_2

(a specific AMO inhibitor), AMO and HAO mRNAs expression were detected in the presence of $(NH_4)_2SO_4$ at similar levels without C_2H_2, suggesting the transcription of these key genes were still active during energy limitation in *N. europaea*[42, 43]. Therefore, the transcription of *amoA* and *hao* might be sustained by internally reserved energy sources. Another proteomic study on the effect of NO_2 on chemostat *N. eutropha* culture demonstrated that increased (compared with oxic condition) AMO proteins and cbb3-type cytochrome c oxidase under oxic-plus-NO_2 conditions, which indicated the need for higher electron flux and PMF in response to energy deficiency when NO_2 was added[44].

1.8 Calvin-Benson-Bassham (CBB) cycle for carbon fixation in AOB

AOB preferentially utilize CO_2 as the assimilative carbon source. *N. europaea* and *N. eutropha* possess the *cbb* operon that is composed of five structure genes, *cbbLSQON*[34, 45], for carbon fixation (Figure 3). Both strains have the green-like type I ribulose bisphosphate carboxylase/oxygenase (RubisCO) consisting of two subunits, the large subunit (encoded by *cbbL*) and small subunit (encoded by *cbbS*). The putative regulatory *cbbR* genes[46] upstream of *cbbL* are identified in both genomes. While *cbbSQN* genes of *N. eutropha* are most similar with those in *N. europaea*, *N. eutropha* CbbRLS proteins showed highest similarity with *Nitrbacter winogradsky* Nb-255, a nitrite-oxidizing bacterium[34]. A study on the expression profiles of ammonia-induced or energy-induced genes in *N. europaea* indicated that NH_3 was not a signaling molecule for *cbbLS* transcription[43]. The lower expression levels for

energy-harvesting mRNAs when cells had no exogenous energy sources further indicated that the regulation of *cbb* operon depend on *N. europaea* cellular energy status[43].

In addition to the *cbb* operon, *N. eutropha* is, to our knowledge, the only aerobic AOB that harbors carboxysome biosynthetic genes which could be involved in concentrating intracellular CO_2 derived carbon reserves. The connections between regulation of RuBisCO synthesis, occurrence of carboxysome, and CO_2 availability in *Halothiobacillus neapolitanus* (previously *Thiobacillus neapolitanus*), from which the first carboxysome was isolated[47], suggests a role for carboxysome in carbon fixation. Genes for carboxysome shell protein (*csoS1A*, *csoS1B*, *csoS2*, *csoS3*), the defining structural characteristics for carboxysomes, have been identified in *N. eutropha*. The expression of *ccmL* (CO_2 concentrating mechanism) gene is required during the assembly of a carboxysome[48]. Analysis of carboxysomes in chemoautotorophs by activity tests or electron microscopic studies revealed the microcompartment was filled with type I RuBisCO, and accounted for about 60% of the carboxysomal protein[49-51]. Given that O_2 is a competing substrate to CO_2 for RuBisCO, concentrated RuBisCO inside the carboxysome and the potential ability to differentiate transfer CO_2 into carboxysome through the shell proteins might improve the efficiency of carbon fixation[52].

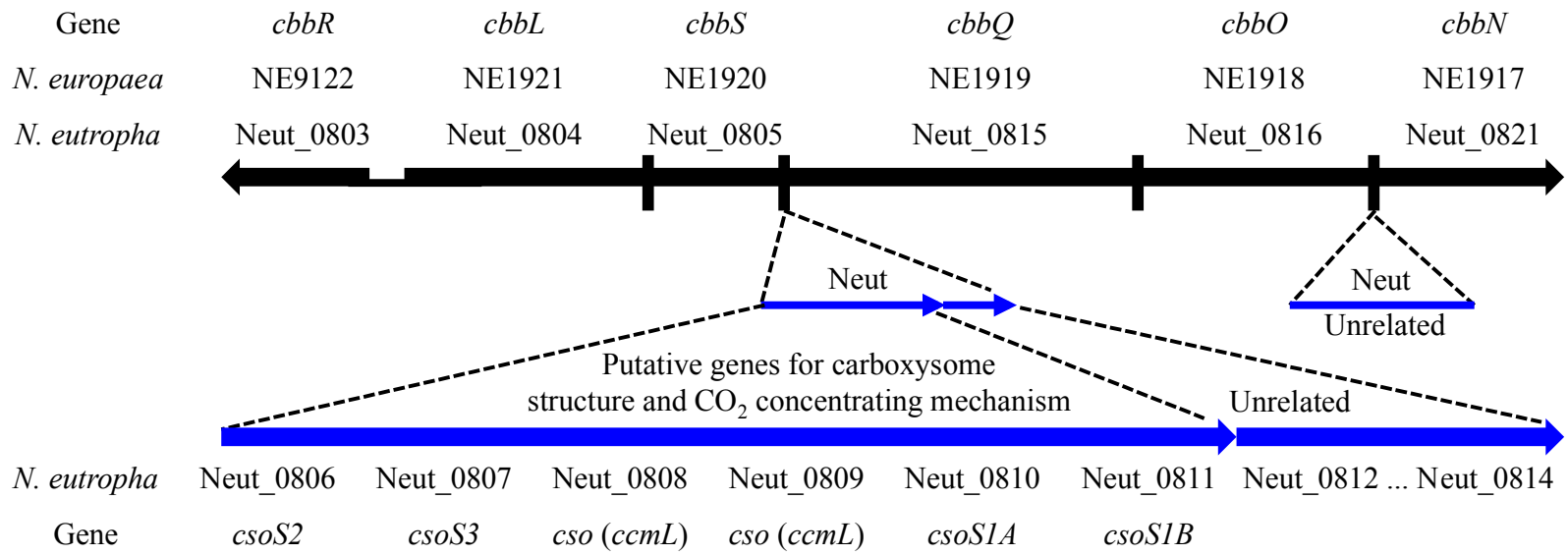

Figure 1.3. Carbon fixation-related genes (*cbb* operon) in *N. europaea* and *N. eutropha* (top) and putative genes for carboxysome and CO_2 concentrating mechanism (*cso* operon) in *N. eutropha* (bottom). Black lines showed orthologous genes in both species. Blue lines indicated presence of genes only in *N. eutropha* genome. (Adapted from Stein et al., 2007[34])

1.9 Research objectives and hypotheses

A platform using methane as precursor carbon source for biological nitrogen removal. The overall objective of this research is to develop a platform to convert readily available internal (within the WRRFs) carbon source, methane-enriched biogas, into methanol for denitrification (Figure 1.4). To achieve this, experiments are conducted using (1) mixed culture nitrifying bacteria to evaluate the practical application potential (2) pure culture AOB experiments to understand the mechanisms and impacts of methane cometabolism at transcriptional and translational level.

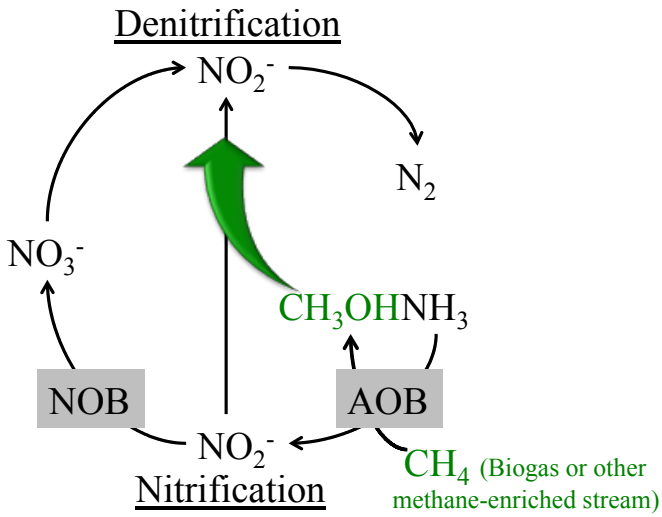

Figure 1.4. Proposed scheme of integrated biomethanol production and BNR process.

Specific Objectives

1. **Evaluate the factors related to biomethanol production using mixed culture nitrifying activated sludge in a continuous flow process**. Taher and Chandran [19] have previously demonstrated the proof-of-concept of using mixed culture nitrifying biomass for biomethanol production in batch mode. The study also

identified operation parameters affecting biomethanol production including sources of electron donor, feed strategies, and the impact of methanol on nitrifying biomass in batch reactors. In this research, we further examine the feasibility of biomethanol production using mixed culture nitrifying biomass in a continuous flow process. Operational factors including electron donor (NH_3 or NH_2OH), hydraulic retention time (HRT) are evaluated to further enhance methanol production efficiency and yields.

2. **Evaluate the responses of mixed culture nitrifying community (AOB and NOB) to long-term continuous methane exposure.** While the biomethanol production process relies on ammonia and methane cometabolism in AOB, the impacts on overall nitrifying community have not been discussed. To understand how nitrifying bacteria respond to long-term methane exposure, we expand our scope to evaluate the impacts of methane on AOB and NOB activity by monitoring ammonia and nitrite oxidation rates during reactor operation, in parallel with quantitative gene expression analysis targeting key metabolic genes in both AOB and NOB

3. **Characterize the physiological and molecular responses of methane cometabolism in *N. europaea*.** Although the capability of AOB to co-oxidize methane and release methanol is well documented in literature, the main focus has traditionally been on the interaction and kinetics between methane and AMO in batch reactors. In this research, chemostat reactors are used for cultivation of pure *N. europaea* cultures with methane supply. Liquid-chromatography-mass

spectrometry-based label-free proteomic analysis and quantitative gene expression analysis targeted at key metabolic genes are applied to investigate the responses of *N. europaea* to methane at transcription (RNA), translation (protein), and reactor levels.

Hypotheses

The research proposed here aims to examine the feasibility of biomethanol production using mixed culture nitrifying biomass and to extend our knowledge on the metabolic versatility of methane co-metabolism by AOB, using a systems biology approach. Based on previous studies on methane and methanol metabolism in *N. europaea* (Figure 1) or mixed culture nitrifying activated sludge, we hypothesize that

1. **Continuous biomass replenishment is advantageous for methanol production**. The fundamental scheme is to exploit the fast reaction rates of AMO to additional methane and to alleviate the negative impacts caused by exposure to methane or methanol via process design.

Studies on energy limitation[44], carbon limitation[53, 54] or deprivation of both nitrogen and carbon[45] have previously demonstrated different strategies for AOB to cope with unfavorable environmental conditions. Furthermore, it has been shown that *N. europaea* devote a larger fraction of energy for maintenance under inorganic carbon limitation[54], suggesting that the energy metabolism in AOB is flexible. Therefore, we further hypothesize that:

2. **Methane co-oxidation consumes electrons and did not contribute to electron**

replenishment, therefore electron flows in AOB would be disrupted. Methane competes with ammonia for AMO and acts an additional electron sink in AOB, reducing the amount of electrons available for downstream ETC and therefore negatively impacts energy synthesis. Hence we hypothesized that AOB would upregulate genes involved in energy synthesis to overcome the reduction in available electrons.

3. **Methane cometabolism suppresses genes related to carbon-fixation**. The positive link between energy availability and carbon fixation have been demonstrated in previous studies, which showed decreased expression of carbon assimilation genes when additional electron sinks were present in addition to the mandatory presence of energy source for the expression of carbon fixation genes[43].
4. **AOB can acclimate physiologically (or more?) to methane exposure.** The increased relative abundance of *Nitrosomonas* 16S rRNA when a soil microcosm was incubated with urea and methane[55] indicated that though anabolic activity might be lower, AOB growth was not completely inhibited. Thus, we hypothesize that AOB can acclimate to methane exposure under proper environmental or engineered reactor operating conditions and concurrent nitrification and biomethanol production is possible

This dissertation consists of seven chapters.

Chapter 1 presents the introduction to bioconversion of methane to methanol

using AOB, the current knowledge on methane cometabolism in AOB, and the comparison between two model organisms, *N. europaea* and *N. eutropha*, used in this research.

Chapter 2 demonstrates a continuous biomethanol production platform using a mixed culture nitrifying consortia including a mechanistic model to predict biomethanol production capacity while adapting this biomethanol platform into current water resource recovery facilities (WRRFs).

Chapter 3 describes the physiological responses and acclimation of a mixed nitrifying consortia to methane exposure and presents possible mechanisms for AOB to endure prolonged methane exposure.

Chapter 4 compares the global proteome structure, with a focus on nitrogen metabolism and carbon fixation, and functional genes analysis in *N. europaea* in chemostat reactors fed with only ammonia or co-fed with ammonia and methane.

Chapter 5 presents the physiological responses of methane cometabolism in *N. eutropha* in ammonia-fed chemostat reactors in the presence and absence of methane supply.

Chapter 6 demonstrates the whole transcriptome analysis of *N. europaea* and *N. eutropha* and reveals the metabolic regulations of AOB during methane cometabolism.

In Chapter 7, implications on both scientific and engineering aspects and future research directions pertaining to methane metabolism in AOB as well as novel biological resource recovery platforms are discussed.

CHAPTER 2

Methanol production using ammonia oxidizing bacteria in a continuous flow process

This chapter is the basis of the paper:

Yu-Chen Su[1, 3], Sandeep Sathyamoorthy[2, 3], Kartik Chandran[1]*

Methanol Production using Ammonia Oxidizing Bacteria in a Continuous Flow Process (In preparation)

Affiliation:

[1] Department of Earth and Environmental Engineering, Columbia University

500 West 120th Street, Room 1045 Mudd Hall, New York, NY 10027

[2] Black & Veatch, 2999 Oak Road, Suite 490, Walnut Creek, CA 94597

[3] These authors contribute equally to this work.

Abstract

Carbon source such as commercially purchased methanol is widely used for enhancing denitrification at wastewater treatment plants to comply with more stringent effluent nitrogen limits. On the other hand, the precursor of methanol, methane, is being produced during the wastewater treatment process and often is flared to mitigate the impact as a potent greenhouse gas. While bioconversion of methane to methanol results from the wide substrate range of ammonia monooxygease in ammonia oxidizing bacteria has been demonstrated in batch systems, the goal of this research was to develop a continuous biogenic methanol production process using mixed culture nitrifying activated sludge. Methanol was produced in a continuous stirred tank reactor, operated at a hydraulic retention time (HRT) of 2 or 7.5 h, fed with methane gas, air and an electron donor - either hydroxylamine or ammonia. The AOB-specific methanol production capacity with a 7.5 h HRT CSTR using hydroxylamine or a 2 h HRT CSTR using hydroxylamine and ammonia were 12.2±1.2, 16.4 ± 0.90 and 1.22 ± 0.16 mg-MeOH-COD(mg-AOB-COD^{-1}), respectively. A mechanistic process model, linking methanol production to ammonia or hydroxylamine oxidation, was developed and used to compare the benefits of ammonia and hydroxylamine as electron donors. Despite the lower production capacity, ammonia, from either primary effluent or a high strength recycle stream (e.g., reject water from anaerobic digestion after dewatering - centrate) holds utility as an electron donor for this process considering it is readily available, at no cost, from within a water resource recovery facility (WRRF).

Our model showed that a maximum steady state methanol concentration at 23 mg-CODL^{-1} can be achieved with centrate as ammonia source. However, with considerations of using the methanol for subsequent denitrification process, influent ammonia should be 10 – 20 mg-NL^{-1}. In conclusion, these results show that biogenic methane to methanol conversion in a continuous flow system is feasible and can potentially contribute to the enhancing the sustainability of WRRFs.

2.1 Introduction

There is a global effort to expand the traditional role of wastewater treatment facilities to integrate recovery of resources. These efforts have in the past primarily relied on beneficial reuse of water and biosolids. However, recent research has focused on the production of commodity chemicals including nutrients for fertilizer production [56, 57], biofuels[58], bioplastics[59], and commodity chemicals including methanol[60]. Methanol is the most widely used exogenous carbon source in water resource recovery facilities (WRRFs) for denitrification to achieve low total nitrogen levels[61]. However, the cost of methanol for denitrification is dependent on competing demand from industries such as utility chemicals manufacturing. Furthermore, in some cases, safety concerns related to methanol storage and handling facilities might preclude the purchase and transport of commercial methanol. Therefore, biogenic production of methanol and *in-situ* utilization within a WRRF presents a particularly valuable opportunity to reduce the dependence on external carbon sources and enhance overall WRRF sustainability.

Conversion of methane to methanol by ammonia oxidizing bacteria (AOB) is facilitated by ammonia monooxygenase (AMO), which shares similar chracteristic with the particulate methane monooxygenase (pMMO) in methane oxidizing bacteria (MOB)[62]. The oxidation of ammonia (NH_3) (Eq. 1) or methane (Eq. 3), a competing substrate for ammonia[16], requires two electrons which are generated through the oxidation of hydroxylamine (NH_2OH) to nitrite (NO_2^-) (Eq. 2)[63] (Figure 2.1).

$$NH_3 + O_2 + 2H^+ + 2e^- \rightarrow NH_2OH + H_2O \quad (1)$$

$$NH_2OH + H_2O \rightarrow NO_2^- + 5H^+ + 4e^- \quad (2)$$

$$CH_4 + O_2 + 2H^+ + 2e^- \rightarrow CH_3OH + H_2O \quad (3)$$

For MOB, methanol, which is the intermediate for energy metabolism and carbon assimilation pathways, is further oxidized by methanol dehydrogenase (MDH)[64]. In order to achieve methanol production using MOB, addition of MDH inhibitors has been widely studied[65]. On the other hand, there is no known enzymes for methanol metabolism present in the genomes of common AOB[34, 66], therefore offers an alternative platform for biomethanol production. Biogenic conversion of methane to methanol has been previously demonstrated at the laboratory scale, using mixed cultures and axenic cultures of AOB[16, 60, 67] fed with either NH_3 or NH_2OH. A recent study has demonstrated especially high rates and yield of biomethanol production using NH_2OH as the electron donor[60]. The process benefit of using NH_2OH as the electron donor rather than NH_3, resulting from the lack of competition for reducing equivalents, is evident. However, hydroxylamine needs to be purchased while ammonia is readily available in WRRFs either in the mainstream sewage itself or in sidestreams such as anaerobic digestion dewatering post-centrifugation (centrate) or post-filtration (filtrate). Therefore, although integration of bioconversion of methane to methanol in WRRFs holds promise, important questions remain as to the efficacy and viability of such a process using continuous cultures to produce significant methanol yields. Additionally, biogenic methanol production has not been demonstrated using continuous flow bioreactors.

The overall objective of this research was to evaluate the biogenic production of methanol using a mixed culture nitrifying community in a continuous stirred tank

reactor (CSTR) and compare the methanol production performance using either ammonia or hydroxylamine as the electron donor in a CSTR. To accomplish this objective we employed a combination of experimental studies and mathematical modeling.

2.2 Materials and methods

2.2.1 Nitrification enrichment culture

A nitrifying enrichment culture was developed in a 11.2 L parent reactor to provide active nitrifying bacteria for the methanol production experiments. The parent reactor feed contained: 1,000 mgNH_3-NL^{-1}, 3.3 mgL^{-1} $FeSO_4 \cdot 7H_2O$, 3.3 mgL^{-1} $MnSO_4 \cdot 7H_2O$, 0.7 mgL^{-1} $(NH_4)_6Mo_7O_{24} \cdot 4H_2O$, 0.8 mg$L^{-1}$ $CuCl_2 \cdot 2H_2O$, 3.0 mgL^{-1} $ZnSO_4 \cdot 7H_2O$, 0.6 mgL^{-1} $NiSO_4 \cdot 6H_2O$, 0.3 gL^{-1} $MgSO_4 \cdot 7H_2O$, 0.2 gL^{-1} KH_2PO_4, 0.5 gL^{-1} K_2HPO_4, and 0.7 gL^{-1} $NaHCO_3$. The parent reactor was operated at room temperature (23 ± 1 ^oC) with a hydraulic retention time (HRT) and a target solids retention time (SRT) of 1 day and 20 days, respectively. The parent reactor dissolved oxygen (DO) concentration was measured (YSI, Yellow Spring, OH) and maintained at 3 ~ 4 mgL^{-1} using filtered lab air (0.2 μm, Whatman). Parent reactor pH was continuously monitored and maintained at 7.50 ± 0.05 using 1M $NaHCO_3$ (Etatron dosing system, Clearwater, FL). Parent reactor performance was regularly monitored by tracking influent NH_3, reactor COD and effluent NH_3, NO_2 and NO_3 concentrations (Figure S2.1 and S2.2).

2.2.2 Methanol production experiments

Methanol production experiments were conducted in a 1.5-liter test CSTR (Figure 2.1) at ambient lab temperature (23 ± 1 ºC). Four liters of mixed liquor from the parent nitrification enrichment reactor was collected and prepared for use in the CSTR by centrifuging (4,000xg, 5 minutes) and washing in a nitrogen-free medium (Table S2.1) twice. The washed biomass was resuspended in the nitrogen-free medium to achieve a target COD of 1,000 mg L^{-1}. A unique CSTR design was employed wherein biomass was itself pumped into the CSTR, to mimic integrated mainstream-sidestream nitrogen treatment practiced currently in increasingly more WRRFs while simultaneously mitigating inhibition of AOB by the methanol produced. The target HRT was achieved by controlling the biomass feed rate. In all experiments, the nitrogen source (i.e., electron donor) was prepared at a concentration of 589 mg-N L^{-1} and supplied to the CSTR using a syringe pump (Kent Scientific, Torrington, CT) at a rate of 11.4 mL h^{-1}, resulting in a mass rate of 6.7 mg-N h^{-1}. Air was provided using an air blower (Tetra, Blacksburg, VA) and methane was provided using 99.99% methane gas (PurityPlus 4.0, TechAir). Gas flow rates were controlled using rotameters (Cole Parmer, Vernon Hills, IL). The methane and oxygen flow rates were maintained at 0.1 L min^{-1} in all experiments. All experiments were carried out under non-limiting DO conditions (>1.5 mg L^{-1}). CSTR pH was continuously monitored (Jenco, San Diego, CA) and manually maintained at 7.50 ± 0.05 with 1 M $NaHCO_3$.

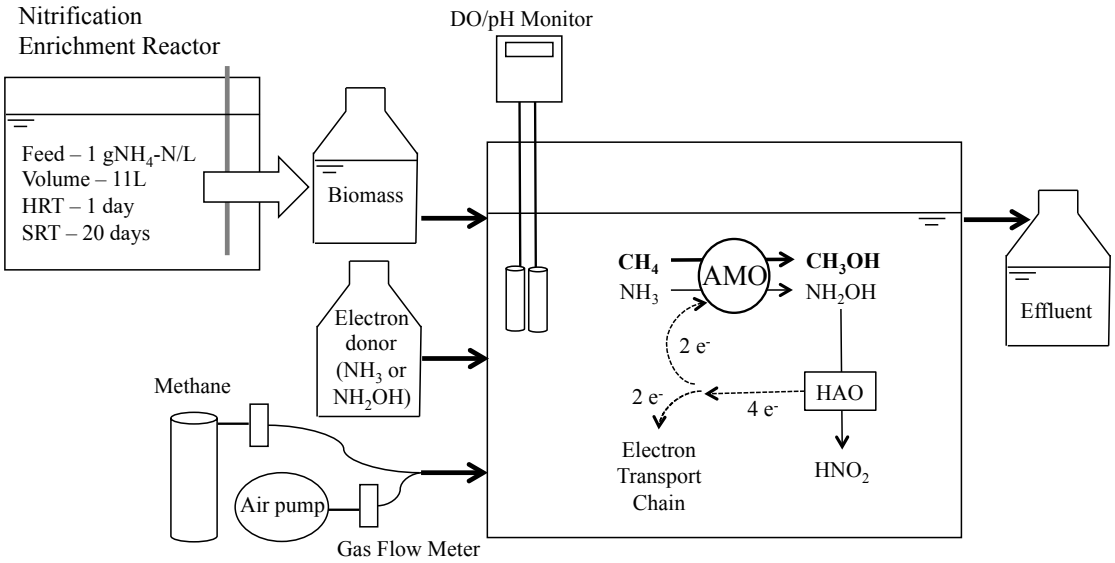

Figure 2.1. Experimental setup of the CSTR for methanol production. Shown in the reactor, for reference purposes, is the conversion of ammonia and methane as well as the electron flow within AOB.

We evaluated methanol production using the CSTR operated at HRTs of 2 h and 7.5 h. The 7.5 h HRT was utilized to benchmark methanol production using NH_2OH as the electron donor in the CSTR operated in a fashion comparable to previous batch experiments of Taher and Chandran, 2014. The HRT of 2 h was selected to reflect a practicable industrial scale system, for which both NH_3 and NH_2OH were evaluated as electron donors.

2.2.3 Analytical methods

Methanol concentration was determined using gas chromatography equipped with flame ionization detection (GC-FID, SRI Instruments, Torrance, CA). The GC was fitted with a 60 m x 0.53 mm ID x 5 □m df capillary MXT-1 column (Restek, Bellefonte, PA). The carrier gas was helium at a constant flow rate of 20 $mlmin^{-1}$ and the GC oven temperature was maintained at 120 ^{o}C. One microliter sample was

injected manually through the on-column injection port. Ammonia nitrogen concentration was measured using gas-sensing combination Ion Selective Electrode (Thermo Fisher, Waltham, MA) for 7.5 h HRT experiments, and a colorimetric assay (HACH method 10031, HACH, Loveland, CO) for 2 h HRT experiments. Hydroxylamine was measured as described previously[68]. For 7.5 h HRT experiments, nitrite and nitrate concentrations were measured using a colorimetric assay[69] (reagents purchased from Ricca chemical, Arlington, TX) and an Ion Selective Electrode (Thermo Fisher, Waltham, MA), respectively. For 2 h HRT experiments, the concentrations of nitrite and nitrate were quantified using ion chromatography coupled with a conductivity detector (Dionex ICS 2100). Separation was achieved using a Dionex Ionpac AS-18 (2 × 250 mm) with a Dionex AG-18 guard column (2 × 50 mm) and isocratic separation at 0.25 ml min^{-1} using a 25 mM KOH eluent. COD was measured using a digestion method (Method 8000, Hach, Loeveland, CO).

2.2.4 DNA extraction and quantification

Biomass DNA was extracted with a DNeasy mini kit on a Qiacube robotic workstation (Qiagen, Valencia, CA) following the manufacturer's protocol. DNA concentration was subsequently measured using UV absorbance (NanoDrop Lite, Thermo Scientific, Waltham, MA). Extracted DNA was stored at -80 ^{o}C prior to further use. Quantitative real time polymerase chain reaction (qPCR) was used to quantify the gene copy concentrations related to the total eubacteria 16S rRNA gene[70], AOB ammonia monooxygenase gene subunit A[71], *Nitrospira* spp.[72] and *Nitrobacter*

spp.[73] 16S rRNA gene (Table S2.2).

2.2.5 Mathematical modeling

The objective of the mathematical model developed herein was to quantitatively link methanol production to ammonia or hydroxylamine oxidation by AOB within the Activated Sludge Model[74] framework. The process model utilized in this research comprised five processes (Table 1): ammonia oxidation to hydroxylamine catalyzed by AMO, hydroxylamine oxidation to nitrite catalyzed by hydroxylamine oxidoreductase (HAO), nitrite oxidation by NOB, decay of AOB and decay of NOB. Methanol production was linked to ammonia and hydroxylamine oxidation by AOB as described in Eq.4.

$$\frac{dS_{MeOH}}{dt} = \left\{ \left(P_{C-AMO-AOB} \left[\mu_{MAX,AOB-AMO} \left(\frac{S_{NH}}{K_{NH} + S_{NH}} \right) \right] \right) + \left(P_{C-HAO-AOB} \left[\mu_{MAX,AOB-HAO} \left(\frac{S_{NH2OH}}{K_{NH2OH} + S_{NH2OH}} \right) \right] \right) \right\} X_{AOB} \quad (4)$$

Here, S_{MeOH} is the methanol concentration, $\mu_{MAX,AOB\text{-}AMO}$ is the maximum specific ammonia oxidation rate by AOB, S_{NH} is the ammonia concentration, K_{NH} is the ammonia half saturation coefficient, $\mu_{MAX,AOB\text{-}HAO}$ is the AOB maximum specific growth rate, S_{NH2OH} is the hydroxylamine concentration, K_{NH2OH} is the hydroxylamine half saturation coefficient, X_{AOB} is the AOB concentration and t is time. In our model, $\mu_{MAX,AOB\text{-}HAO}$ is linked to AOB growth while $\mu_{MAX,AOB\text{-}AMO}$ is not, to reflect that source of electrons for energy metabolism and bio-synthesis are derived from NH_2OH oxidation by HAO and not NH_3 oxidation by AMO[75]. The methanol production rate in Eq.4 is linked to the biomass specific rate of ammonia or hydroxylamine oxidation using the dimensionless production capacity terms $P_{C\text{-}AMO\text{-}AOB}$ and $P_{C\text{-}HAO\text{-}AOB}$,

Table 2.1. Component mass balance and process rates for process model used to describe nitrification and methanol production.

	Nitrogen Species				Biomass		Methanol	
Process	**S_{NH}**	**S_{NH2OH}**	**S_{NO2}**	**S_{NO3}**	**X_{AOB}**	**X_{NOB}**	**S_{MeOH}**	**Process Rate**
Oxidation of NH_3 by AOB	-1	1					$P_{C-AMO-AOB}$	$\left[\mu_{MAX,AOB-AMO}\left(\frac{S_{NH}}{K_{NH}+S_{NH}}\right)\right]X_{AOB}$
Growth of AOB on NH_2OH	$-i_{NBM}$	$-\left(\frac{1}{Y_{AOB}}\right)$	$\left(\frac{1}{Y_{AOB}}\right)$		1		$P_{C-HAO-AOB}$	$\left[\mu_{MAX,AOB-HAO}\left(\frac{S_{NH2OH}}{K_{NH2OH}+S_{NH2OH}}\right)\right]X_{AOB}$
Decay of AOB					-1			$b_{AOB}X_{AOB}$
Growth of NOB	$-i_{NBM}$		$-\left(\frac{1}{Y_{NOB}}\right)$	$\left(\frac{1}{Y_{NOB}}\right)$		1		$\left[\mu_{MAX,NOB}\left(\frac{S_{NO2}}{K_{N02}+S_{NO2}}\right)\right]X_{NOB}$
Decay of NOB						-1		$b_{NOB}X_{NOB}$

Table 2.2. Process model parameters used in the methanol production experiments.

Description	Variable	Unit of Measure	Literature Values		Selected Value
			Range/Values	Ref.(s)	
Common					
Nitrogen fraction of biomass	i_{NBM}	(mg-N·mg-COD^{-1})	0.07	[76, 77]	0.07
AOB biokinetics and stoichiometry					
max. specific ammonia oxidation rate	$\mu_{max,AOB\text{-}AMO}$	(day^{-1})	0.2 – 1.6	[78]	0.90
max. specific hydroxylamine oxidation rate	$\mu_{max,AOB\text{-}HAO}$	(day^{-1})	0.2 – 2.2	[57, 60]	0.90
decay rate	b_{AOB}	(day^{-1})	0.06 – 0.40	[78, 79]	0.15
half saturation value for S_{NH}	K_{NH}	(mg-N·L^{-1})	0.14 – 2.3	[80, 81]	0.50
half saturation value for S_{NH2OH}	K_{NH2OH}	(mg-N·L^{-1})	0.7*, 2.4	[57]	0.70
Ammonia-N yield	Y_{AOB}	(mg-COD·mg-N^{-1})	0.11 – 0.21	[78, 82]	0.15
NOB biokinetics and stoichiometry					
max. specific growth rate	$\mu_{max,NOB}$	(day^{-1})	0.2 – 2.5	[80]	0.90
decay rate	b_{NOB}	(day^{-1})	0.08 – 1.7	[80, 83]	0.15
half saturation value for S_{NO2}	K_{NO2}	(mg-N·L^{-1})	0.05 – 3.0	[79, 84, 85]	0.50
Nitrite-N yield	Y_{NOB}	(mg-COD·mg-N^{-1})	0.06 – 0.10	[82]	0.09
Biomass Concentrations					
Ammonia oxidizing bacteria	X_{AOB}	(mg-CODL^{-1})	NA		*estimated using qPCR*
Nitrite oxidizing bacteria	X_{NOB}	(mg-CODL^{-1})			
Methanol Production Capacity of AOB					
ammonia-N as electron donor	$P_{C\text{-}AMO}$	(g-COD g-COD^{-1})	NA		*fit value*
hydroxylamine-N as electron donor	$P_{C\text{-}HAO}$	(g-COD·g-COD^{-1})			

Notes: (*)K_{NH2OH} of 0.7 is from unpublished data of Taher and Chandran, 2014

respectively. $P_{C\text{-}HAO\text{-}AOB}$ (i.e., the CH_3OH production capacity linked to hydroxylamine oxidation) is strictly indicative of the net effect of the return of electrons from HAO to AMO, which are subsequently utilized for methanol production (Eqs. 2 and 3). $P_{C\text{-}HAO\text{-}AOB}$ was estimated by minimizing the sum of square residuals (SSR) between measured and modeled CH_3OH concentration from the 7.5 h HRT CSTR. The estimated value of $P_{C\text{-}HAO\text{-}AOB}$ was subsequently used to predict CH_3OH production in the CSTR operated with 2 h HRT. The data from the NH_3-fed CSTR (2 h HRT) was used to independently estimate $P_{C\text{-}AMO\text{-}AOB}$. In all cases, nitrogen species concentrations were predicted using the nitrification model described in Table 1 (model) and Table 2 (biokinetic parameters). The mathematical model developed herein comprises seven ordinary differential equations - one each for X_{AOB}, X_{NOB}, S_{NH}, S_{NH2OH}, S_{NO2}, S_{NO3} and S_{MeOH} - and 15 parameters. Literature values were utilized for biokinetic and stoichiometric parameters for AOB and NOB as detailed in Table 2. AOB and NOB concentrations utilized in the model were estimated using the gene copy concentrations as described previously[86]. We assumed that ordinary heterotrophs from this nitrification enrichment community could not use methanol as a carbon or energy source. Thus, the concentration of ordinary heterotrophs (X_{OHO}) was not explicitly modeled. Biokinetic and stoichiometric parameters were utilized to model methanol production in the CSTR and independently estimate the AOB methanol production capacity using ammonia or hydroxylamine as the electron donor ($P_{C\text{-}AMO\text{-}AOB}$ or $P_{C\text{-}HAO\text{-}AOB}$). Parameter estimation was accomplished using MATLAB 2011a (Mathworks, Natick, MA) using the *lsqnonlin* routine. The 95% confidence

intervals for all estimated parameters were determined using the *nlparci* routine. Model performance was evaluated using the Nash-Sutcliffe Efficiency (NSE), which ranges from $-\infty$ to 1; negative values of NSE indicate poor model predictions and strong predictive capability is generally characterized by NSE > 0.7[87].

The influence of AOB biokinetic and stoichiometric parameters on the methanol production capacity was evaluated using 2000 Monte Carlo simulations coupled with non-parametric dimensionless elasticity coefficients[88]. Five biokinetic parameters, $\mu_{MAX,AOB\text{-}AMO}$, $\mu_{MAX,AOB\text{-}HAO}$, b_{AOB}, $\mu_{MAX,NOB}$ and b_{NOB}, and three stoichiometric parameters, K_{NH}, K_{NH2OH} and K_{NO2}, were randomly selected using a Latin hypercube sampling method[89] from uniform distributions that span the range of literature values shown in Table 2. These randomly selected biokinetic and stoichiometric values were used to predict nitrogen species concentration and estimate the methanol production capacity (Eq. 4). We selected a design influent ammonia nitrogen concentration and conducted MC simulations varying the AOB and NOB biokinetic and stoichiometric parameters within the applicable range of the multivariate model utilized to develop the parameter elasticities (Table S2.5). In all MC simulations, we fixed the AOB biomass concentrations at 200 mg-CODL^{-1} and set X_{NOB} using an X_{NOB}/X_{AOB} ratio of 0.34[80]. Estimates for $P_{C\text{-}AMO\text{-}AOB}$, calculated through application of the elasticity model, were subsequently used to determine steady state methanol production rates in a CSTR operated at an HRT of 2 h. We evaluated the use of 100, 200 and 500 MC simulations and determined that there was no difference between results using 200 and 500 MC simulations (Mann Whitney test with $\alpha = 0.05$).

2.3 Results and discussion

2.3.1 Continuous methanol production using hydroxylamine as electron donor

The maximum CH_3OH concentration achieved using NH_2OH as the electron donor at a CSTR HRT of 7.5 h, was 41.0 ± 3.4 $mgCODL^{-1}$ (Figure 2.2, bottom left panel). Operation of the CSTR at 2 h HRT resulted in a maximum CH_3OH concentration of 21 ± 4.6 $mg\text{-}CODL^{-1}$ (Figure 2.2, bottom middle panel). Notwithstanding the different maximum methanol concentreations, the peak biomass specific CH_3OH production rates ($r_{CH3OH\text{-}NH2OH}$) were independent of CSTR HRT and in the range of 0.05–0.06 $mg\text{-}CH_3OH\text{-}COD^{-1}mg\text{-}biomass\text{-}CODh^{-1}$ (Figure 2.3), which was equivalent to ~0.6 $mg\text{-}CH_3OH\text{-}COD^{-1}mg\text{-}AOB\text{-}CODh^{-1}$ (Table 2.3). The maximum $r_{CH3OH\text{-}NH2OH}$ achieved in the CSTR using NH_2OH was approximately 60% of that previously reported in a batch reactor (0.82 $mg\text{-}CH_3OH\text{-}COD^{-1}mg\text{-}AOB\text{-}CODd^{-1}$, Table S2.3). The steady state $r_{CH3OH\text{-}NH2OH}$ with the CSTR operated with a 2 h HRT (0.38 ± 0.26 $mg\text{-}CH_3OH\text{-}COD^{-1}mg\text{-}AOB\text{-}CODh^{-1}$) was higher than the $r_{CH3OH\text{-}NH2OH}$ with 7.5 h HRT (0.17 ± 0.12 $mg\text{-}CH_3OH\text{-}COD^{-1}mg\text{-}AOB\text{-}CODh^{-1}$). The lower $r_{CH3OH\text{-}NH2OH}$ at the higher HRT is likely due to AMO inhibition resulting from longer exposure to methane or methanol in the CSTR, both of which are known AMO inhibitors[60]. Conversely, the higher $r_{CH3OH\text{-}NH2OH}$ achieved with a lower HRT indicate that AMO inhibition can be effectively alleviated through appropriate HRT control.

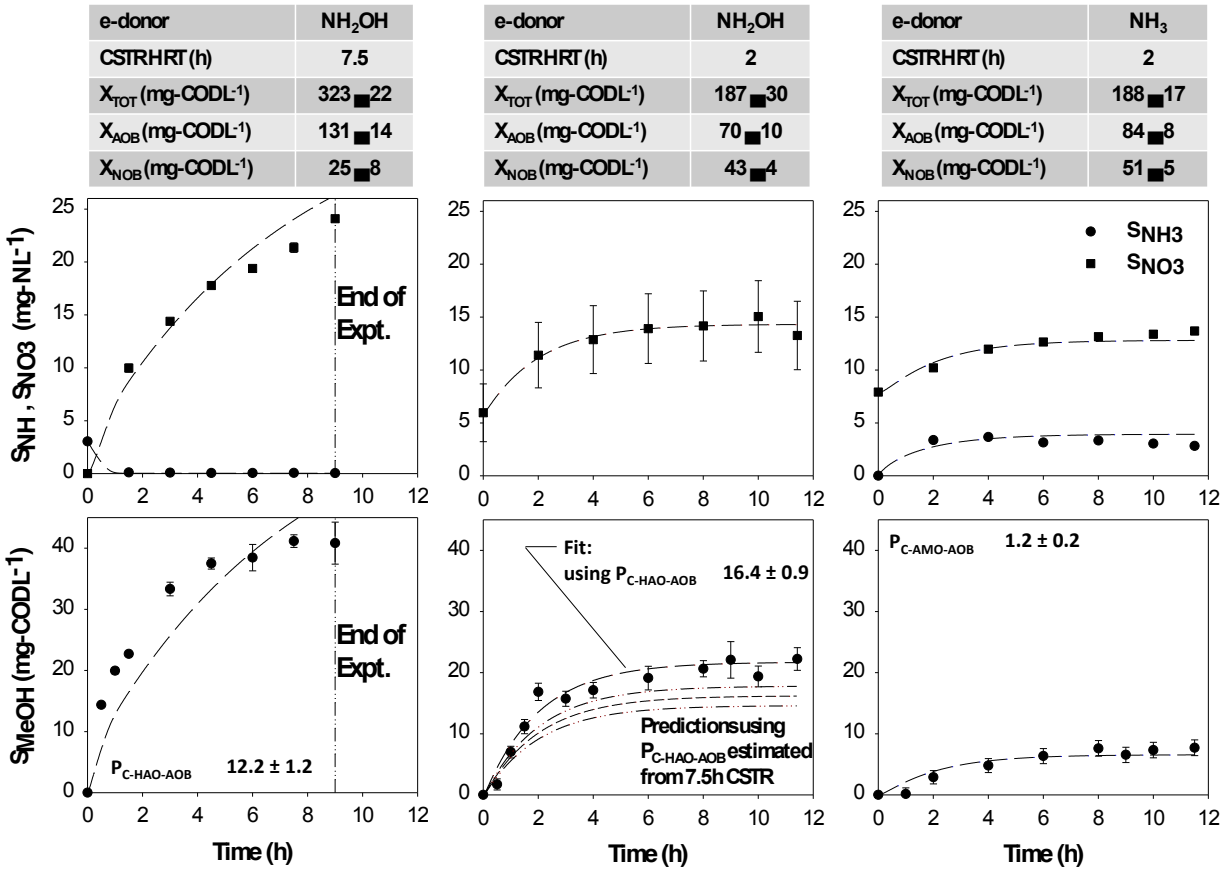

Figure 2.2. Measured concentrations of nitrogen species (top panels) and methanol (bottom panels) for 2 h and 7.5 h HRT CSTR experiments with hydroxylamine (left and middle panels) and ammonia (right panels) as the electron donor. Also shown are predictions for the nitrogen species and fits for methanol. Included above the figures are the AOB and NOB biomass concentrations utilized to model the experimental data from each experiment.

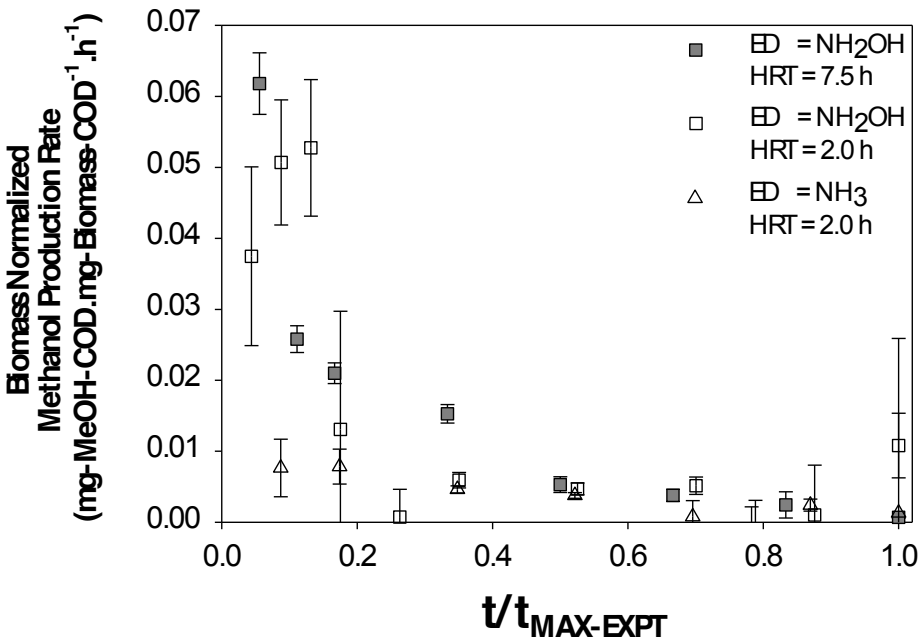

Figure 2.3. Biomass specific methanol production rates for 2 h and 7.5 h HRT CSTR experiments with hydroxylamine and ammonia as the electron donor (ED).

2.3.2 Comparison of NH_2OH and NH_3 as electron donors for methanol production

Operation of the methanol production CSTR at 2 h HRT using NH_3 as the electron donor resulted in a maximum methanol concentration of 7.1 ± 2.8 mg-CODL^{-1} (Figure 2, bottom right panel). The maximum biomass specific CH_3OH production rates achieved using NH_3 ($r_{CH3OH-NH3}$), 0.19 ± 0.05 mg-CH_3OH-COD^{-1}mg-AOB-CODh^{-1}, was 32% of the analogous maximum $r_{CH3OH-NH2OH}$. This $r_{CH3OH-NH3}$ in the CSTR is comparable with previous batch studies using mixed nitrifying populations[60] or axenic *N. europaea* cultures[16] (Table S2.3). The steady state $r_{CH3OH-NH3}$ was 0.10 ± 0.05 mg-CH_3OH-COD^{-1}mg-AOB-CODh^{-1}, which was 26% of the steady state $r_{CH3OH-NH2OH}$. The lower steady state methanol concentration and production rate using NH_3 as the electron donor are related to two

factors. The first is the competition for AMO between CH_4 and NH_3[16, 90, 91]. Second, co-oxidation of CH_4 to CH_3OH doesn't result in a replenishment of reducing equivalents as would normally occur during NH_2OH oxidation by HAO. In contrast, the external addition of NH_2OH would obviate both competitive inhibition of AMO and any potential limitation of reducing equivalents. Nonetheless, methanol production rates utilizing NH_3 in our research are comparable to those previously reported for methanol production in batch reactors[60, 92]. Furthermore, ammonia is an attractive electron donor for biogenic methanol production considering that it is readily available, at no cost, in a WRRF. The application of ammonia does not add any exogenous nitrogen loads into a WRRF in contrast to NH_2OH.

Table 2.3. Summary of operational conditions and biogenic methanol production in mixed nitrifying cultures CSTR.

Electron Source	HRT (h)	Max S_{MeOH} $mgCODL^{-1}$	**Specific MeOH Production Rate** $mg\text{-}CH_3OH\text{-}COD^{-1}(mg\text{-}AOB\text{-}CODd)^{-1}$	
			Max	Steady state
NH_2OH	7.5	41.0 ± 3.4	0.63 ± 0.03	0.17 ± 0.12
NH_2OH	2	21.0 ± 4.6	0.65 ± 0.24	0.38 ± 0.26
NH_3	2	7.1 ± 2.8	0.19 ± 0.05	0.10 ± 0.05

The nitrogen normalized steady state methanol production ratio using hydroxylamine and ammonia as the electron donor were 2.6 and 0.9 mg-COD $mg\text{-}N^{-1}$, respectively Despite the potential of AMO inhibition by methane and methanol present in the CSTR, 65% of the NH_3-N fed to the CSTR was oxidized to NO_3-N at steady state. This observation also links the biomethanol production process to a broader prospect

that concurrent nitrification and methanol production using AOB is feasible. In fact, while the goal of this study is to use on-site methane for denitrification, previous reports have demonstrated the possibility of simultaneous nitrification and denitrification using methane as carbon source[8, 93]. However, while previous studies achieved methane oxidation and nitrification by engineering a mixed culture consortia with MOB (from landfill cover soil or sludge with a history of methane exposure) and AOB, our study aims to exploit all the components of the process (ammonia, methane, AOB) within the WRRFs.

2.3.3 Process model describing methanol production

The nitrification model effectively described the nitrogen species data in all three experiments (Figure 2.2 top panels) with NSE values greater than 0.70 (Table S2.4). The estimated value of $P_{C\text{-}HAO\text{-}AOB}$ using the NH_2OH-fed CSTR operated at 7.5 h HRT (Figure 2.2, bottom left panel) was 12.2 ± 1.2 mg-CH_3OH-COD(mg-AOB-COD^{-1}). We expected that $P_{C\text{-}HAO\text{-}AOB}$ is independent of reactor operating conditions as shown in hydroxylamine-fed experiments. Application of the best-fit estimate of $P_{C\text{-}HAO\text{-}AOB}$ from the 7.5 h HRT experiment effectively described the CH_3OH concentration during the first hour of operation of the NH_2OH-fed CSTR operated with an HRT of 2 h. However, for the remaining experiment period, model values consistently under predicted the CH_3OH concentrations (Figure 2.2, bottom middle panel). Referring to Eq. 4, under prediction of the methanol production rate could result from impacts on AOB biokinetic (i.e., $\mu_{MAX,AOB\text{-}HAO}$) or stoichiometric parameters (i.e., K_{NH2OH}). Taher

and Chandran, 2013 indicate that $\mu_{MAX,AOB\text{-}HAO}$ is not impacted by CH_3OH. Application of an alternate model (details in the *Model Evaluation of Inhibition of AOB by Methanol* section of SI) only marginally improved the fit of CH_3OH concentration in the 2 h HRT CSTR (NSE = 0.74, compared to 0.70 for the predictive model) despite the additional fitting parameter. We did not measure the dissolved methane concentration in the CSTR and are therefore not able to assess its potential inhibitory impact. Further research is warranted to explore whether inhibition resulting from CH_4 exposure should be incorporated into the process model framework to describe concurrent ammonia and methane oxidation by nitrifying communities. The value of $P_{C\text{-}HAO\text{-}AOB}$ obtained by independently fitting CH_3OH concentration from the 2-h NH_2OH-fed CSTR was 16.4 ± 0.90 mg-CH_3OH-COD(mg-AOB-COD^{-1}), approximately 34% greater than that obtained using the data from the 7.5 h CSTR.

The value of $P_{C\text{-}AMO\text{-}AOB}$ estimated using this CH_3OH production in the NH_3-fed CSTR operated at 2 h HRT was 1.22 ± 0.16 mg-CH_3OH-COD(mg-AOB-COD^{-1}). As expected the methanol production capacity using NH_3 as the electron donor is lower than that using NH_2OH. A sensitivity analysis suggested that a one percent increase in $\mu_{MAX,AOB-AMO}$ would result in a 0.64% reduction in $P_{C\text{-}AMO\text{-}AOB}$ (*Methanol Production Capacity using Ammonia - Sensitivity Analysis* section of SI)). This inverse relationship may be explained through inspection of Eq. 4 – a higher ammonia oxidation rate due to an increase in $\mu_{MAX,AOB-AMO}$ would result in a lower value of $P_{C\text{-}AMO\text{-}AOB}$ to describe the methanol production data. On the other hand, an increase

in K_{NH}, which would result in a lowering of the ammonia oxidation rate, would require a higher value of $P_{C\text{-}AMO\text{-}AOB}$. Our analysis suggests that $P_{C\text{-}AMO\text{-}AOB}$ is less sensitive to changes in K_{NH} ; a 1% increase in K_{NH} would result in less than a 0.2% change in $P_{C\text{-}AMO\text{-}AOB}$. $P_{C\text{-}AMO\text{-}AOB}$ is relatively insensitive to changes in b_{AOB} ($\varepsilon^*_{b_{AOB}/P_{C-AMO-AOB}} = 0.06 \pm 0.01$).

2.4 Implications

Results from our study indicate that biogenic methanol production in a continuous flow process is both feasible and practicable using ammonia rather than hydroxylamine as the electron donor. This is a significant step towards integrating methanol production with WRRFs. Our results suggest that a methane to methanol production platform using ammonia as an electron donor could be beneficial for methanol use within a WRRF rather than for production of methanol as a commodity chemical. Key questions remain however as to how a methanol production platform may be integrated within a WRRF. These include, the source of ammonia-N, potential for methanol consumption by methylotrophs and impact of exposure to methane or methanol on AOB metabolism.

A range of ammonia-nitrogen sources are available for a biogenic methanol production platform within a WRRF, including the influent or primary effluent (~10 – 15 mg-NL^{-1}[94]), biological process effluent (the ammonia-N concentration will vary depending on the biological process in the range of 5 – 10 mg-NL^{-1} for WRRFs not practicing nutrient removal and as low as 0.5-1 mg-$NL^{-}1$ for biological nutrient

removal systems) and, where available, digester reject effluent (i.e., centrate; > 500 mg-NL^{-1}[95, 96]). We employed the elasticity coefficients developed in this research to assess the efficacy of a methanol production platform using these different ammonia nitrogen sources. Results from our evaluation suggest that steady state methanol concentration as high as 23 mg-$CODL^{-1}$ could be achieved using, for example, centrate fed to the CSTR (Figure 2.4, top panel). With the influent ammonia-N less than 20 mg-NL^{-1}, a nitrogen normalized methanol production ratio of 0.9 – 1.3 mg-CODmg-N^{-1} is achievable (Figure 2.4, middle panel), however at higher influent ammonia-N concentrations, the methanol production rate to feed-nitrogen ratio decreases dramatically. Considering that the effluent from the methanol production platform could be a beneficial supplemental carbon source sent directly to a post denitrification reactor, it is important that the effluent ammonia-N concentration be low enough to ensure robust operation of the liquid stream process. Our evaluation suggests that to achieve an effluent ammonia-N concentration of ≤ 1 mg-NL^{-1} with the conditions evaluated herein, the influent ammonia-N concentration should be ≤ 10 - 20 mg-NL^{-1} (Figure 2.4, bottom panel). Collectively, results from this preliminary evaluation suggest that if a high strength ammonia-N stream is available within a WRRF, it would be a useful choice for the methanol production platform. Alternatively, primary effluent may hold utility as the ammonia-N feed. It is important to recall that the estimates for $P_{C\text{-}AMO\text{-}AOB}$ are valid when the AOB and NOB biokinetic parameters are within the range shown in

Table S2.5. Therefore, caution is warranted in attempting to extrapolate these results outside this range.

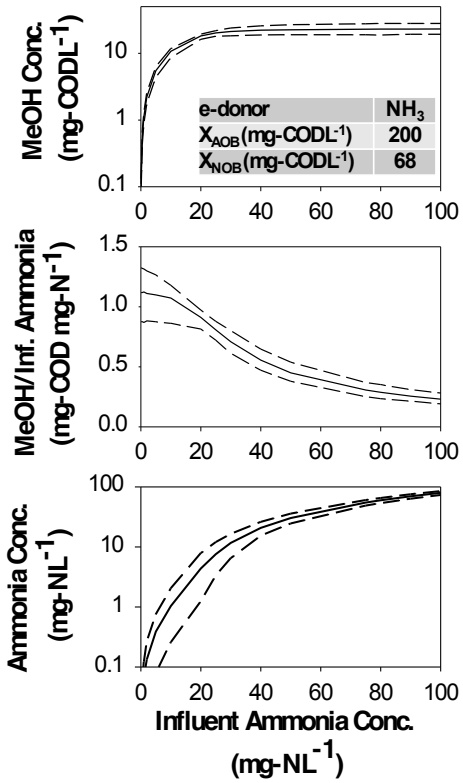

Figure 2.4. (Top panel) Methanol concentration. (Middle panel) Steady state methanol production to nitrogen feed ratio (mg-COD/mg-N). (Bottom panel) Ammonia concentration. For each plot the solid line represents that median value from 500 MC simulations. The lower and upper dashed lines represent the 5th and 95th percentile values, respectively from 500 MC simulations. Shown in the top panel are the AOB and NOB biomass concentrations used in these simulations.

2.5 Supporting information

The supporting information includes (1) nitrogen-free medium composition for methanol production experiment (2) performance profile of the nitrifying enrichment culture (3) primers used for bacteria quantification in this study (4) Summary of studies evaluating biogenic methanol production using mixed nitrifying cultures or axenic cultures of ammonia oxidizing bacteria (5) model evaluation of inhibition of AOB by methanol (6) sensitivity analysis of methanol production capacity.

Table S2.1. Composition of the nitrogen free medium used to re-suspended biomass for methanol production experiments in the CSTR.

Component	Concentration (mg/L)
$FeSO_4.7H_2O$	3.33
$MnSO_4.H_2O$	3.33
$(NH_4)_6Mo_7O_{24}.4H_2O$	0.67
$CuCl_2.2H_2O$	0.83
$ZnSO_4.7H_2O$	2.98
$NiSO_4.6H_2O$	0.57
$MgSO_4.7H_2O$	252
KH_2PO_4	204
$K_2HPO_4.3H_2O$	523
$NaHCO_3$	700

2.5.1 Performance of the nitrifying enrichment culture

Concentrations of ammonia, nitrite, nitrate, and biomass were continuously monitored to assess the nitrification performance of the nitrifying enrichment culture. Initially the parent reactor was fed with 500 mg NH_3-N L^{-1} and operated at 1-day HRT and 5-day SRT. To obtain higher AOB biomass concentration, the feed ammonia concentration was increased to 1000 mg NH_3-N L^{-1} and the SRT was increased to 20-day. The parent reactor was disturbed by the changes of operation conditions and stabilized again in about 100 days. Biomass for experiment using NH_2OH as electron donor and 7.5 h HRT (ED = NH_2OH, HRT = 7.5 h) was collected during the transition period. For 2 h HRT experiments (ED = NH_2OH or NH_3, HRT = 2 h), biomass was collected after parent reactor nitrification performance was stabilized.

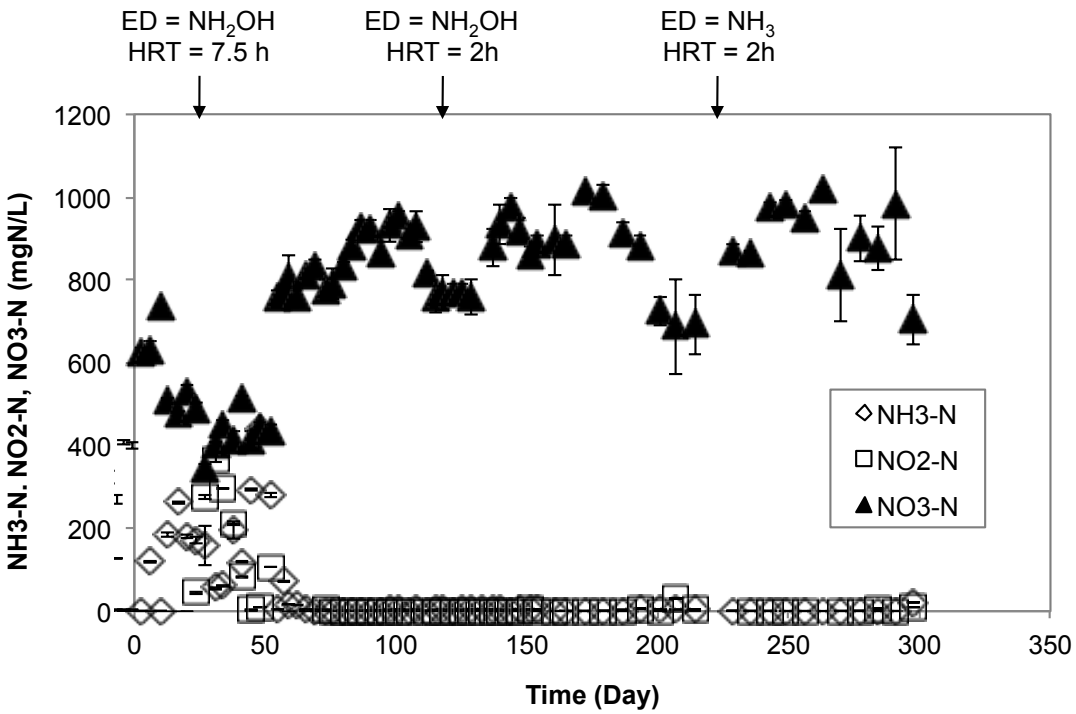

Figure S2.1. Ammonia, nitrite, and nitrate concentrations of the nitrifying enrichment culture. The disturbance from 0 to 100 days was resulted from changes in operation conditions. The arrows indicated the period when biomass was collected for methanol production experiments. Error bars represent one standard deviation of duplicate measurements.

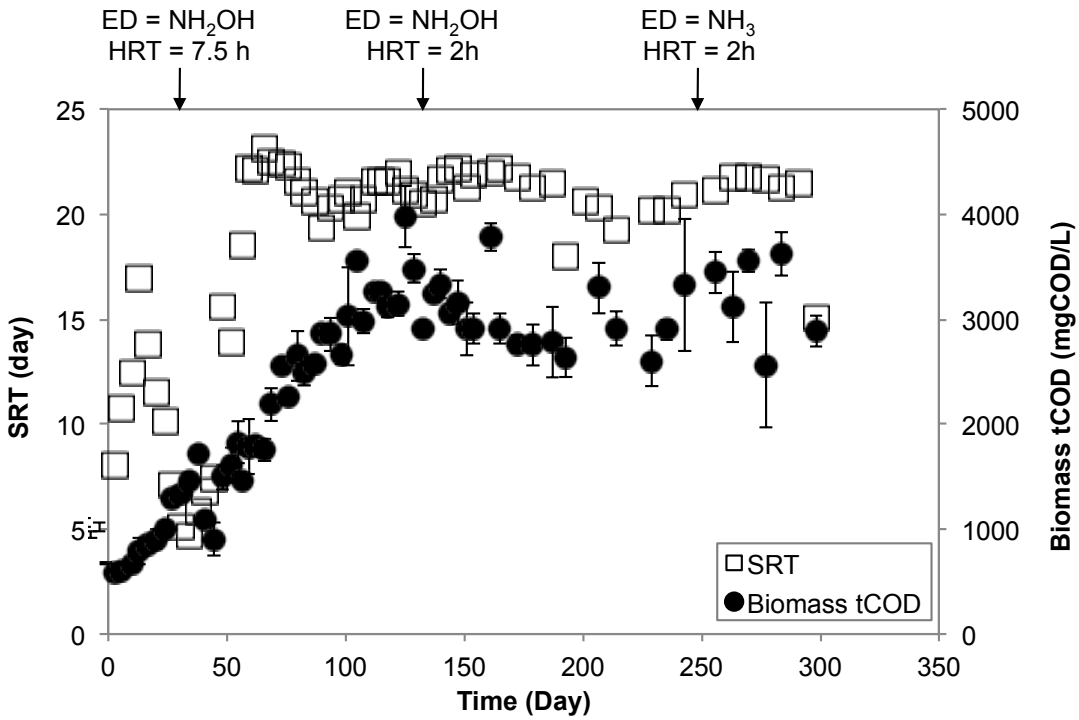

Figure S2.2. Biomass tCOD and calculated solids retention time (SRT) of the nitrifying enrichment culture. The increase in SRT and biomass concentration was resulted from the changes in operation conditions. The arrows indicated the period when biomass was collected for methanol production experiments. Error bars represent one standard deviation of duplicate measurements.

Table S2.2. Primers used for bacterial quantification in the methanol production experiments.

Target Gene	Primer set	Sequence (5'-3')	PCR product size (bp)	Annealing temp (°C)	Reference
Nitrospira 16S	NTSPAf	CGCAACCCCTGCTTTCAGT	67	67	[72]
	NTSPAr	CGTTATCCTGGGCAGTCCTT			
Nitrobacter 16S	Nitro-1198f	ACCCCTAGCAAATCTCAAAAAACCG	227	58	[97]
	Nitro-1423r	CTTCACCCCAGTCGCTGACC			
Universal 16S	1055F	ATGGCTGTCGTCAGCT	353	55.5	[98]
	1392R	ACGGGCGGTGTGTAC			
amoA	amoA-1F	GGGGTTTCTACTGGTGGT	491	60	[99]
	amoA-2R	CCCCTCKGSAAAGCCTTCTTC			

Table S2.3. Summary of studies evaluating biogenic methanol production using mixed nitrifying cultures or axenic cultures of ammonia oxidizing bacteria.

Description	Electron Source	Max S_{MeOH} [*2] mg COD L^{-1}	Specific MeOH Prod. Rate mg-CH_3OH-COD^{-1}(mg-AOB-CODd)$^{-1}$ Max	Average/Steady state	Note	Ref.
Batch Reactors						
N europaea cell suspension [*1]	NH_3	27.3	0.80	0.35	1 mM NH_3-N	16
	NH_3	28.7	0.52	0.42	10 mM NH_3-N	
N europaea cell suspension [*1]	None	N/A	N/A	0.10		17
	NH_3	N/A	N/A	0.59	10 mM NH3-N	
N europaea cell suspension [*1]	None	12.4	0.09	0.03	30 ºC	100
	NH_3	21.2	0.10	0.06	30 ºC, 0.1 mM NH_3-N pulse feed	
	NH_3	20.4	0.09	0.06	30 ºC, 0.2 mM NH_3-N pulse feed	
Mixed liquor	NH_3	23.5 ± 0.5	0.21	0.06	NH_3 feed batch	19
	NH_2OH	27.5 ± 0.8	0.30	0.07	NH_2OH feed batch	
	NH_3 + NH_2OH	31.5 ± 1.2	0.22	0.07	Simultaneous NH_3 & NH_2OH feed batch	
	NH_3+ NH_2OH	40.7 ± 0.2	0.20	0.09	Alternate NH_3 & NH_2OH feed batch	
	NH_2OH	59.9 ± 1.1	0.82	0.39	Biomass replenishment	

[1] Biomass concentration conversion factors: 1 mg dry wt =1.42 mg COD; 1 mg wet wt mL^{-1} = 344 mg COD L^{-1}.

[2] Methanol concentration conversion factor: 1 mM methanol = 48 mg COD L^{-1} methanol.

Table S2.4 Summary of Process Model Performance.

Electron Donor	NH_2OH	NH_2OH	NH_2OH	NH_2OH	NH_3
CSTR HRT (h)	7.5	2	2	2 & 7.5	2
S_{MeOH} Modeling Approach	Fit	***Predicted***	Fit	Fit	Fit
$N_{FITTING\ PAR}$	1	N/A	1	2	1
	$P_{C\text{-}HAO\text{-}AOB}$	--	$P_{C\text{-}HAO\text{-}AOB}$	$P_{C\text{-}HAO\text{-}AOB}$ $K_{MeOH\text{-}INH}$	$P_{C\text{-}AMO\text{-}AOB}$
Fit Values					
$P_{C\text{-}HAO\text{-}AOB}$	12.2 ± 1.2	*12.2 ± 1.2*	16.4 ± 0.9	10.8 ± 7.2	--
$K_{MeOH\text{-}INH}$	--	--	--	6.6 ± 5.6	--
$P_{C\text{-}AMO\text{-}AOB}$	--	--	--	--	1.22 ± 0.2
Methanol Time Course Goodness of Fit/Prediction					
NSE	0.82	0.70	0.95	0.74	0.90
Nitrogen Species Goodness of <u>Prediction</u> Metrics					
NSE	0.96	0.97	0.97	0.96	0.96

2.5.2 Model evaluation of inhibition of AOB by methanol

To explore whether the difference in estimates of PC HAO AOB from the 2 h and 7.5 h experiments may be explained by self inhibition resulting from exposure to CH_3OH, we modified Eq.4 using NH_2OH to include a mathematical switching function to moderate the CH_3OH production rate at high CH_3OH concentration as shown in Eq.S 4.1. This approach is consistent with the IWA ASM model framework.

$$\frac{dS_{MeOH}}{dt} = \left\{ \left(P_{C-HAO-AOB} \left[\mu_{MAX,AOB-HAO} \left(\frac{S_{NH2OH}}{K_{NH2OH} + S_{NH2OH}} \right) \right] \left(\frac{K_{MeOH-INH}}{K_{MeOH-INH} + S_{MeOH}} \right) \right) \right\} X_{AOB}$$

--- Eq S4.1

Here, $K_{MeOH\ INH}$ describes the extent to which CH_3OH production is inhibited by the presence of CH_3OH. All other parameters are as previously described. Application of the updated model to concurrently fit CH_3OH concentration profiles from the 2 h and 7.5 h HRT CSTR resulted in estimates of $P_{C\ HAO\ AOB}$ and $K_{MeOH\ INH}$ of 10.8 ± 7.2 mg-CH_3OH-COD(mg-biomass-COD^{-1}) and 6.6 ± 5.6 mg-CH_3OH-$CODL^{-1}$, respectively. Use of these fitting parameters only marginally improved the fit of CH_3OH concentration in the 2 h HRT CSTR (NSE = 0.74, compared to 0.70 for the predictive model) despite the additional fitting parameter. Furthermore, comparison of the Akaike Information Criterion for CH_3OH suggests that use of the alternate model is not warranted[101]. Thus, poor model performance may not be a result of self inhibition by CH_3OH in the CSTR.

2.5.3 Methanol production capacity using ammonia - Sensitivity analysis

There is no statistically significant correlation between the posterior distributions of parameters in each of the MC simulations (Table S4.5). Parameter sensitivity analysis was conducted utilizing results from 575 out of the 2,000 MC simulations which had NSE values greater than 0.7 for the nitrification model (using ammonia and nitrate data) indicating that the model suitably described nitrification in the CSTR. Consequently, the range of parameter values was smaller than those initially utilized in the MC simulations (Table S4.5). Most notably, $\mu_{MAX,AOB\text{-}AMO}$ ranged from 0.82−1.6 d^{-1} compared to 0.20−1.6 d^{-1} utilized in the initial MC simulations.

$P_{C\text{-}AMO\text{-}AOB}$ ranged from 1.03 to 1.40 (25th percentile = 1.12; 75th percentile = 1.28) in the 575 MC simulations. The mean value from the MC simulations is 1.20 ± 0.10 compared to the estimated value of 1.22 ± 0.16 from the deterministic simulation. An initial evaluation of elasticities indicated that only three of the eight predictors varied in the MC simulations ($\mu_{MAX,AOB\text{-}AMO}$, b_{AOB}, and K_{NH}) were statistically significant (i.e., p value ≤ 0.05). This is not surprising considering that $P_{C\text{-}AOB\text{-}AMO}$ is related to AOB and not NOB and more specifically to ammonia oxidation (Table 4.1). The significance of b_{AOB} may be explained due to its influence on determining X_{AOB}. The elasticity model was therefore limited to these three predictors. Residuals from the OLS regression were homoscedastic and normally distributed. The NSE of the elasticity model is 0.954 indicating that application of the linear elasticity model is effective. Shown in Figure 4.4 are the elasticities with standard errors for $\mu^*_{MAX,AOB-AMO}$, $b^*_{AOB}$and K^*_{NH}. Results indicate that $P_{C\text{-}AMO\text{-}AOB}$ is most sensitive to

changes in $\mu_{MAX,AOB-AMO}$ through a relatively strong inverse relationship ($\varepsilon^*_{\mu_{MAX,AOB-AMO}/P_{C-AMO-AOB}}$= -0.64 ± 0.006) and changes in K_{NH} through a less strong positive relationship ($\varepsilon^*_{K_{NH}/P_{C-AMO-AOB}}$= 0.19 ± 0.002). $P_{C\text{-}AMO\text{-}AOB}$ is relatively insensitive to changes in b_{AOB} ($\varepsilon^*_{b_{AOB}/P_{C-AMO-AOB}}$= 0.06 ± 0.008).

Table S2.5. Range of biokinetic parameters in 2,000 and 575 MC simulations with NSE > 0.70 for N-species.

Description	Variable		Range for 2,000 MC Simulations	Range in 575 MC Simulations ($NSE_{N\text{-species}} > 0.70$)
AOB biokinetics and biostoichiomety				
max. specific ammonia oxidation rate	$\mu_{max,AOB\text{-}AMO}$	(day^{-1})	0.2 – 1.6	0.82 – 1.6 (*)
max. specific hydroxylamine oxidation rate	$\mu_{max,AOB\text{-}HAO}$	(day^{-1})	0.2 – 2.2	0.2 – 2.2 (*)
decay rate	b_{AOB}	(day^{-1})	0.06 – 0.4	0.06 – 0.4
half saturation value for S_{NH}	K_{NH}	($mg\text{-}N{\cdot}L^{-1}$)	0.15 – 2.5	0.15 – 2.5 (*)
half saturation value for S_{NH2OH}	K_{NH2OH}	($mg\text{-}N{\cdot}L^{-1}$)	0.2 – 2.5	0.2 – 2.5
NOB biokinetics and biostoichiometry				
max. specific growth rate	$\mu_{max,NOB}$	(day^{-1})	0.2 – 2.5	0.21 – 2.5 (*)
decay rate	b_{NOB}	(day^{-1})	0.08 – 1.7	0.08 – 1.7
half saturation value for S_{NO2}	K_{NO2}	($mg\text{-}N{\cdot}L^{-1}$)	0.05 – 3.0	0.05 – 3.0

(*) indicates that distribution of values from 575 MC simulations with $NSE_{N\text{-species}} > 0.70$ is statistically different from distribution of values from initial 2,000 MC simulations (Mann Whitney test with $\alpha = 0.05$; Note that none of the distributions are statistically different with $\alpha = 0.01$).

CHAPTER 3

Characterization of nitrifying enrichment consortia in a coupled nitrification and biomethanol production process

This chapter is the basis of the paper:

Yu-Chen Su and Kartik Chandran*

Physiological characterization and community analysis of nitrifying enrichment consortia in a coupled nitrification and biomethanol production process (In preparation)

Affiliation:

Department of Earth and Environmental Engineering, Columbia University

500 West 120th Street, Room 1045 Mudd Hall, New York, NY 10027

Abstract

Biogenic methanol production using nitrifying activated sludge and methane offers an alternative and sustainable carbon source for biological nitrogen removal (BNR). While the process relies on ammonia (NH_3) and methane (CH_4) cometabolism in ammonia oxidizing bacteria (AOB), the effects of CH_4 on mixed culture nitrifying consortia were less discussed. To evaluate the responses of nitrifying bacteria to methane, a 1.5-L continuous flow reactor was inoculated with nitrifying biomass and was fed with 1000 mg NH_3-N/L and CH_4. During prolonged methane exposure, the solute profiles showed ammonia oxidation rates were maintained above 90% with a consistent methanol effluent concentration at 20 mg COD/L. Though the observed yield coefficients of AOB and NOB decreased more than 50% during methane exposure, specific ammonia and nitrite oxidation rates increased 190% and 250%, respectively. Analysis of key genes involved in AOB and NOB catabolism and AOB anabolism demonstrated transient impacts at transcription level, suggesting the adaptation of nitrifying microcosm. Sequencing of 16S rRNA gene amplicons showed that *Nitrosomonas* genus (AOB) remained dominant at the end of exposure but the relative abundance of *Nitrobacter* genus (nitrite oxidizing bacteria) decreased from

8.3% (pre-exposure) to 4.0%. Moreover, the detection of methanol-utilizing denitrifying bacteria indicated the potentiality of using methane as precursor carbon and AOB as biocatalyst to produce methanol for a combined nitrification-denitrification process. In summary, here we demonstrated the acclimation of nitrifying consortia to methane, which can be advantageous for the application of biomethanol production in BNR processes. Furthermore, the increase in the relative abundance of methanol-utilizing methylotrophic denitrifiers revealed by 16S rRNA gene sequencing indicates the potential integration of a simultaneous nitrification, biomethanol production and denitrification process.

3.1 Introduction

Methanol is the most widely used exogenous carbon source in water resource recovery facilities (WRRFs) for conventional denitrification[61]. An alternative source for methanol within a facility presents a particularly valuable opportunity to reduce the dependence on external carbon sources and enhance overall WRRF sustainability. Methanol can be produced chemically or biologically [102]. Biogenic methanol production from methane, which is commonly present in WRRFs with anaerobic digestion process, had been proposed and demonstrated using methanotrophic bacteria or ammonia oxidizing bacteria[15]. Methanol production using pure culture ammonia oxidizing bacteria (AOB) [16-18] as well as mixed culture nitrifying activated sludge[19] are of interest because the biological process precludes high temperature, high pressure, and energy-intensive catalytically conversion. The results were promising that mixed culture nitrifying activated sludge which was enriched in AOB showed high methanol production rates and high yields when compared with pure culture studies[19]. Furthermore, utilizing AOB in nitrifying activated sludge is advantageous which preclude the sterile operation required for pure culture applications and biomass is easily accessible and abundant in WRRFs that perform BNR.

Biomethanol production by AOB is relied on the activity of ammonia monooxygenase (AMO) enzyme to oxidize methane to methanol[16]. AMO is involved in the first step of ammonia oxidation and hydroxylamine is being produced. Hydroxylamine oxidation by hydroxylamine oxidoreductase (HAO) then results in nitrite production

and releasing reducing equivalents for AOB metabolism[103].

$$NH_3 + O_2 + 2e^- \xrightarrow{AMO} NH_2OH + H_2O \cdots\cdots\cdots (1)$$

$$NH_2OH + H_2O \xrightarrow{HAO} NO_2^- + 5H^+ + 4e^- \cdots\cdots (2)$$

$$CH_4 + O_2 + 2e^- \xrightarrow{AMO} CH_3OH + H_2O \cdots\cdots\cdots (3)$$

While the biomethanol production process relies on ammonia and methane cometabolism in AOB, the impacts on overall nitrifying community are relatively less studied. The increased relative abundance of *Nitrosomonas*-like and nitrite oxidizing bacteria (NOB) 16S rRNA genes when soil microcosm was incubated with urea (as nitrogen source) plus methane[55] indicated that though anabolic activity might be lower, AOB and NOB growth was not completely inhibited. Thus, we hypothesize that AOB and NOB are capable of acclimating to methane exposure and concurrent nitrification and biomethanol production is possible. Moreover, we further expanded our scope to evaluate the impacts of cometabolic biomethanol production on both AOB and NOB activity, which is crucial for the practical application of the biomethanol production platform.

3.2 Materials and methods

3.2.1 Cultivation of nitrifying enrichment consortia with continuous methane exposure

To study the responses of nitrifying community to the coexistence of ammonia and methane, a 1.5-liter continuous stirred tank reactor (CSTR) was inoculated with nitrifying enrichment biomass from a parent full nitrification reactor. The test CSTR was fed with mineral medium as previously described[104] with 1000 mg NH_3-N/L

(Table S3.1). The hydraulic retention time (HRT) and solids retention time (SRT) were controlled at 1-day and 20-day, respectively (Fig S3.1). The pH was automatically controlled with a pH controller (Jenco Instrument, San Diego CA) at 7.50 ± 0.05 using 1M $NaHCO_3$. Dissolved oxygen was continuously monitored using a Clark-type dissolved oxygen probe (YSI, Yellow Springs, OH) and was remained unlimited (above 1.6 mg O_2/L) throughout the experiment. Air (0.9 L/min) and nitrogen (0.1 L/min) (Purity 4.0, TechAir, White Plains, NY) were filtered and supplied during pre-exposure and post-exposure phase while 0.9 L/min air plus 0.1 L/min methane (Purity 5.0, TechAir, White Plains, NY) was applied during methane exposure phase (co-feeding phase). The full nitrification capacity of the test reactor was confirmed by routine performance measurements before methane was supplied. During reactor operation, samples were taken for nitrogen species, methanol, total COD measurement, and molecular analysis.

3.2.2 Analytical methods

Reactor performance was monitored by measuring the concentrations of total ammonia (ammonia + ammonium, S_{NH3}) (Method 10031, Hach, Loveland, CO), hydroxylamine (intermediate of ammonia oxidation in AOB, S_{NH2OH})[68], nitrite (S_{NO2}) (Ricca, Pocomoke City, MD), nitrate (S_{NO3}) (Dionex ICS2100 with AS18 column, Fisher Scientific, CA), and reactor total COD (Method 8000, Hach, Loveland, CO) in the reactor. Methanol concentrations (S_{CH3OH}) were measured using MXT-1 column (Restek, Bellefonte, PA) and a GC8610C gas chromatography equipped with flame

ignition detector (SRI Instrument, Torrance, CA) to assess the cometabolic transformation of methane.

3.2.3 Determination of biomass concentrations and observed yield coefficient

Approximately 0.4 mL pelleted biomass for DNA extraction was stored in -80 °C freezer until being extracted using QIAcube (Qiagen, Valencia, CA) according to the manufacturer's instructions. Primers (Table S3.2) target on AOB, NOB and eubacterial 16S rRNA gene fragments were used in quantitative polymerase chain reaction (qPCR) with SYBR Green chemistry to estimate the bacterial concentrations (Determination of bacterial concentrations based on qPCR and total COD measurement in Section 3.6.1). Observed yield coefficient (Y_{obs}) for AOB and NOB was estimated based on biomass concentrations, HRT (□), SRT (□$_c$), and nitrogen profiles[80].

$$Y_{obs,AOB}=\frac{X_{AOB}\tau}{\theta_c(S_{NO2}+S_{NO3})}$$

$$Y_{obs,NOB}=\frac{X_{NOB}\tau}{\theta_c S_{NO3}}$$

3.2.4 RNA extraction and functional gene analysis

To evaluate the expression of functional genes during different phases, cells were harvested from 1 mL biomass and treated with RNAprotect reagent (Qiagen, Valencia, CA) before stored in -80 °C freezer until being extracted using QIAcube. Approximately 0.5 μg of total RNA was reversed transcribed to cDNA using QuantiTect Reverse Transcription kit (Qiagen, Valencia, CA). Primers (Table S3.2)

target on ammonia monooxygenase (*amoA*), hydroxylamine oxidoreductase (*hao1*), nitrite reductase (*nirK*), nitric oxide reductase subunit B (*norB*), ribulose-1, 5-bisphosphate carboxylase large subunit (*cbbL*), nitrite oxidoreductase (*nxrA*) were used in qPCR with SYBR Green chemistry. The expression levels of each functional gene were normalized with respective 16S rRNA gene expression. For each gene, the average of normalized gene expression during pre-exposure phase was used as baseline for expression fold changes comparison. Fold changes were calculated by dividing the normalized gene expression value by baseline expression. The expression of *amoA*, *hao1* (AOB), and *nxrA* (NOB) were monitored as indicators for AOB and NOB catabolic activities while expression of *cbbL* gene was further examined to evaluate AOB anabolic potential.

3.2.5 DNA sequencing for microbial community analysis

DNA samples at the end of pre-exposure (experiment day 8) and the end of co-feeding phase (experiment day 23) were further used for 16S rRNA sequencing on the Ion PGM system (Life Technologies). Sequencing reads were processed with mothur[105] and blasted against the SILVA rRNA database[106]. In brief, raw reads were trimmed with average Q score of 20 and reads smaller than 300 bp were discarded. After initial screening, qualified reads were aligned with silva rRNA database (version 123) and possible chimeric sequences were identified and removed from the alignment. The alignment was then classified by taxonomy based on silva rRNA database (version 123).

3.3 Results

3.3.1 Transient peaks of nitrification intermediates

Two replicate reactors were operated and data from one of the replicates were demonstrated (biological replicate shown in Fig S3.3). Before methane supplementation, the test CSTR showed full nitrification with stable S_{NH3}, S_{NO2}, S_{NO3} at 0.56 ± 0.35 mg NH_3-N/L, 0.50 ± 0.87 mg NO_2-N/L, and 950.9 ± 44.3 mg NO_3-N/L, respectively (n = 9). S_{NH2OH} were below the detection limit (~0.014 mg NH_2OH-N/L) (Fig 3.1A). The nitrification performance data during pre-exposure phase was then used as reference for subsequent comparisons.

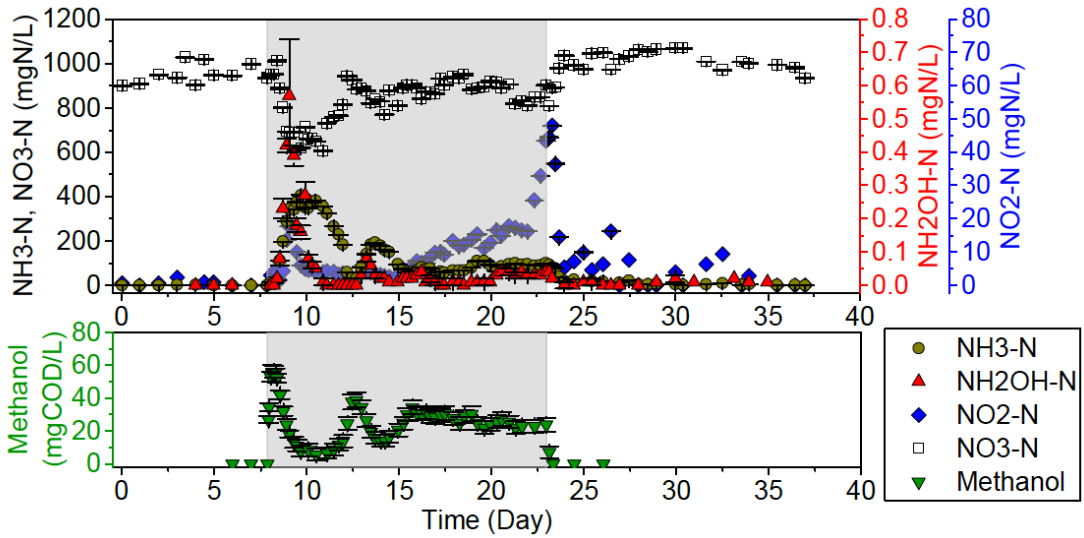

Figure 3.1. Nitrogen (A) and methanol (B) profile. Shaded area indicate methane exposure phase. Error bars indicate one standard deviation of duplicate measurements.

After the baseline was established, nitrogen gas was switched to 0.1 L/min methane and the overall gas flow rate was retained at 1 L/min. Significant increase of S_{NH3} and S_{NO2}, at 11.21 ± 0.25 mg NH_3-N/L and 2.06 ± 0.02 mg NO_2-N/L, respectively, were observed after 4 hours of methane exposure, while S_{NH2OH} increased from non-detect

level to 0.019 ± 0.001 mg NH_2OH-N/L in 12 hours of methane exposure. Peaks of S_{NH2OH} and S_{NO2} were observed at 28-hour of methane cofeeding, up to 0.570 ± 0.169 mg NH_2OH-N/L (maximum during co-feeding period) and 18.25 ± 0.03 mg NO_2-N/L, respectively, followed by S_{NH3} peak at 406.3 ± 0.9 mg NH_3-N/L (maximum during co-feeding period) approximately 43-hour after methane supplementation. Similarly, concurrent peaks of S_{NH2OH} (0.078 ± 0.007 mg NH_2OH-N/L) and S_{NO2} (4.84 ± 0.02 mg NO_2-N/L) showed up at exposure day 5 and a later S_{NH3} peak (192.3 ± 0.4 mg NH_3-N/L) was observed at exposure day 5.8 (Fig 3.1A). After the transient peaks, S_{NH3} and S_{NH2OH} were stabilizing at 90.22 ± 0.06 mg NH_3-N/L and 0.031 ± 0.002 mg NH_2OH-N/L, respectively (n = 8), from exposure day 12 until the end of co-feeding. S_{NO2}, however, begun to increase after the second S_{NO2} peak (at exposure day 5) to a maximum 39.22 ± 0.03 mg NO_2-N/L before methane supply was terminated. The total nitrogen concentration was 992.2 ± 42.2 mg N/L (n = 60), which showed no significant nitrogen loss during co-feeding.

3.3.2 Impacts of methane exposure to AOB and NOB were reversible

Within 8 hours after methane supply was stopped, S_{NH3} and S_{NH2OH} decreased to 82.0 ± 0.19 mg NH_3-N/L and 0.018 ± 0.003 mg NH_2OH-N/L, respectively, and further decrease in S_{NH3} and S_{NH2OH} were observed. As reactor operation continued under the same condition as pre-exposure period, however, S_{NH3} were fluctuated between 0.2 – 5 mg NH_3-N/L while S_{NH2OH} decreased below the detection limit.

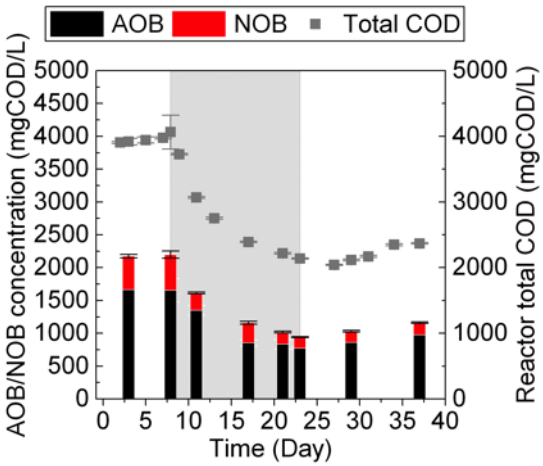

Figure 3.2. Total COD concentrations and estimated AOB/NOB concentrations. Error bars indicate one standard deviation of duplicate measurements (tCOD) or triplicate qPCR analysis.

Unlike S_{NH3} and S_{NH2OH} which started to decrease shortly after methane was switched back to nitrogen, an increase in S_{NO2} from 39.22 ± 0.03 mg NO_2-N/L to ~46 mg NO_2-N/L was observed. After 8 hours of operation in the absence of methane, S_{NO2} started to decreased but unable to stabilize at pre-exposure level (~0.50 mg NO_2-N/L). Rather, S_{NO2} were fluctuated between 0.2 – 10 mg NO_2-N/L (Fig 3.1A).

3.3.3 Biomethanol production and ammonia and hydroxylamine oxidation

No methanol was detected during pre-exposure phase. Within an hour of methane co-feeding, S_{CH3OH} increased from non-detect level to 26.8 ± 2.1 mg COD/L (Fig 3.1B). S_{CH3OH} peak preceded the rising of S_{NH3} and S_{NH2OH} at approximately 50 mg COD/L within 4 hours of methane supply and eventually stabilized at 24.2 ± 1.4 mg COD/L (n = 8) as co-feeding continued. The changes in S_{CH3OH} were related to both S_{NH3} and S_{NH2OH} profiles. Accumulation of AOB metabolites in the sequence of methanol, hydroxylamine then ammonia were observed in preliminary experiments

and both replicates during early stage of co-feeding (Fig S3.2 and S3.3). As S_{NH3} increased, S_{CH3OH} declined. S_{CH3OH} started to increase as S_{NH3} was decreasing. On the other hand, the decrease in S_{CH3OH} was captured within the period of a complete S_{NH2OH} peak (Fig 3.1).

3.3.4 Determination of bacterial yield coefficient and substrate oxidation rates

Reactor total COD concentrations were stabled at 4064 ± 257 mg COD/L (n = 4) during pre-exposure phase and gradually decreased during methane cofeeding (Fig 3.2). Bacterial concentrations showed that AOB and NOB concentrations decreased 53% ad 69%, respectively (Fig 3.2), during co-feeding period.

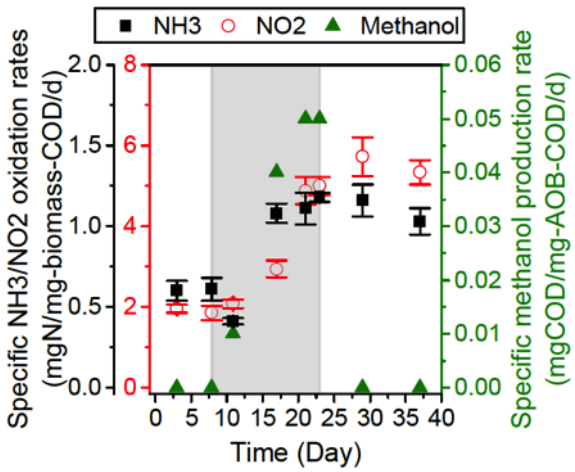

Figure 3.3. AOB-specific ammonia oxidation/methanol production rates and NOB-specific nitrite oxidation rates. Error bars indicate one standard deviation calculated from AOB/NOB substrate concentrations and biomass concentrations.

Further analyses on the observed yield coefficient (Y_{obs}) showed that Y_{obs_AOB} decreased from 0.089 ± 0.008 mg-COD/mg-N oxidized (pre-exposure) to 0.041 ± 0.001 mg-COD/mg-N oxidized (end of co-feeding) and Y_{obs_NOB} decreased from 0.029 ± 0.002 mg-COD/mg-N oxidized to 0.009 ± 0.001 mg COD/mg N oxidized. On

the other hand, AOB-specific ammonia oxidation rates and NOB-specific nitrite oxidation rates showed 1.9-fold and 2.5-fold increase, respectively, at the end of co-feeding (Fig 3.3). The net biomethanol production rates also increased from 0.006 mg-CH_3OH-COD/mg-AOB-COD/d at early stage of methane co-oxidation to 0.047 ± 0.004 mg-CH_3OH-COD/mg-AOB-COD/d at the end of co-feeding period (Fig 3.3).

3.3.5 Recovery of genes expression involved in catabolism and carbon fixation

In terms of the genes coding for key catabolic pathways in AOB and NOB, a lower (compared to other selected genes) and steady recovery of *amoA* expression was captured during the co-feeding period. However, the expression level only partially recovered to 62% ± 7% of pre-exposure level (Fig 3.4A). Expression of *hao1*, *cbbL* and *nxrA* returned to pre-exposure level within 4.5 day of co-feeding (Fig 3.4A, C and D), coinciding with the end of first S_{NH3} peak (Fig 3.1A). On the other hand, expression of *nirK* changed in parallel with the fluctuation of S_{NO2} (Fig 3. 4B). The 300-fold and 70-fold spikes for *nirK* expression were observed coincided the two transient S_{NO2} peaks and the increase in *nirK* expression levels were observed in parallel with the increasing S_{NO2}. In terms of anabolism in AOB, following an initial short-term reduction, expression of *cbbL* (coding for CO_2 fixation gene) recovered during co-feeding and co-metabolism to even higher than pre-exposure levels (up to twice the pre-exposure levels) (Fig 3.4C). During post-exposure phase, expression of *amoA* and hao*1* showed an increase but dropped below baseline before the experiment was stopped, while *cbbL* and *nxrA* expression returned to baseline.

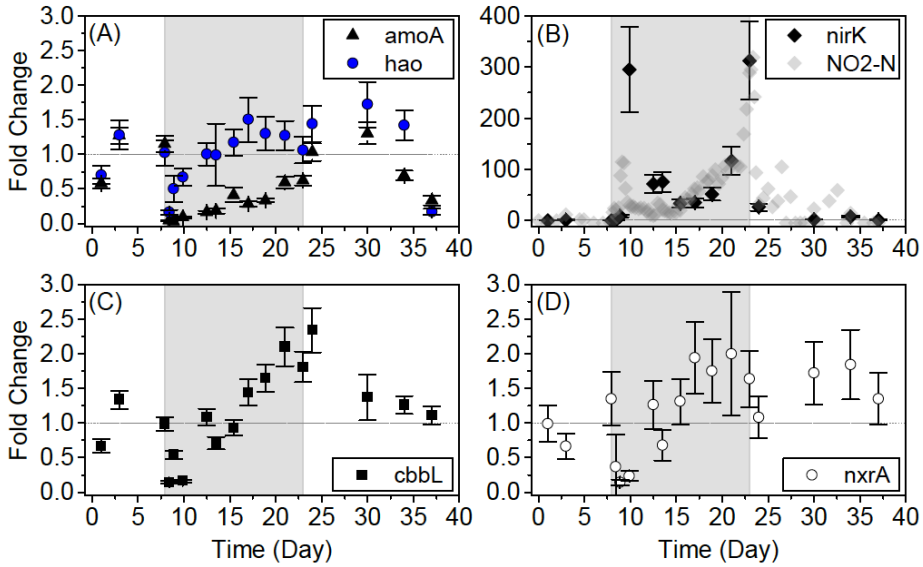

Figure 3.4. Fold changes of gene expression target on *amoA* and *hao1* (A), *nirK* (B), *cbbL* (C), and *nxrA* (D). Expression levels of each gene were normalized with AOB16S rRNA gene (for AOB genes) or Nb16S rRNA gene (for NOB genes). Fold changes were calculated relative to the expression levels during pre-exposure phase.

3.3.6 16S amplicon sequencing revealed endurance of *Nitrosomonas* genus and emerging methylotrophic denitrifying bacteria

Total 24601 and 26015 reads resulted from 16S amplicon sequencing were analyzed for pre-exposure phase and methane co-feeding phase, respectively. The relative abundance of *Nitrosomonas* genus remained dominant as presented by approximately 70 % of the total reads at both time points (Fig 3.5). The relative abundance of *Nitrobacter* genus, which represents the NOB community, decreased from 8.28 % to 4.03 %. It was intriguing that the relative abundance of bacteria related to methanol-based denitrifying population, *Hyphomicrobium* genus (from 0.04 % to 0.68 %) and *Methyloversatilis* genus (from non-detection level to 0.02 %), were observed[107]. Ten-fold increases of the members from the *Comamonadaceae* family, which can denitrify using glycerol as carbon source[108, 109], from 0.92 % to 9.47 %

were shown. Facultative methylotroph, which grows on methanol, from the well-characterized *Methylobacterium* genus[110] also showed an increase from non-detected to 0.03 % (Fig 3.5).

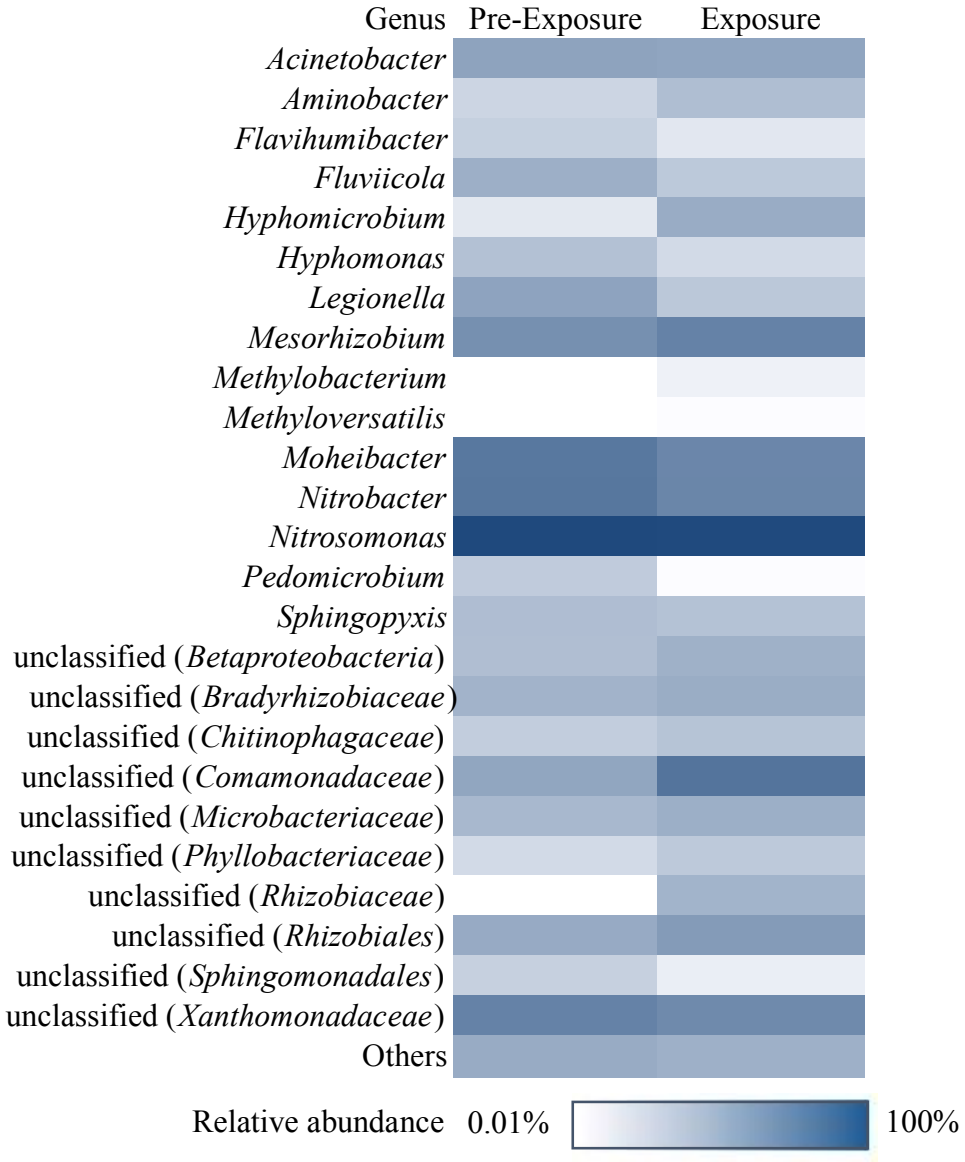

Figure 3.5. Microbial composition during pre-exposure phase and at the end of methane exposure phase. Relative abundances (at genus level) higher than 0.1% of the total reads are presented.

3.4 Discussion

3.4.1 Coupled nitrification and biomethanol production as nitrifying biomass acclimated to methane

While previous studies described the competitive role and inhibitory effect of methane on ammonia oxidation in AOB in short-term batch experiments[24, 28, 29], results present here is one of the few studies conducted in a continuous flow process. Furthermore, we expanded the scope from biomethanol production[18, 19, 111] to the responses of AOB and NOB during prolonged methane exposure and biomethanol production. The multilevel results including solute profiles, substrate oxidation rates and gene expression suggested that adaptation of AOB and NOB to ammonia and methane co-feeding. The stabilized S_{NH3}, S_{CH3OH}, AOB concentrations and ammonia oxidation rates indicated that AOB accomplished the adjustments for methane co-oxidation (discussed in Section 3.4.4), while increasing S_{NO2} suggested that NOB was still in the process of adaptation. As all operational parameters remained the same throughout the experiment, the changes in NOB activity were likely due to the presence of methane. While it was proposed that methane-oxidizing bacteria outcompete NOB in the soil samples incubated with ammonia and methane[112], no direct evidence showed the effects of methane or methanol on NOB. However, previous studies have demonstrated the inhibition of elevated S_{NH2OH} to NOB[113]. Finally, the increasing biomass concentration and nitrification (ammonia to nitrate) efficiency (Fig 3.1A) suggested that the inhibitory effects of methane co-feeding on AOB and NOB were reversible.

3.4.2 Ammonia-nitrogen for biomethanol production

As AOB acclimated to ammonia and methane co-feeding, the specific methanol production rates also increased by 8-fold, reached ~0.05 mg-CH_3OH-COD/mg-AOB-COB/d (Fig 5.3), which was at the same order with previous reported values from pure culture batch studies[16-18] but lower than previous mixed culture studies[19, 111]. Taher and Chandran (2013)[19] demonstrated that a maximum specific methanol production rate at 0.82 mg-CH_3OH-COD/mg-AOB-COB/d can be achieved when hydroxylamine was fed as nitrogen source and biomass was replaced every two hours in a fed-batch system. While nitrogen supply (in the forms of ammonia or hydroxylamine) serves as electron donors to sustain the electron flows in AOB, it is more reasonable to use on-site ammonia source rather than purchasing hydroxylamine externally even if using hydroxylamine can avoid the competition with methane for AMO. Nevertheless, the fed-batch experiment fed with ammonia-nitrogen still showed higher specific methanol production rate at 0.21 mg-CH_3OH-COD/mg-AOB-COB/d [19]. A subsequent study with ammonia as nitrogen source and with continuous biomass replacement demonstrated biomethanol production at 0.08 ± 0.02 mg-CH_3OH-COD/mg-AOB-COB/d in a continuous flow process[111]. Considering the competition between ammonia and methane, it is expected that specific methanol production rates are lower in current study. The S_{NH3} at the end of methane co-feeding in this study were 90.22 ± 0.06 mg NH_3-N/L (Fig 3.1), which was unfavorable for

biomethanol production comparing with the S_{NH3} during continuous biomass replacement (below 10 mg NH_3-N/L)[111]. Possible strategies to avoid he inhibitory effect of ammonia to biomethanol production could be controlling the ammonia feed rate (mg NH_3-N/L/d) and HRT to lower the S_{NH3} in the reactor while maintaining active nitrifying culture (more specifically, maintain AOB).

3.4.3 Functional genes expression reflect bacterial activities at reactor level

During NH_3 and CH_4 co-feeding, initial reduction followed by recovery in the expression of amoA and hao1 in AOB (Fig 3.3A) indicated that AOB catabolic pathways were directly responsive to presence and metabolism of methane. The nxrA gene expression also changed rapidly during early stage of co-feeding (Fig 3.3D) and the transient fluctuations agreed with S_{NH2OH} and S_{NO2} peaks, which indicate that NOB catabolism might be affected by S_{NH2OH} as demonstrated previously[113]. The parallel trends in *nirK* expression and S_{NO2} also revealed the indirect impact of concurrent NH3 and CH_4 metabolism that resulted in transient nitrite accumulation (Fig 3.1). In terms of AOB anabolism, the trend in *cbbL* expression suggests the adaptation of AOB anabolism machinery to counteract the decreased availability of reducing equivalents during the period of CH_4 oxidation, so that cell growth could still be sustained. While expression of *nirK*, *cbbL* and *nxrA* genes recovered to baseline levels during the post-exposure phase, varying degrees of recovery and subsequent fluctuations in the expression of *amoA* and *hao1* were observed and likely reflect sustained changes to the catabolic potential of AOB to external disturbance as

observed previously[114].

3.4.4 Shifted metabolic balance toward catabolism in AOB

The impact of methane on AOB growth was previously demonstrated in *Nitrosomonas europaea*, presumably due to disrupted electron flows for biosynthesis. Figure 3.6 illustrates the proposed mechanism for the redistribution of electrons in AOB.

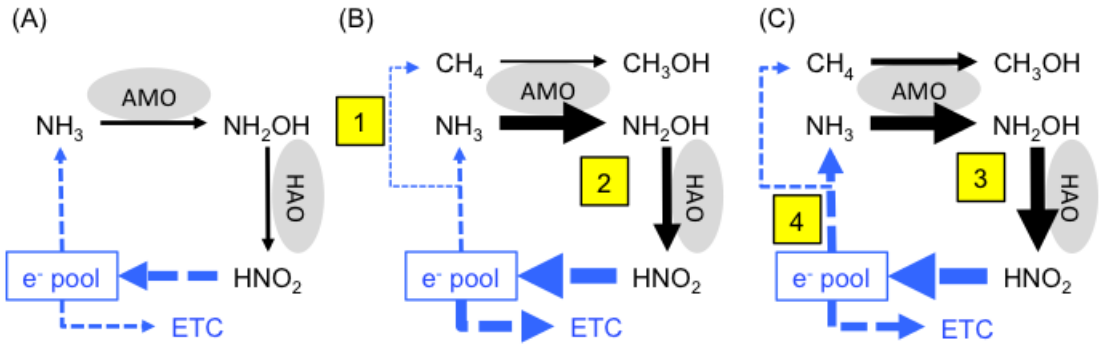

Figure 3.6. Proposed mechanism for acclimation of AOB to methane co-oxidation. Ammonia and hydroxylamine oxidation are catalyzed by AMO and HAO (gray circles). Blue lines indicate electron flows and the blue block represents the electron pool. Line thickness implies the rates of redox reaction or electron flux. The yellow blocks indicate a series of events during the acclimation process.

During pre-exposure phase, the electrons generated from hydroxylamine oxidation are transferred to ubiquinone/ubiquinol electron pool, from which electrons return to AMO (for subsequent ammonia oxidation) or continue toward downstream electron transport chain (ETC) for energy synthesis (Fig 3.6A)[20]. Methanol is being produced as soon as methane becomes available and being oxidized by AMO (Fig 3.6B, step 1). Methane oxidation is an electron-consuming process and the produced methanol will not be metabolized for further electron generation in AOB, which results in

insufficient electron flux when compare with pre-exposure phase. The transient S_{NH2OH} (Fig 3.6, step 2) and increasing ammonia oxidation rates (Fig 3.2) suggested that electron production was accelerated in AOB to compensate the electron deficiency. The decrease in S_{NH2OH} (Fig 3.6C, step 3) followed by decrease in S_{NH3} and increasing S_{CH3OH} (Fig 3.6C, step 4) indicated that the redistribution of electrons was fulfilled after the adjustments in ammonia and hydroxylamine oxidation were completed. The increasing ammonia oxidation rates (Fig 3.2) and decrease in Y_{obs_AOB} further implied that though higher electron production rate was maintained, lower fraction of electrons or the resulted energy were used for biosynthesis.

The profiles of the first S_{NH2OH} and S_{NO2} peaks matched the recovery in *hao1* and *nxrA* genes expression (Fig 3.4), suggested that both AOB and NOB catabolism were being regulated during early co-feeding phase however the mechanisms might be different. While the changes in nitrogen metabolism or gene expression in AOB could be related to electron redistribution as proposed above (Fig 3.6), the changes in NOB could be in response to inhibitory effects of elevated S_{NH2OH} [113]. Similarly, the higher nitrite oxidation rates and lower Y_{obs_NOB} suggested that lower fraction of electrons or the resulted energy was devoted to NOB growth.

Alternatively, since that hydroxylamine oxidation is the actual step for electrons production, the S_{NH2OH} peak could be resulted from rate-limiting hydroxylamine oxidation while AOB accelerated both steps (Fig 3.6B, step 2). The AOB then fine-tuned hydroxylamine oxidation rates to the level when the requirement for reducing equivalents can be satisfied (Fig 3.6B, step 3). Assuming NOB was affected

only by CH_4 exposure, the S_{NO2} peaks could be detected when the transient S_{NO2} production rates during this period (step 2) were higher than S_{NO2} consumption rates by NOB. Considering the solute profiles, substrate oxidation rates and gene expression data, it is more likely that AOB metabolism was affected in response to methane first and NOB was mainly impacted by the elevated S_{NH2OH}.

3.4.5 Increase in relative abundance of methylotrophic denitrifying bacteria indicated the possibility for simultaneous nitrification and denitrification

In addition to qPCR, high throughout sequencing targeting bacterial 16S rRNA fragments was applied to investigate the changes in microbial composition in more detail. It was noticed that the relative abundance (copy number basis) of *Nitrosomonas* genus and Nitrobacter genus were different between qPCR results and 16S amplicon sequencing data. While qPCR results from DNA sample collected at the end of pre-exposure phase showed approximately 45% of the total copy number belonged to *Nitrosomonas* genus and 15% of the total copy number belonged to *Nitrobacter* genus, 16S amplicon sequence showed ~68% and ~8%, respectively. The bias in 16S amplicon sequencing data might be resulted from the selection of primer, which is related to different targeting regions on bacterial 16S rRNA fragment, as part of the sequencing procedure[115, 116]. However, given the consistent workflow for the sequence analysis of our samples, the comparison between the two samples should still be valid. Microbial community revealed by 16S amplicon sequencing showed that (1) *Nitrosomonas* genus remained dominant during ammonia and methane

co-feeding phase (2) decrease in relative abundance of *Nitrobacter* genus (3) increasing population of methanol-utilizing denitrifying bacteria (Fig 3.5). The increase in methylotrohpic denitrifying bacteria including *Hyphomicrobium* genus and *Methyloversatilis* genus[107] implied the potentiality of using methane as precursor carbon source and AOB as biocatalyst to produce methanol for denitrification. Furthermore, the increasing relative abundance of members from the *Comamonadaceae* family, which is capable of using acetate, glycerol, or polyhydroxyalkanoates for denitrification[108, 109, 117, 118] indicate that carbon supply in the from of methane can lead to formation of other daughter metabolites in addition to methanol. Though denitrifying bacteria was emerging during ammonia and methane co-feeding cultivation, the lack of observed nitrogen loss indicated that the operation condition was inappropriate for denitrification to occur perhaps due to unlimited dissolved oxygen. Therefore, oxygen control should be considered to facilitate denitrification and to achieve nitrogen removal (ammonia to nitrogen gas).

3.4.6 Precaution of undesirable enrichment of obligate aerobic methylotrophs

It was noticed that the relative abundance of bacteria belongs to the *Methylobacterium* genus, which is capable of growing on one-carbon compounds including methane or methanol using oxygen as a terminal electron acceptor[119], was also increasing. Since that only little evidence for methanotrophic growth was provided by Van Aken et al (2004)[119] and the lack of genes involved in methane oxidation is present in Methylobacterium genus, methane utilization by *Methylobacterium* genus remains

inconclusive[120]. However, either case (methanotrophic growth or methanol utilization using oxygen rather than nitrite/nitrate as terminal electron acceptors) would negatively affect the effectiveness of biomethanol production for biological nitrogen removal. With regard to obligate aerobic methanol-utilizing bacteria, one of the possible strategies would be controlling oxygen levels to limit the availability of terminal electron acceptors. Still, unwanted enrichment of methanotrophs should also be taken into account given the ubiquitous presence of methanotrophs in natural environment and its ability to further metabolize methanol. As discussed in Yang et al (2011)[121], with NH_4^+/CH_4 molar ratio higher than 30, nitrogen would be non-limited for methanotrophs (nitrogen limitation when NH_4^+/CH_4 molar ratio < 0.1)[122], however further increase in NH_4^+ would negatively impact methane oxidation by methanotrophs through competition for the active binding sites of methane monooxygenase. In addition to substrate competition, nitrite toxicity could also negatively affect the activity of methanotrophs[123, 124]. Therefore, the high NH_4^+/CH_4 molar ratio (assuming 10% saturation of methane) between 30 (at 5 mg NH_3-N/L) to 2370 (at 400 mg NH_3-N/L) and the increasing S_{NO2} in this study should establish an unfavorable environment for methanotrophs. However, the target NH_4^+/CH_4 molar ratio should be low for biomethanol production in order to reduce the degree of competitive inhibitory effect of ammonia on methane oxidation in AOB as discussed in previous sections.

3.5 Implications

Our results clearly demonstrate continuous AOB-mediated biomethanol production in a nitrification reactor fed with ammonia and methane, both are readily accessible within WRRFs. Acclimation of the nitrifying biomass to co-exposure and co-oxidation of ammonia and methane were shown at multiple levels (reactor performance, biomass concentrations and genes expression). This adaptation of AOB was achieved by modulating their catabolic (energy synthesis) and anabolic (biomass synthesis) pathways. Interestingly, accumulation of nitrite and a more substantive decrease in Y_{obs_NOB} (compared to Y_{obs_AOB}) indicated the possibility for partial nitrification (ammonia-N to nitrite-N) coupled with biomethanol production, thereby opening the prospect for even more resource-efficient concurrent carbon and nitrogen management and removal. The 16S amplicon sequencing data further revealed the potential for simultaneous nitrification and denitrification under ammonia and methane co-feeding operation. Currently ongoing extensions of this broader work include further process optimization for AOB-mediated biomethanol production in both mainstream and sidestream nitrification (full- or partial-) processes as well as structured process modeling to facilitate such optimization and eventual process scale-up and adoption.

3.6 Supporting information

The supporting information includes (1) reactor setup and operational conditions (2) preliminary results of 2-day ammonia and methane co-feeding experiment (3)

performance data from the biological replicate reactor (4) primers used in this study (5) details for determination of bacterial concentrations.

Table S3.1. Primers used for bacterial quantification and gene expression analysis for the continuous exposure experiments.

Target Gene	Primer Set	Sequence (5'-3')	PCR product size (bp)	Annealing temp (°C)	Reference
Nitrospira 16S	NTSPAf	CGCAACCCCTGCTTTCAGT	67	67	[72]
	NTSPAr	CGTTATCCTGGGCAGTCCTT			
Nitrobacter 16S	Nitro-1198f	ACCCCTAGCAAATCTCAAAAAACCG	227	58	[97]
	Nitro-1423r	CTTCACCCCAGTCGCTGACC			
AOB16S	CTO 189fAB	GGAGRAAAGCAGGGGATCG	116	60	[125]
	CTO189fC	GGAGGAAAGTAGGGGATCG			
	RT1r	CGTCCTCTCAGACCARCTACTG			
Universal 16S	1055F	ATGGCTGTCGTCAGCT	353	55.5	[98]
	1392R	ACGGGCGGTGTGTAC			
amoA	amoA-1F	GGGGTTTCTACTGGTGGT	491	60	[99]
	amoA-2R	CCCCTCKGSAAAGCCTTCTTC			
hao1	hao1Fq	TGAGCCAGTCCAACGTGCAT	85	57	[114]
	hao1Rq	AAGGCAACAACCCTGCCTCA			
nirK	nirK157F	GTGGCTCTGATCCGATGATT	152	58	[53]
	nirK534R	GGCTGTTTTGTCGTCAGGAT			
cbbL	cbbL1223f	TGGTGGCGGTACTTTAGGTC	140	57	[53]
	cbbL1371r	TGTGTTTTGCAGCCTCTGTC			
nxrA	F1norA	CAGACCGACGTGTGCGAAAG	322	55	[126]
	R1norA	TCYACAAGGAACGGAAGGTC			

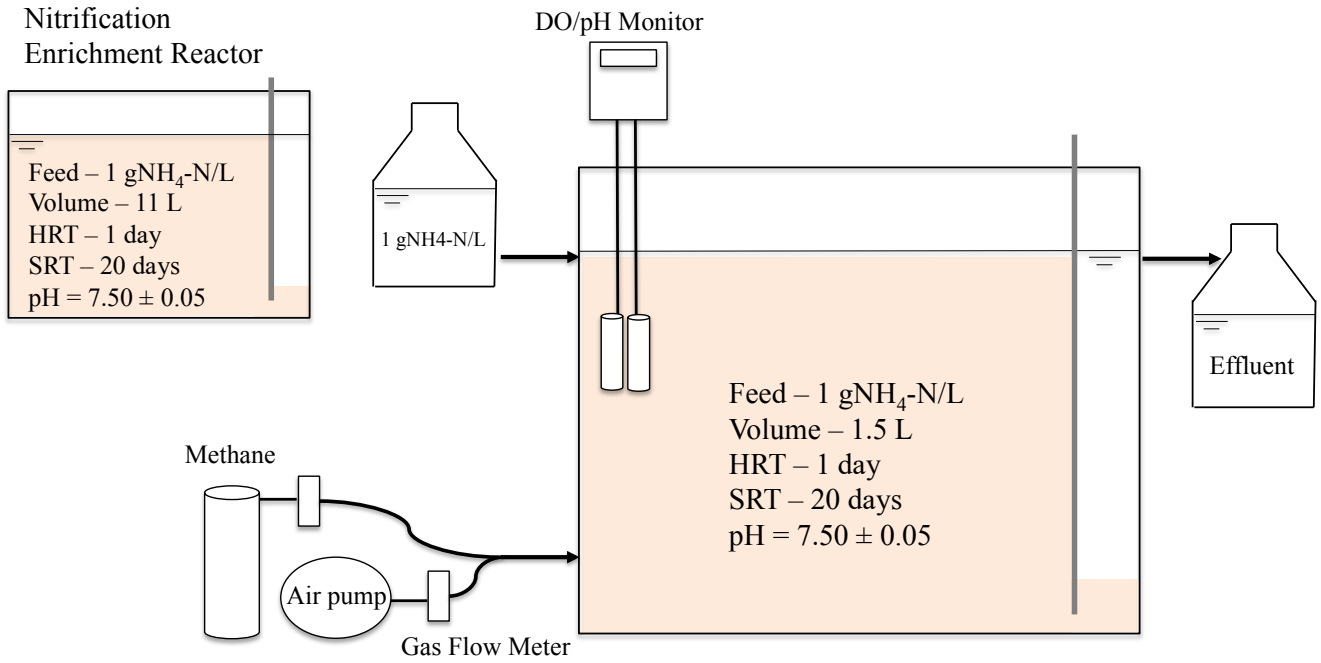

Figure S3.1. Reactor setup and operational conditions for the continuous methane exposure experiments.

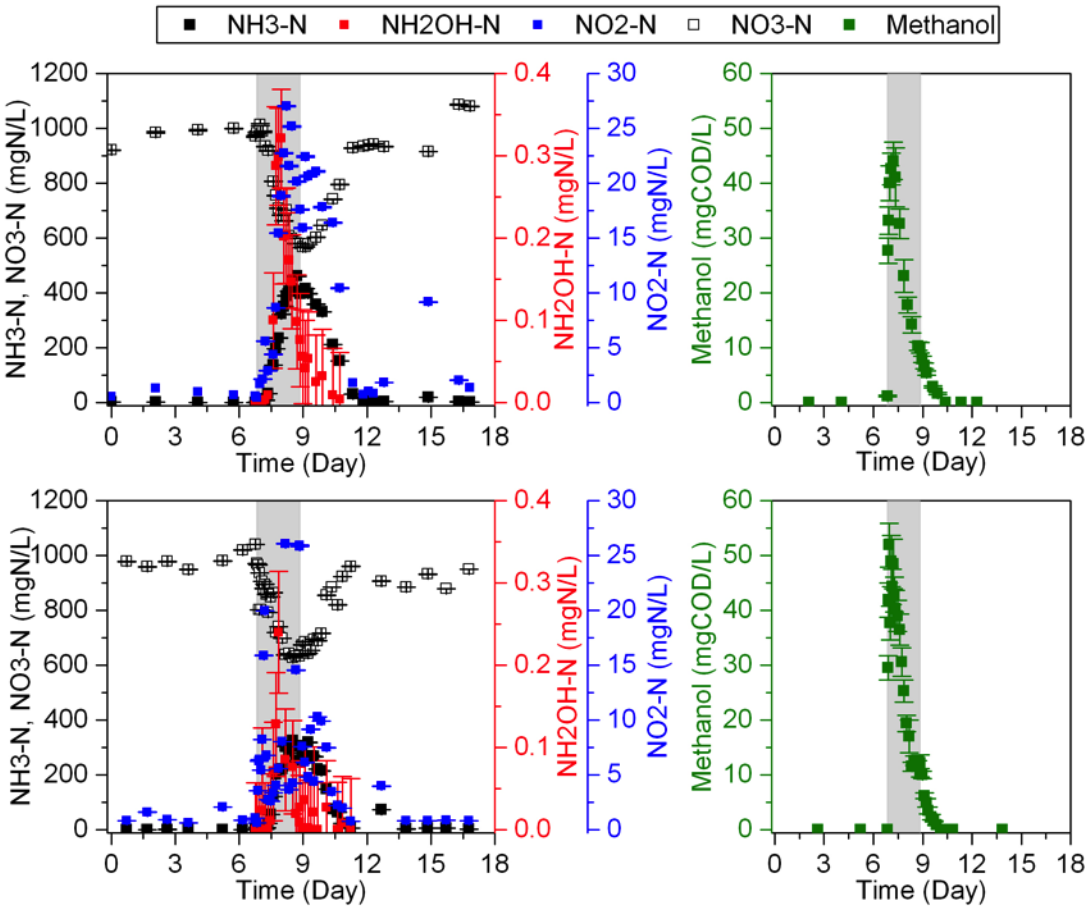

Figure S3.2. Preliminary results of 2-day methane exposure demonstrated the reversible impacts of methane exposure on nitrification. Error bars indicate one standard deviation from duplicate measurements.

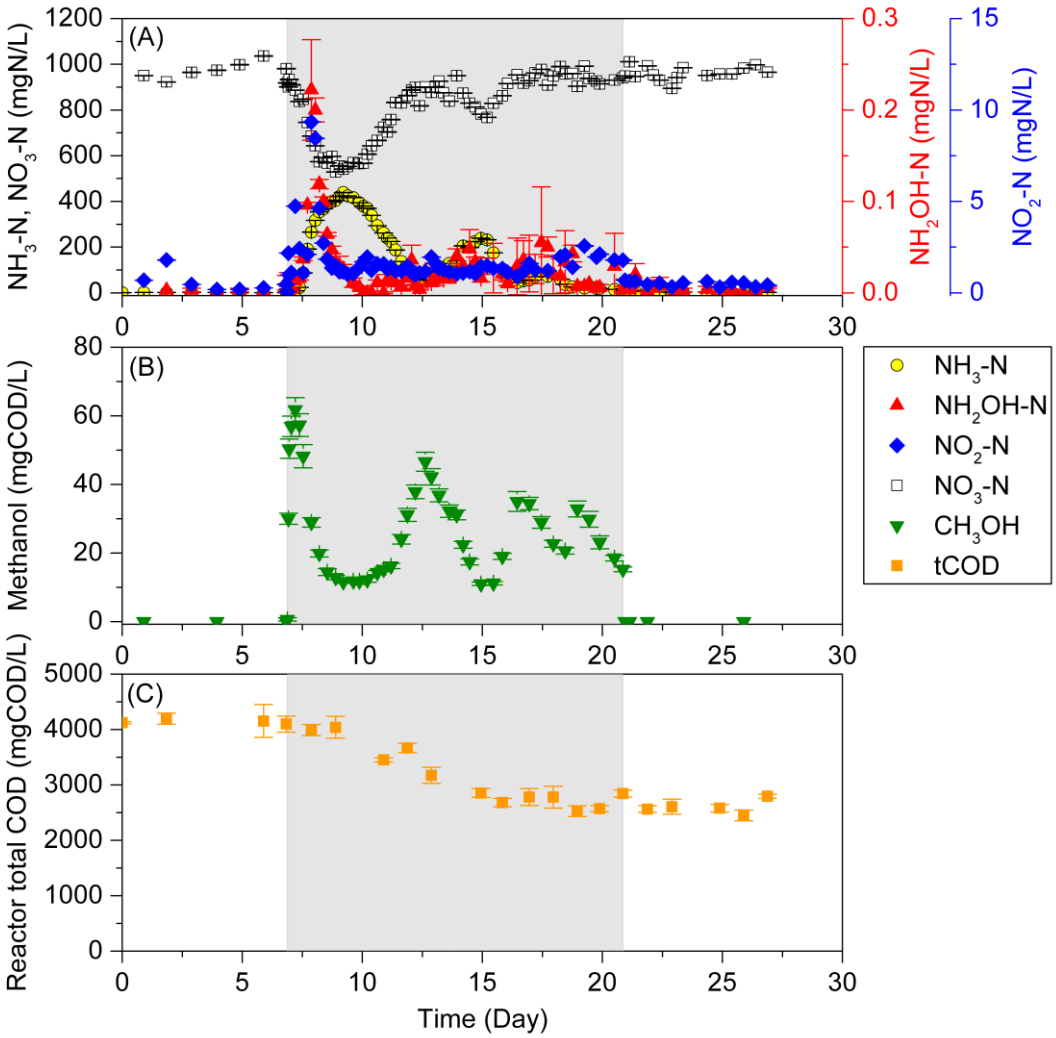

Figure S3.3. Nitrogen (A), methanol (B), and reactor tCOD (C) profiles in the replicate reactor. Shaded area indicate methane exposure phase. Error bars indicate one standard deviation of duplicate measurements.

3.6.1 Determination of AOB and NOB concentrations based on total COD and qPCR

AOB and NOB concentrations were calculated using reactor total COD concentration (tCOD) and AOB/NOB fractions, which are calculated based on qPCR results. Reactor total COD measured by COD digester vials are composed of AOB, NOB, non-nitrifying bacteria and inert concentrations. The active fraction of the nitrifying enrichment biomass with 20-d SRT was calculated assuming a specific decay rate (b) of 0.17 d^{-1} [127] and a biomass debris fraction (f_d) of 0.1 mgCOD/mgCOD [128]. AOB and NOB fractions are calculated based on the information that each AOB, NOB, and eubacteria cell contain 1 copy of AOB16S[129], 1 copy of NOB16S[130], and 4.2 copies of EUB16S[97], respectively.

$$Active\ fraction = \frac{1}{1 + f_b \cdot b \cdot q_c}$$

$$Total\ bacterial\ concentration = tCOD \cdot active\ fraction$$

$$AOB\ concentration = Total\ bacterial\ concentration \cdot AOB\ fraction$$

$$NOB\ concentration = Total\ bacterial\ concentration \cdot NOB\ fraction$$

CHAPTER 4

Proteomic and transcriptional responses of methane cometabolism in *Nitrosomonas europaea*

This chapter is the basis of the paper:

Yu-Chen Su[1], Sandeep Sathyamoorthy[2], Kartik Chandran[1,*]

Proteomic and transcriptional responses of methane cometabolism in *Nitrosomonas europaea* (In preparation)

Affiliation:

[1] Department of Earth and Environmental Engineering, Columbia University

500 West 120th Street, Room 1045 Mudd Hall, New York, NY 10027

[2] Black & Veatch, 2999 Oak Road, Suite 490, Walnut Creek, CA 94597

Abstract

Nitrosomonas europaea is a chemolithoautotrophic ammonia oxidizing bacteria (AOB) that derives energy from the oxidation of ammonia using ammonia monooxygenase (AMO). The wide range substrate of AMO allows AOB to cometabolically oxidize alternative substrates such as methane, however the responses of AOB at whole cell level have not been characterized. The goal of this study was to investigate the physiological responses of choemostat *N. europaea* culture to methane. Concurrent ammonia and methane oxidation by *N. europaea* resulted in methanol production but with a decreased biomass yield. Label-free proteomic profiling revealed that the relative abundances of key proteins involved in catabolism (AMO, HAO) were not changing during methane exposure. However, increased relative abundances of intermediate and terminal electron acceptors, NirK, NorY, and CoxA, and decreased carbon-fixation protein subunit CbbL were observed during methane exposure. Furthermore, the elevated *nirK* mRNA transcripts detected during methane exposure and during recovery of chemostat, up to 100-fold and 60-fold of pre-CH_4 exposure level, respectively, suggests the important physiological roles of NirK. In summary, here we demonstrated the negative and reversible impacts of methane exposure on *N. europeaea*. Proteomic data suggest that continuous methane exposure induced a rearrangement of electron and energy partitioning between anabolic and catabolic pathways in *N. europaea*.

4.1 Introduction

Nitrosomonas europaea is an ammonia oxidizing bacterium (AOB) that participates in the transformation of nitrogen compounds in global nitrogen cycle and engineered environment. As a chemolithoautotrophic bacterium, *N. europaea* uses CO_2 as carbon source and acquires energy from the oxidation of ammonia (NH_3) to nitrite (HNO_2). During AOB catabolism, ammonia is first oxidized to hydroxylamine (NH_2OH) by ammonia monooxygenase (AMO) (eq 1), and then NH_2OH is further oxidized to nitrite (NO_2^-) by hydroxylamine oxidoreductase (HAO) (eq 2). For each mole of NH_2OH oxidation, four moles of electrons are released and transferred to ubiquinone pool, where two moles of electrons are directed back to AMO for subsequent NH_3 oxidation and the others are used for NADH synthesis or move toward electron transport chain and generate proton motive force[20]

$$NH_3 + O_2 + 2e^- \xrightarrow{AMO} NH_2OH + H_2O \quad (1)$$

$$NH_2OH + H_2O \xrightarrow{HAO} NO_2^- + 5H^+ + 4e^- \quad (2)$$

Ammonia monooxygenase, which shares many similar characteristics with the particulate methane monooxygenase (pMMO)[21], is the key enzyme that initiates AOB catabolism. The common substrates for AMO and pMMO including NH_3, methane (CH_4), and various recalcitrant pollutants[22]. Methane, as a competitive inhibitor for NH_3[24-26], hinders NH_3 oxidation and subsequent electron-releasing NH_2OH oxidation.

$$CH_4 + O_2 + 2H^+ + 2e^- \xrightarrow{AMO} CH_3OH + H_2O \quad (3)$$

The interaction between CH_4 and AOB has been studied using *Nitrosococcus oceanus*,

Nitrosospira multiformis, and *Nitrosomonas europaea*[16, 17, 24-26, 131]. However, while previous studies were focus on the kinetics of methane oxidation or optimal conditions for methanol production, a more comprehensive view of the interaction between CH_4 and AOB had not been addressed. For instance, the oxidation of methane consumes electrons (eq 3), which could deplete available reducing equivalents for AOB energy synthesis. While methane competitive inhibits ammonia oxidation and not contributes to electron replenishment, we hypothesized that nitrogen metabolism in *N. europaea* and the electron flows resulted from ammonia oxidation would be affected. In this study, the impacts of methane exposure and co-oxidation with NH_3 on *N. europaea* were evaluated using a systems biology approach at the gene expression, comparative proteomics, and physiological levels.

4.2 Materials and methods

4.2.1 Cultivation of *N. europaea* in chemostat reactors

N. europaea was cultivated in Bio Flo115 fermenter systems (Eppendorf) using medium containing 280 mg NH_3-N L^{-1} and essential minerals (Table S4.1). The working volume was 2.2-liter and the dilution rate was 0.45 d^{-1} (influent flow rate = 0.99 L d^{-1}). The water-jacketed reactor was maintained at 26 °C and pH was automatically controlled at 7.50 ± 0.05 using 50 g L^{-1} $NaHCO_3$ solution. Oxygen was supplied using lab air (1 L min^{-1}) and filtered through 0.2 μm cellulose filter (Millipore, Billerica, MA). Reactors performance were continuously monitored and maintained at steady state before proceed to ammonia and methane co-feeding

experiment. Steady state was defined as follow: the average effluent ammonia concentration of three consecutive days was not statistically different (t-test with α = 0.05) from the average ammonia concentration of three previous time points.

4.2.2 Ammonia and methane co-feeding experiment

The ammonia and methane co-feeding experiment was consisted of three phases: pre-CH_4 exposure phase, methane exposure phase during which ammonia and methane was supplied simultaneously, and post-CH_4 exposure phase. During pre-CH_4 exposure phase, 0.9 L min^{-1} lab air and 0.1 L min^{-1} nitrogen (Tech Air, White Plains, NY) supplied and the total gas flow rate was maintained at 1 L min^{-1}. When steady state was achieved, nitrogen was switched to 0.1 L min^{-1} methane (Tech Air, White Plains, NY) to evaluate the impact of methane on *N. europaea*. Due to continuous biomass washout, methane supply was replaced by 0.1 L min^{-1} nitrogen after 3 days of exposure to avoid further biomass washout. The reactors were operated under the same conditions as pre-CH_4 exposure phase until reactors returned to steady state.

4.2.3 Analytical methods

Reactor performance was monitored by measuring the concentrations of total ammonia (ammonia + amonium, S_{NH3}) (Method 10031, Hach, Loveland, CO), hydroxylamine (S_{NH2OH})[68], and nitrite (S_{NO2}) (Dionex ICS2100 with AS18 column, Fisher Scientific, CA) concentrations. Cell concentrations were monitored by direct cell count (brightline hemocytometer, Hausser Scientific, Horsham PA) under phase

contrast microscope (Canon). Methanol concentrations (S_{CH3OH}) were measured using MXT-1 column (Restek, Bellefonte, PA) and a GC8610C gas chromatography equipped with flame ignition detector (SRI Instrument, Torrance, CA) to assess the co-oxidation of methane.

4.2.4 Protein extraction and label-free protein identification

At the end of each phase, approximately 10^{10} cells were collected on ice for protein extraction. Cell was centrifuge in 50 mL conical tubes for 30 minutes at 5000 rcf under 4 °C (Beckman Coulter, Brea, CA). Pellet was washed with ice-cold PBS buffer (Thermo Fisher, MA) for three times. Lysis buffer was prepared with 7.9 mL LC/MS grade water (Thermo Fisher, MA), 1 mL 10X TBS (0.5M Tris at pH 7.5 and 1.5M NaCl), 1 mL 3% SDS solution, and 100 μL protease inhibitor cocktail (Sigma-Aldrich, MO). Washed pellet was resuspended in 250 μL lysis buffer and sonicated using Branson Sonifier 450 (Branson Ultrasonics Corporation, CO) for three cycles with following condition: total time 1:30, duty cycle 50%, amplitude 20%. Lysed sample was centrifuged for 30 minutes at 16100 rcf under 4 °C to remove cell debris. Supernatant was collected and protein concentrations were determined using Qubit protein assay kit (Thermo Fisher, MA). Approximately100 μg of protein from each sample was used for SDS-PAGE (4-12% Tris-Glycine Mini Protein Gel, Life Technology, CA) with Xcell SureLock Mini-Cell sytem (Life Technology, CA). Samples at each lane were sliced into 12 fragments and digested with trypsin (Sigma-Aldrich, MO) and 75 fmol of yeast alcohol dehydrogenase was added as an

internal standard. Analyses were performed using NanoAcquity UPLC (Waters Corp) coupled with Synapt G2 QTOF HDMS mass spectrometer equipped with an ion mobility separation (IMS) cell (Waters Corp., Milford, MA), which alternated low- and high-energy scans (MSE data-independent acquisition) with a scan time of 0.6 s. (Waters Corp., Milford, MA). Spectrum output files were analyzed with Protein Lynx Global Server (Version 2.5, RC9, Waters Corp., Milford, MA). *N. europaea* protein database was downloaded from UniProtKB (as of 2.19.2016). The database included 2376 protein sequences and protein sequences of yeast alcohol dehydrogenase, porcine trypsin, and human keratins were manually added into the database. Raw data was searched against the manually curated database with a false discovery rate of 1%. Positive protein identification was defined as proteins exist in one of the two technical replicates and in both biological replicates with 95% confidence based on Student's t-test. Student's t-test was also used to compare relative protein abundance at different phases.

4.2.5 RNA extraction and functional gene analysis

To evaluate the expression of target genes at different phases, cell were harvested from 20−100 mL biomass and treated with RNAprotect reagent (Qiagen, Valencia, CA) before stored in -80 °C freezer until being extracted using QIAcube (Qiagen, Valencia, CA) according to the manufacturer's instructions. Approximately 1 μg of total RNA was reversed transcribed to cDNA using QuantiTect Reverse Transcription kit (Qiagen, Valencia, CA). Primers (listed in Table S2.2) targeting on ammonia

monooxygenase (*amoA*), hydroxylamine oxidoreductase (*hao1*), nitrite reductase (*nirK*), nitric oxide reductase (*norB*), cytochrome c oxidase subunit I (*coxA*), ribulose-1, 5-bisphosphate carboxylase large and small subunit (*cbbL*, *cbbS*) were used in qPCR with SYBR Green chemistry and the expression levels were normalized with respective 16S rRNA gene expression. Fold changes in relative gene expression were calculated using the average normalized gene expression values during pre-CH_4 exposure phase as denominator and the normalized gene expression values at each time points as numerator.

4.3 Results

4.3.1 Ammonia oxidation and cell growth were negatively but reversibly affected by methane exposure

During the pre-CH_4 exposure period when ammonia-nitrogen was the sole substrate for AMO, the steady-state S_{NH3} and S_{NO2} were 5.48 ± 1.92 mg NH_3-N L^{-1} (n = 9) and 263 ± 4 mg NO_2-N L^{-1} (n = 8) (Fig 4.1A). Upon exposure to methane, increase in S_{NH3} were observed in 12 hours and continued to increase. After methane was replaced by nitrogen, further accumulation of S_{NH3}, up to ~211 mg NH_3-N L^{-1}, were observed. After 9 days of operation under the same condition as pre-CH_4 exposure period, ammonia oxidation and cell growth were observed again. When reactor achieved steady state again, the S_{NH3} were 3.89 ± 0.73 mg NH_3-N L^{-1} (n = 8) (Fig 4.1A) and showed no significant differences (α = 0.05) compared with pre-CH_4 exposure phase.

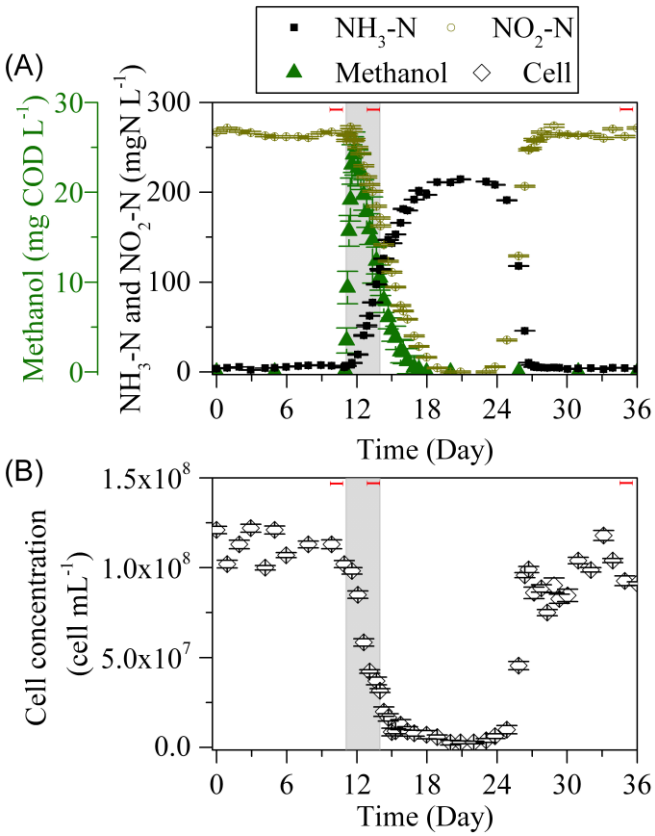

Figure 4.1. Concentrations of nitrogen compounds, methanol (A) and cell concentration (B) during ammonia co-feeding experiment (Fig S4.1 for biological replicate). Gray area indicate methane exposure phase. Red bars indicate the period during which effluent cells were collected for proteomic analysis. Error bars represent the standard deviation of duplicate (nitrogen compounds), triplicate (methanol) measurements. Error bars for cell concentrations represent the standard deviation of cell counts from ten grids on the hemocytometer.

Methanol was detected an hour after methane was supplemented and S_{CH3OH} reached 19.2 ± 2.4 mg COD L^{-1} in 9 hours of ammonia and methane co-feeding (Fig 4.1A). The maximum S_{CH3OH} at ~24 mg COD L^{-1} were observed 18 hours after methane supply and S_{CH3OH} started to decrease within 24-hour of exposure.

The cell concentrations were $1.1 \times 10^8 \pm 9.1 \times 10^6$ cell mL^{-1} (n = 6) during pre-CH_4 exposure phase and dropped significantly to $3.2 \times 10^7 \pm 1.0 \times 10^6$ cell mL^{-1} after 3 days of exposure (Fig 4.1B), which were approximately 30% of cell compared with pre-CH_4 exposure phase. As the reactor returned to steady state, cell densities were

$9.7 \times 10^7 \pm 1.3 \times 10^7$ cell mL^{-1} which showed no significant differences ($\alpha = 0.05$) when compared with pre-exposure phase.

4.3.2 Comparative proteomic analysis in the presence and absence of additional methane supply.

Proteins considered existence for each phase were identified if (i) presence in at least one injection of each sample and (ii) presence in duplicate experiments. We further validated the results by reviewing the protein concentrations in each biological replicates. A total of 523 different proteins (approximately 22% of the *N. europaea* proteome) were identified with 313 proteins common in all phases (Fig S4.3). Among these common proteins, 17 of the proteins remained in the top 20 most abundant proteins in all three phases. To evaluate the effects of methane exposure on *N. europaea*, we further focused on proteins related to nitrogen metabolism, electron flow and carbon fixation (summarized in Fig 4.2).

The relative abundance of proteins related to ammonia and hydroxylamine oxidation (AmoCAB and HAO) remained stable throughout the experiments. However, two proteins in the nitrite reductase cluster[33], NirK (NE0924) and Pan1 (NE0927), were both exclusively detected during methane exposure. Another terminal electron acceptor, cytochrome c oxidase subunit I encoded by *coxA* (NE1016), was also detected exclusively during methane exposure while other cytochrome c oxidase subunits (NE1017 and NE1013) were detected in all phases and showed significant changes (Fig 4.3A).

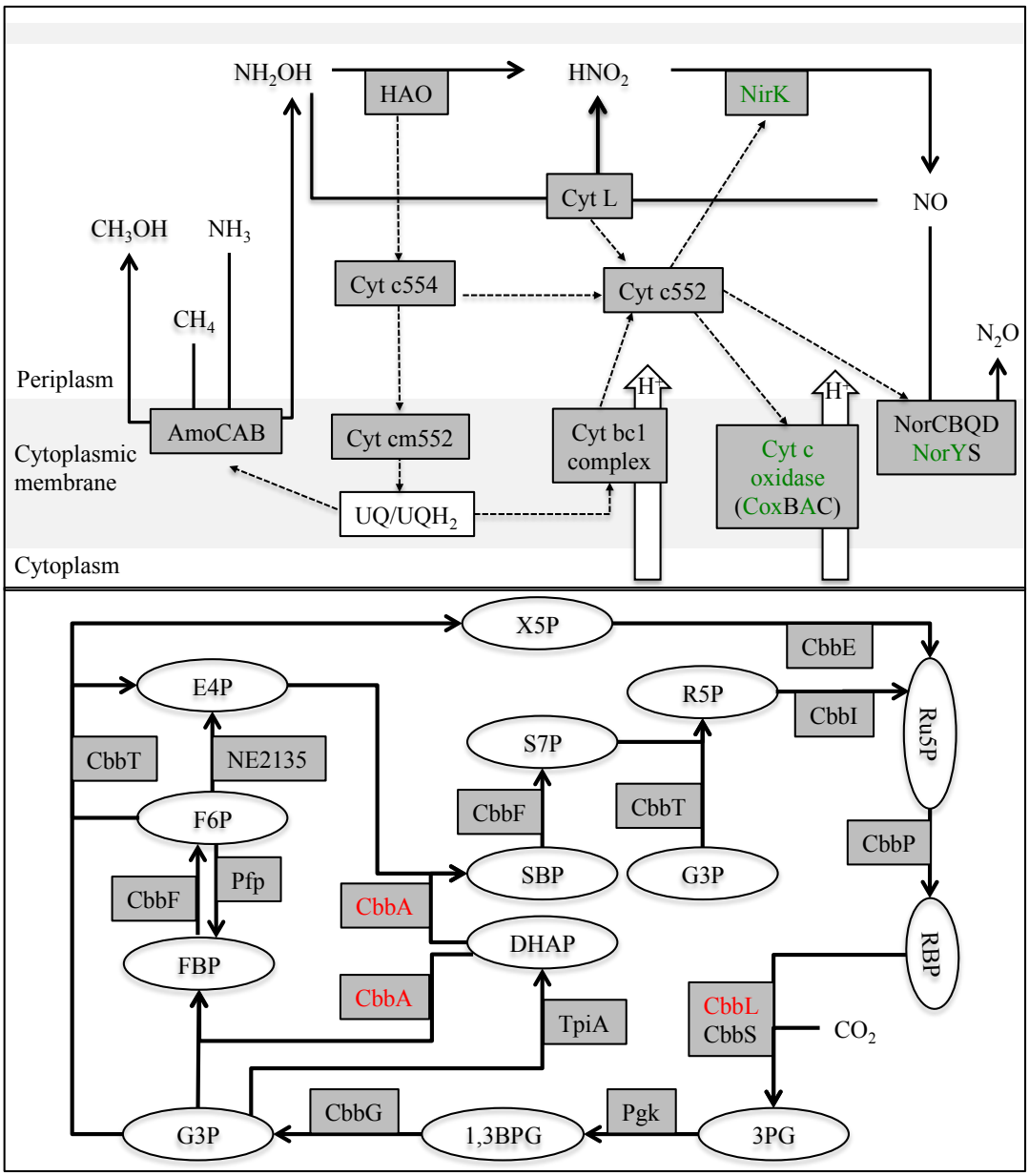

Figure 4.2. Nitrogen metabolism (A) and carbon fixation (B) pathways in *N. europaea* (Adapted form Chandran et al (2011)[37] and Berg [132]). Transformation of nitrogen and carbon containing compounds and associated enzymes (square) are illustrated. Methane is oxidized to methanol by AMO and no further metabolism is discussed Solid lines indicate redox reactions and dashed lines indicate electron flows. Proteins detected by proteomic analysis are labeled in gray. Green and red texts indicate the significant increase or decrease, respectively, in relative abundance (α = 0.05) during methane exposure compare to pre-exposure phase.

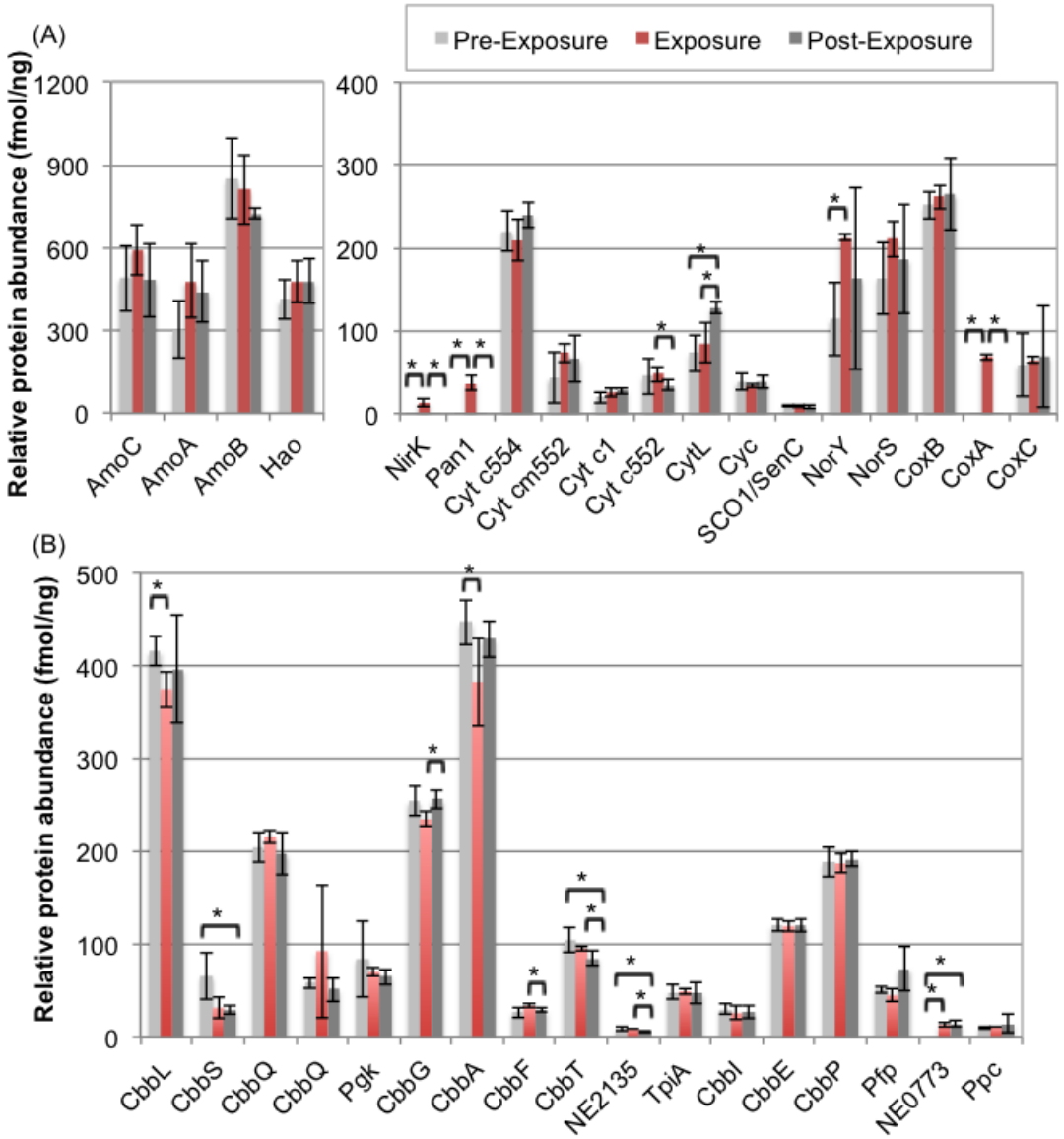

Figure 4.3. Relative abundance of proteins related to (A) nitrogen metabolism and electron transfer and (B) carbon fixation (based on KEGG pathway neu00710) in *N. europaea*. Error bars represent standard deviations based on the technical and biological replicates. Asterisks indicate statistically significant differences ($\alpha = 0.05$). Cbbs (29.2 ± 4.5 fmol/ng) during post-exposure was detected in R1 but not detected in R2. NE2135 (6.1 ± 1.1 fmol/ng) during post-exposure was detected in R2 but not detected in R1.

Cytochrome P460, one of the two enzymes able to catalyze hydroxylamine to nitrite oxidation, showed higher concentration in post exposure sample than pre exposure.

Due to the intrinsically linked nitrogen and carbon metabolism in *N. europaea*, proteins involved in carbon fixation were also investigated. Our data showed that within the all the proteins involved in carbon fixation (based on KEGG pathway neu00710) were detected during methane exposure and CbbL and CbbA showed significant lower relative abundance (compared with pre-CH_4 exposure phase, α = 0.05) during methane exposure (Fig 4.3B).

4.3.3 Methane exposure induced stress response proteins expression

It was noted that of the 37 proteins present exclusively during methane exposure (listed in Table S4.3), 5 of them were related to stress response. Therefore, we further focused on the changes in the relative abundance of stress response proteins related mechanisms (Table S4.4). Our results showed that two proteins defined as ATP-dependent Lon protease were detected. While Lon (NE0033) was found throughout the experiment, LonA (NE1278) was only detected during methane exposure. The ATP-depenent protease subunit HslV (NE2260) and the ATPase subunit HslU (NE2261) were both detected exclusively during methane exposure. Results also showed the increase in relative abundance of heat shock proteins (HSPs) (GrpE, HtpG, DnaK, NE2074, ClpB), function as molecular chaperones, and the predicted functional partners (NE1155, ClpA) during methane exposure. GroEL (NE0028), a general HSPs family protein, also increased during methane supply.

4.3.4 Transcriptional analysis of genes involved in nitrogen metabolism and carbon fixation

To understand how methane supply affects *N. europaea* at transcription level, biomass samples were collected for RNA extraction and used for RT-qPCR analysis. Expression of *amoA*, *hao1* (genes encoded the first two enzymes involved in AOB electron-yielding process), *coxA* (subunit A of cytochrome c oxidase, the terminal electron acceptor), *nirK* and *norB* (alternative electron sinks involved in nitrogen metabolism) (illustrated in Fig 4.2) were evaluated. The expression of *amoA* responded more rapidly to methane exposure than *hao1* expression (Fig 4.4A). The decrease in the expression of *amoA* and *hao1*, to 37% and 67% of pre-exposure level, respectively, were detected within 6 hours of methane exposure. The expression level of *amoA* dropped below 15% of pre-exposure level within 1 day of methane exposure while the expression of *hao1* gradually decreased to ~19% of pre-exposure level in 3 days (Fig 4.4A). The recoveries in *amoA* and *hao1* expression before the recovery of cell concentrations were observed when methane supply was terminated. In approximately 9 days, the expression of *amoA* and *hao1* returned to pre-exposure level as cell concentrations approached pre-exposure level. On the other hand, the increase in *nirK* expression, up to ~100-fold of pre-exposure level, was detected within 24 hours of methane exposure and gradually decreased to ~30-fold of pre-exposure level (Fig 4.4A).

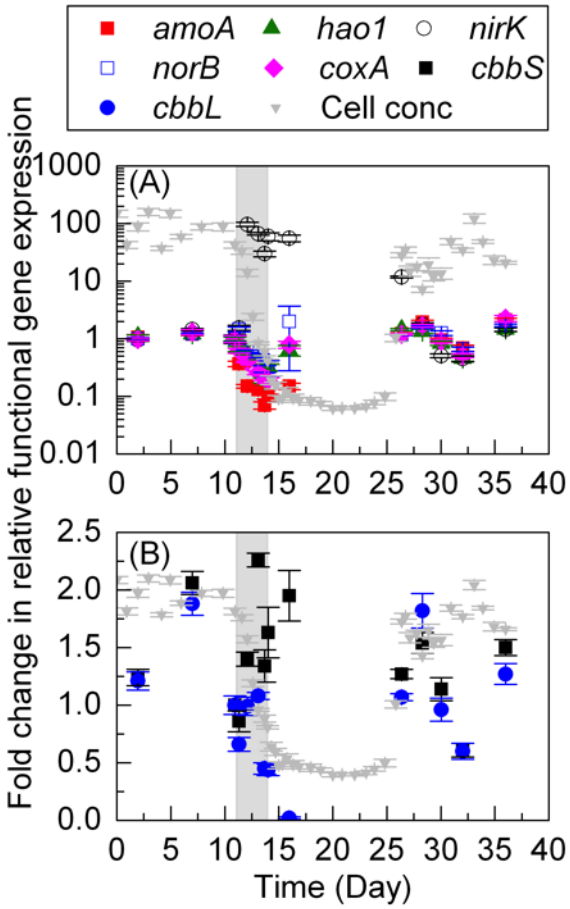

Figure 4.4. Expression profiles of genes related to nitrogen metabolism and terminal electron acceptors (A) and carbon fixation (B) (see Fig S4.3 for biological replicate). Cell concentrations are depicted as a reference of reactor operation and the scale for cell concentrations is not shown. Gray area indicate methane exposure phase. Error bars represent standard deviation from triplicate qPCR analysis.

However, the transient increase in *nirK* expression, up to 60-fold of pre-exposure level, was observed during early post-exposure phase (Fig 4.4A). As cell concentrations approached the pre-exposure level, *nirK* expression decreased rapidly and returned to pre-exposure level. Two genes encode enzymes related to proton motive force production (cytochrome c oxidase subunit A, *coxA*) and *nirK* functional partner (nitric oxide reductase subunit B, *norB*) were also analyzed (Fig 4.4A). The expression of *norB* increased to ~1.47-fold of pre-exposure level after 6 hours of

methane exposure and decreased to 30% of pre-exposure level. The decrease in *coxA* expression was detected at the beginning of methane exposure and the lowest expression level achieved was ~20% of pre-exposure level. The rapid recovery of *norB* and *coxA* genes expression were detected 2 days after methane supply was terminated and the expression of both genes returned to pre-exposure level when the reactor returned to steady state.

The analysis of genes involved in carbon fixation showed that the expression of *cbbL* was stable during methane exposure for 2 days but the expression levels dropped to ~ 45% of pre-exposure level as methane exposure continued (Fig 4.4B). On the other hand, the expression of *cbbS* showed a transient decrease during early methane exposure phase and the expression was maintained above pre-exposure level up to 2-fold during methane exposure. The differences in the recovery of *cbbL* and *cbbS* genes expression were also detected during post exposure phase. A further decrease in *cbbL* expression from 45% to 2% of pre-exposure level were detected during early post-exposure phase but the expression of *cbbS* was maintained at ~2-fold of pre-exposure level. When cell concentrations returned to steady state, both *cbbS* and *cbbL* expression returned to pre-exposure level.

4.4 Discussion

4.4.1 Ammonia and methane co-oxidation in chemostat reactors

Methane co-oxidation in ammonia oxidizing bacteria had been demonstrated for decades[16]. While previous studies focused on the activity and kinetics of AMO in

batch systems, we demonstrated here the responses of active growing cells to ammonia and methane co-feeding in chemostat reactors. The increase in S_{NH3} and S_{CH3OH} (the product of methane oxidation) indicated the competition between ammonia and methane for AMO. While the electron flows which refill UQ/UQH_2 electron pool in AOB are initiated by ammonia oxidation, no known enzymes in AOB is capable of extract electrons from methane during the oxidation process. The UQ/UQH_2 serves as the electron pool that provides electrons for AMO, NADH synthesis, or electron transport chain[20, 75]. Therefore, the oxidation of methane as an electron-consuming process would also impact the downstream processes including carbon assimilation and energy synthesis.

For wastewater treatment, the cometabolic methane oxidation is of potential application since that methanol, the cometabolic product, is used extensively for denitrification in biological nitrogen removal process[133]. The potential for methanol production using *N. europaea*, the most extensively studied AOB, had been proposed decades ago[16] with few reexaminations[17, 24, 100]. A recent study utilizing nitrifying activated sludge which was abundant in AOB further demonstrated the potential for field application[19]. The rapid increase in S_{CH3OH}, which was attractive for practical application, was also observed in previous batch studies [19]. However, the decrease in S_{CH3OH} after 24 hours of methane exposure, which could be resulted from the competition of elevated S_{NH3} or being deficient in cells for methane oxidation as cell concentrations decreased showed that the process can not be sustained under current experimental design.

4.4.2 Expression of genes encoded energy-harvesting proteins and carbon fixation proteins

AMO and HAO are the two most important enzymes for AOB catabolism. Previous studies on the effects of ammonium, presumably as induction signal[42, 134], on AOB gene expressions showed that *amoA* and *hao* mRNA syntheses were preferentially synthesized under energy-limited conditions[42]. Besides, the fast degrading *amoA* and *hao1* mRNA transcripts in *N. europaea* during starvation have been demonstrated[42]. On the other hand, the proteome structure was relatively stable and potential activity of AMO and HAO was not affected even after a prolonged starvation period[135]. However, in this study we showed that although S_{NH3} were high in the reactor (ammonium was not limiting) during methane exposure, the decrease in *amoA* and *hao1* expression were significant, suggesting that the presence of ammonium was not the only transcriptional regulator for the expression of *amoA* and *hao1*. Additionally, the lower *amoA* expression level could be related to the slower growth[136], which led to decrease in cell concentrations (Fig 4.1B).

The nitrogen and carbon metabolism in AOB are inherently linked together since that energy derived from ammonia oxidation will be used to support cell maintenance and growth. The disrupted ammonia metabolism would inevitably affect cell growth, which was observed during methane addition. While previous study suggested that *N europaea cbbLS* transcripts were depleted faster than *amoA* and *hao1* mRNAs[137] during nutrient limitation, our results showed that *cbbLS* expression were less

sensitive to the changes in physiological states.

4.4.3 Induction of *nirK* expression indicated the role in facilitating electron transfer

The increasing concentrations of nitrite reductase transcripts (Fig 4.5) and proteins (Fig 4.3) suggesting that nitrite reductase played important role when *N. europaea* metabolism was disrupted by methane. The upregulation of *nirK* was also reported at both transcriptional and translational level when *N. europaea* was exposed to chloromethane, a noncompetitive inhibitor of ammonia oxidation that drained reductants away from subsequent metabolic processes[138]. It was generally considered that *nirK* expression in *N. europaea* was related to protect cell against NO_2^- [139] and growth, especially during anaerobic condition with NO_2 as terminal electron acceptor[140, 141]. Previous study also showed indirectly that *nirK* was involved in the electron transport circuit through promoting NH_2OH oxidation by HAO and avoid nitrosative stress buildup[141]. Considered that the S_{NO2} during methane exposure was decreasing (less toxicity) and the oxygen concentration was always non-limiting throughout the experiments, our data indicated a role for NirK to facilitate electron transfer. NirK perhaps modulated the redistribution of electrons partitioning to manage the electron imbalance condition induced by methane cometabolism. The higher *nirK* expression might indicate the attempt to acquire more electrons from cytochrome c552, creating a pulling force from UQ/UQH_2 electron pool (Fig 4.2) or even bypass cytochrome cm552 and UQ/UQH_2 for more efficient electron transport[38].

On the other hand the expression of *norB*, as the predictive functional partner of *nirK*, showed no significant different while the expression of *nirK* was highly upregulated (Fig 4.5A). This result were in agreement with the accumulating evidence that *nirK* and *norB* expression are not necessarily linked[140, 142] and the expression of *norB* to *N. europaea* appeared to be inessential to aerobic respiration[143].

The increase of a subfamily of cytochrome c oxidases encoded by *norY* (NE0683) could be related to nitrite reductase expression. While NorB was physiologically and genetically characterized in AOB (reviewed by Stein, 2011[38]), NorSY, previously annotated as CoxBA2 in *N. europaea*, was less studied and was hypothesized to contribute to N_2O production during growth of *N. europaea* under oxic condition[144, 145]. The increase in relative abundance of NorY and NirK during methane exposure might indicate the functional relationship in mediating electron flow as proposed by Stein et al (2013)[134].

4.4.4 Methane exposure induced the expression of stress response proteins

Stable proteomic structure appeared to be a feature of *N. europaea* when coping with fluctuating environmental conditions[146]. Nonetheless, the increasing relative abundance of stress response proteins during methane exposure were evident (Table S4.4). A previous study on cometabolic chloroform degradation by *N. europaea* showed a very similar pattern of upregulated stress response proteins[138] at transcription level, however the treatment led to irreversible loss of AMO activity[147]. GroEL (NE0028), a general HSPs family protein proposed as an indicator of stress in

activated sludge system[148], also increased when supplying methane. The lower concentrations of the stress response proteins at the end of experiments again suggested that the expression of these stress proteins were induced by methane supply.

4.5 Conclusions

Cometabolic methane oxidation in ammonia oxidizing bacteria is of interest not only for the evolutionary linked ammonia/methane catabolism module[149] but also for its potential application[19]. In this study, we used a systems biology approach to assess the bacterial responses at mRNA and protein level and correlated with the responses at reactor level. Our results suggested that methane did not act solely as a competitive inhibitor for ammonia oxidation but had more profound impacts on electron distribution and carbon metabolism in *N. europaea*. The upregulation of NirK at transcriptional and translational levels indicates its function as a regulator for electrons when *N. europaea* electron flow was disrupted during methane exposure. The decrease in cell concentrations corresponded with lower carbon fixation protein abundance, which also suggested that electrons were diverted away from anabolism.

4.6 Supporting information

The supporting information includes (1) Profiles of nitrogen compounds, methanol and cell concentration during ammonia co-feeding experiment in the replicate chemostat (2) Venn diagram of proteins identified before, during, and post methane

exposure (3) Expression profiles of genes related to nitrogen metabolism, terminal electron acceptors and carbon fixation in the replicate chemostat (4) List of proteins identified exclusively during methane exposure phase (5) Changes in relative abundance of proteins related to stress response (6) Composition of medium containing 280 mg NH_3-N L^{-1} and essential elements for *N. europaea* cultivation (7) Primer sets used in this study.

Table S4.1. Composition of medium containing 280 mg NH_3-N L^{-1} and essential elements for *N. europaea* cultivation.

Chemicals	Concentration	
Ammonium sulfate	1.32	g/L
Magnesium Sulfate Heptahydrate	0.2	g/L
Calcium chloride dihydrate	20	mg/L
Potassium phosphate dibasic	87	mg/L
EPPS	2.52	g/L
Sodium bicarbonate	2	g/L
EDTA ferric sodium salt	1	mg/L
Copper (II) sulfate pentahydrate	0.25	mg/L
Sodium molybdate dihydrate	0.1	mg/L
Manganese(II) Chloride Tetrahydrate	0.172	mg/L
Zinc sulfate heptahydrate	0.2	mg/L
Cobalt(II) chloride hexahydrate	0.004	mg/L

Table S4.2 Prime sets used in *N. europaea* experiments.

Target gene	Primer set	Sequence (5'-3')	PCR product size (bp)	Annealing temp (°C)	Reference
amoA	amoAFq	GGA CTT CAC GCT GTA TCT G	136	61	[150]
	amoARq	GTG CCT TCT ACA ACG ATT GG			
hao1	hao1Fq	TGA GCC AGT CCA ACG TGC AT	85	57	[114]
	hao1Rq	AAG GCA ACA ACC CTG CCT CA			
nirK	nirK157F	GTG GCT CTG ATC CGA TGA TT	152	58	[142]
	nirK534R	GGC TGT TTT GTC GTC AGG AT			
norB	norB530f	ATC TTG CCC TCG ACA AAA TG	125	58	[142]
	norB654r	TCA CGA TCC ACA CCA GTC AT			
coxA	coxA784f	GCA TTT GGT GTC GTT TCA GA	105	58	This study
	coxA888r	ACA TGA CAG CAA AGC AAT CG			
cbbS	cbbS_f	CAC ACT GAA CCG GAG TTT CT	94	57	This study
	cbbS_r	CTT CGG CAA GGA TAC GAT CTA C			
cbbL	cbbL1223f	TGG TGG CGG TAC TTT AGG TC	140	57	[142]
	cbbL1371r	TGT GTT TTG CAG CCT CTG TC			
EUB16S	1055F	ATG GCT GTC GTC AGC T	353	55.5	[98]
	1392R	ACG GGC GGT GTG TAC			

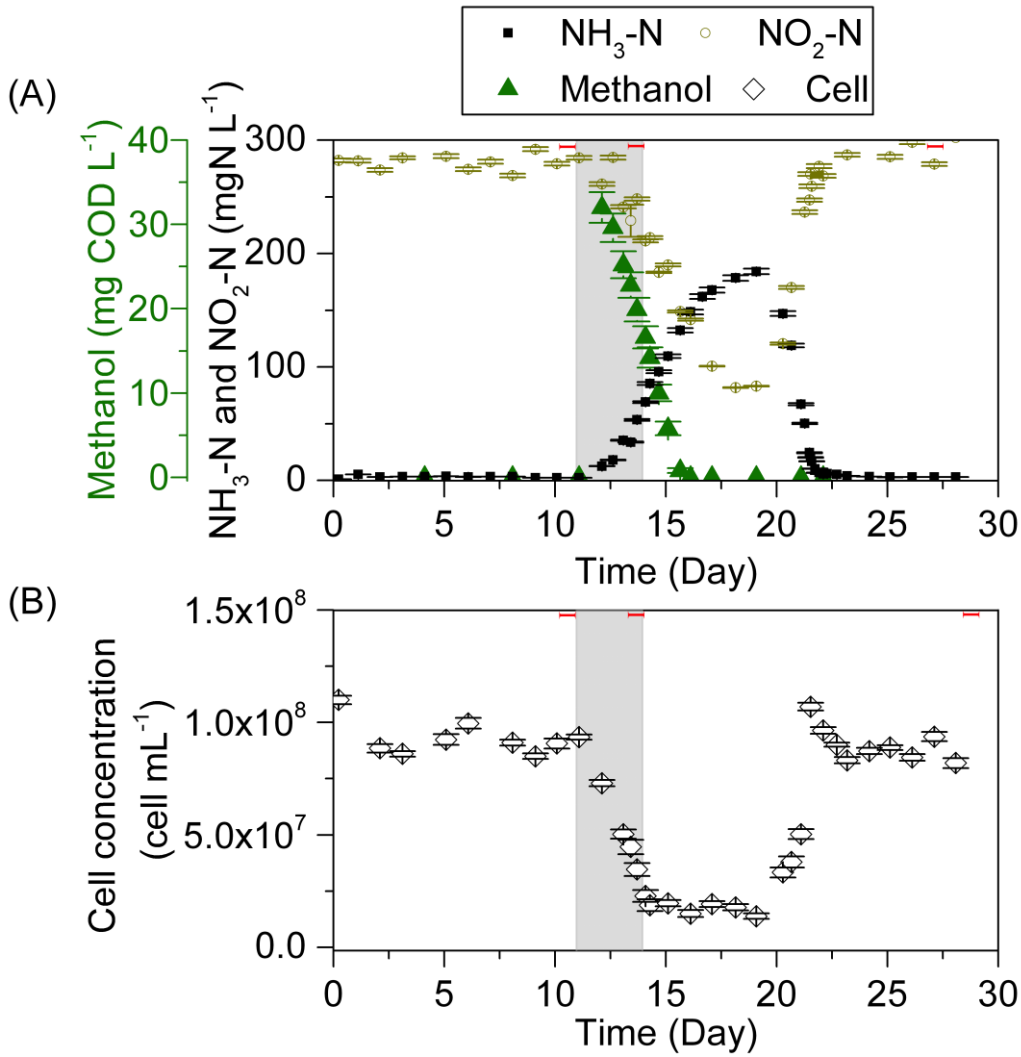

Figure S4.1. (Biological replicate) Concentrations of nitrogen compounds, methanol (A) and cell concentration (B) during ammonia co-feeding experiment. Gray area indicate methane exposure phase. Red bars indicate the period during which effluent cells were collected for proteomic analysis. Error bars represent the standard deviation of duplicate (nitrogen compounds) or triplicate (methanol) measurements. Error bars for cell concentrations represent the standard deviation of cell counts from ten grids on the hemocytometer.

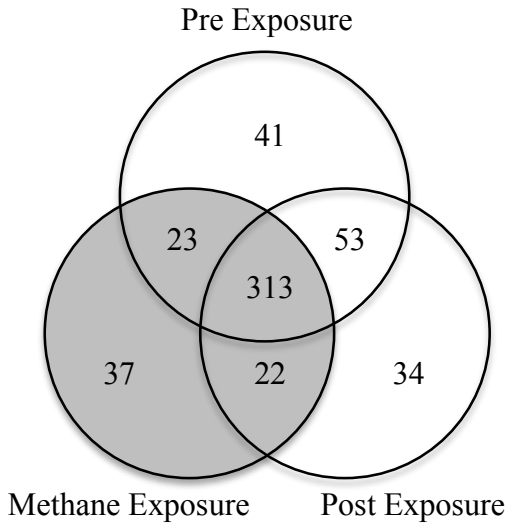

Figure S4.2. Venn diagram of proteins identified before, during, and post methane exposure. A total of 523 proteins (22 % of *N. europaea* proteome) were identified.

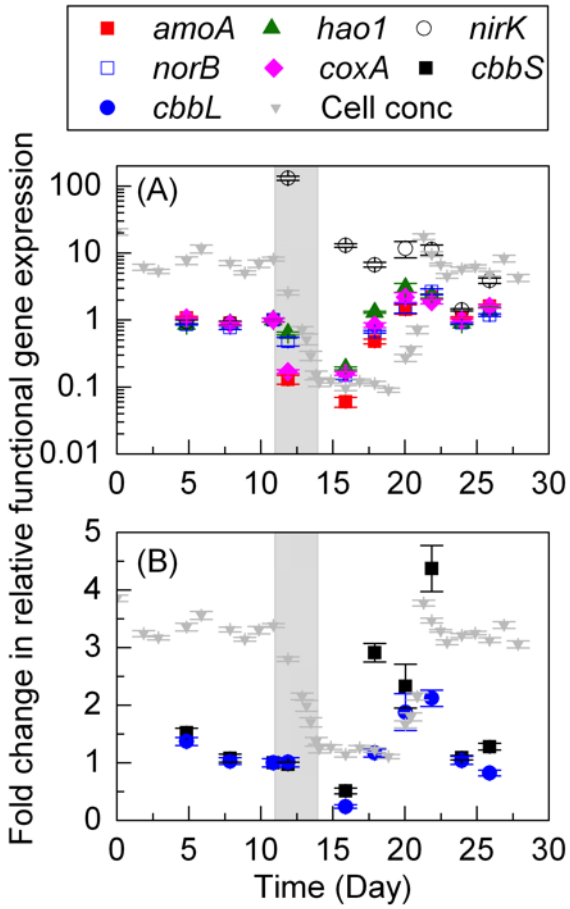

Figure S4.3. (Biological replicate) Expression profiles of genes related to nitrogen metabolism and terminal electron acceptors (A) and carbon fixation (B). Cell concentrations are depicted as a reference of reactor operation and the scale for cell concentrations is not shown. Gray area indicate methane exposure phase. Error bars represent standard deviation from triplicate qPCR analysis.

Table S4.3. Proteins identified exclusively during methane exposure phase. The numbers indicate the average of relative protein abundance (Avg) and standard deviation (SD) calculated from two technical replicates and two biological replicates.

KEGG No.	Uniprot No.	Protein Name	Relative abundance (fmol/ng)	SD
NE2074	Q82T55	Heat shock hsp20 proteins family	73.4	4.1
NE1016	Q82VQ0	Cytochrome c oxidase, subunit I	67.8	2.9
NE2571	Q82RZ4	Metallo-beta-lactamase superfamily	50.9	4.7
NE0909	Q82VZ0	Orn/DAP/Arg decarboxylases family	48.0	9.9
NE1142	Q82VE9	Uncharacterized protein	44.4	15.1
NE1472	Q82UL2	Possible transmembrane protein	42.5	15.4
NE1733	Q82TY2	ClpA, ATP dependent protease, chaperonin	40.4	8.7
NE0084	Q82Y06	Thioredoxin	38.5	9.0
NE0927	Q82VX3	Multicopper oxidase type 1	36.6	9.3
NE2212	Q82SU2	Putative transmembrane protein	35.2	4.9
NE1907	Q82TI0	Uncharacterized protein	31.2	15.5
NE1680	Q82U33	Uncharacterized protein	27.8	6.9
NE1278	Q82V32	Lon protease (ATP-dependent protease La)	27.2	9.8
NE2261	Q82SP6	ATP-dependent protease ATPase subunit HslU	20.3	4.9
NE0196	Q82XQ8	30S ribosomal protein S18	19.4	4.4
NE0424	Q82X71	30S ribosomal protein S11	18.4	4.4
NE1008	Q82VQ8	Uncharacterized protein	17.1	0.6
NE0411	Q82X79	50S ribosomal protein L14	15.4	7.4
NE1450	Q82UN2	Uncharacterized protein family UPF0051	15.0	3.0
NE2149	Q82SZ4	Phosphoglycolate phosphatase	13.7	3.5
NE0924	Q82VX5	Multicopper oxidase type 1	13.6	5.0
NE0060	Q82Y29	Phosphotransferase system mannitol/fructose-specific IIA domain	12.4	4.2
NE1661	Q820K6	Carbamoyl-phosphate synthase	11.6	1.2
NE2260	Q82SP7	ATP-dependent protease subunit HslV	11.5	0.0
NE0644	Q82WM5	Phosphoribosylformimino-5-aminoimidazole carboxamide ribotide isomerase	10.9	0.7

Table S4.4. Relative abundance of proteins related to stress response. The numbers indicate the average of relative protein abundance (Avg) and standard deviation (SD) calculated from two technical replicates and two biological replicates. Asterisks indicate the relative protein abundance are statistically significant differences ($\alpha = 0.05$) from pre-exposure phase.

KEGG No.	UniProt No.	Protein Name	Pre-exposure		Methane exposure		Post-exposure	
			Avg	SD	Avg	SD	Avg	SD
NE0028	Q82Y60	60 kDa chaperonin (GroEL protein) (Protein Cpn60)	320.4	14.7	339.9	2.4	257.3 *	18.4
NE0031	Q82Y57	ATP-dependent Clp protease proteolytic subunit	23.1	1.4	28.9	7.3	24.3	4.7
NE0032	Q82Y56	ATP-dependent Clp protease ATP-binding subunit ClpX	28.2	3.2	20.5 *	1.0	22.9	4.5
NE0033	Q82Y55	Lon protease (ATP-dependent protease La)	12.1	3.1	10.1	0.4	10.5	0.7
NE0379	Q82XA8	Serine proteases, trypsin family	8.6	0.8	*		9.3	1.1
NE0528	Q820A1	ATP-dependent zinc metalloprotease FtsH	54.9	7.8	37.5 *	7.5	42.4 *	2.6
NE0906	Q82VZ3	ATP-dependent zinc metalloprotease FtsH	41.8	12.6	49.6	17.5	33.6	7.8
NE1028	Q82VN8	Universal stress protein	12.4	4.4	*		*	
NE1155	Q82VD9	DnaJ N-terminal domain:DnaJ C terminal domain			12.5 *	2.4	12.8 *	2.3
NE1183	Q82VB3	Serine proteases, subtilase family			123.0 *	77.2	162.1 *	16.4
NE1278	Q82V32	Lon protease (ATP-dependent protease La)			27.2 *	9.8		
NE1421	Q82UR0	Protease HtpX homolog	23.9	8.5	49.3 *	16.5	13.7	6.4
NE1508	Q82UH7	Htra-like serine protease signal peptide protein	34.5	5.7	38.4	1.4	37.6	1.9
NE1733	Q82TY2	ClpA, ATP dependent protease, chaperonin			40.4 *	8.7		
NE1762	Q82TV8	Chaperone protein HtpG	25.9	2.3	44.4 *	4.0	25.9	5.8
NE1782	Q82TT8	Carboxy-terminal processing protease	96.1	41.2	93.4	41.7	86.5	30.2

Table S4.4 (continued). Relative abundance of proteins related to stress response. The numbers indicate the average of relative protein abundance (Avg) and standard deviation (SD) calculated from two technical replicates and two biological replicates. Asterisks indicate the relative protein abundance are statistically significant differences ($\alpha = 0.05$) from pre-exposure phase.

KEGG No.	UniProt No.	Protein Name	Pre-exposure		Methane exposure		Post-exposure	
			Avg	SD	Avg	SD	Avg	SD
NE1825	Q82TQ5	50S ribosomal protein L25 (General stress protein CTC)	73.2	14.2	85.3	2.8	63.6	2.7
NE1949	O06430	Chaperone protein DnaK (HSP70)	93.9	6.3	144.7 *	4.9	79.5 *	1.4
NE1950	O08384	Protein GrpE (HSP-70 cofactor)	20.3	6.2	52.9 *	2.5	20.1	13.9
NE2074	Q82T55	Heat shock hsp20 (Alpha crystallin) proteins family			73.4 *	4.1		
NE2206	Q82SU8	PpiC-type peptidyl-prolyl cis-trans isomerase	88.5	30.6	93.6	33.0	125.3	35.4
NE2260	Q82SP7	ATP-dependent protease subunit HslV			11.5 *	0.0		
NE2261	Q82SP6	ATP-dependent protease ATPase subunit HslU			20.3 *	4.9		
NE2329	Q82SJ3	MucD serine protease MucD	53.8	20.3	69.7	5.8	58.0	24.8
NE2402	Q82SD8	Chaperone protein ClpB	29.0	3.7	60.3 *	3.5	41.3	31.7

CHAPTER 5

Physiological and transcriptional analysis of genes related to nitrogen metabolism in response to methane exposure in *Nitrosomonas eutropha*

This chapter is the basis of the paper:

Yu-Chen Su[1], Luis Arellano-García[1], Kartik Chandran[1*]

Physiological and transcriptional analysis of genes related to nitrogen metabolism in response to methane exposure in *Nitrosomonas eutropha* (In preparation)

Affiliation:

[1] Department of Earth and Environmental Engineering, Columbia University

500 West 120th Street, Room 1045 Mudd Hall, New York, NY 10027

Abstract

The versatile cometabolic activity of ammonia monooxygenase (AMO) in ammonia oxidizing bacteria (AOB) has been documented for decades, however the physiological responses of AOB to cometabolism are less discussed. The goal of this work was to investigate the physiological responses of chemostat *Nitrosomonas eutropha* culture to the presence of methane, a cometabolic substrate for AMO. The introduction of methane led to accumulation of ammonia and washout of biomass. However, the elevated hydroxylamine concentrations from 0.014 ± 0.005 mg NH_2OH-N L^{-1} to 0.036 ± 0.008 mg NH_2OH-N L^{-1} and the increase in specific ammonia oxidation rates from $2.15 \times 10^{-9} \pm 2.45 \times 10^{-9}$ mg NH_3-N $cell^{-1}d^{-1}$ to $5.78 \times 10^{-9} \pm 4.00 \times 10^{-10}$ mg NH_3-N $cell^{-1}d^{-1}$ indicated the catabolic activity in *N. eutropha* were regulated in response to methane exposure. Rapid methanol production at a rate of 2.81 ± 0.16 mg-CH_3OH-COD mg-biomass-$COD^{-1}d^{-1}$ was achieved but *N. eutropha* was unable to sustain methanol production, possibly due to increasing ammonia concentrations. Functional gene analysis on genes involved in catabolism also showed 10-fold decrease in *amoA* and *hao1* transcription activities. The transient increase of *nirK* expression during early methane exposure phase and recovery phase suggested the important physiological roles of NirK, possibly to regulate the electron flux. The impacts of methane exposure were reversible at the reactor level. However, lower transcription levels were detected for genes tracked in this study, indicating a lag for recovery at the transcription level. In conclusion, our results demonstrated the *N. eutropha* was able to adjust the catabolic and anabolic activity in response to methane

exposure. The potential adaptation of *N. eutropha* to methane also provides insight for biofuel production using AOB.

5.1 Introduction

Nitrosomonas eutropha is a chemolithoautotropihc ammonia oxidizing bacteria (AOB) which acquires all it energy from the oxidation of ammonia and fixes CO_2 as its carbon source. Ammonia oxidation in AOB is a two-step process during which ammonia is first oxidized to hydroxylamine by ammonia monooxygenase (AMO) and subsequently to nitrite by hydroxylamine oxidoreductase (HAO). For each mole of hydroxylamine oxidation, four moles of electrons are released and transferred to a quinol pool, from which two moles of electrons are directed back to AMO for ammonia oxidation and residual electrons are used for biosynthesis or passed to terminal oxidases for energy synthesis (Fig 5.1) [20].

$$NH_3 + O_2 + 2e^- \xrightarrow{AMO} NH_2OH + H_2O$$
$$NH_2OH + H_2O \xrightarrow{HAO} NO_2^- + 5H^+ + 4e^-$$

The genome sequence revealed that *N. eutropha* contains similar genes inventory for catabolism with the well-studied model AOB, *Nitrosomonas europaea*. Both *N. eutropha* and *N. europaea* contain two copies of gene clusters that encode AMO and three copies of gene clusters that encode HAO [34]. The wide substrate range of AMO is well documented[103]. The cometabolic oxidation of other AMO substrate is an electron-consuming reaction and no evidence suggests the contribution of the resulting products to further electron replenishment. Previous studies have established the modes of interaction between cometabolic substrates and AMO[23] and the possible impacts of resulting products[147]. Analysis of the active binding site-containing subunit of AMO and particulate methane monooxygenase (pMMO) from methane oxidizing bacteria (MOB) revealed the evolutionary relationship between two enzymes [21], both

able to catalyze methane oxidation.

$$CH_4 + O_2 + 2e^- \xrightarrow{AMO} CH_3OH + H_2O$$

The cometabolic methane oxidation and the enzymatic kinetics have been studied in batch systems using axenic AOB culture including *N. europaea* [17, 23, 25], or *Nitrosococcus oceanus* [24, 26].

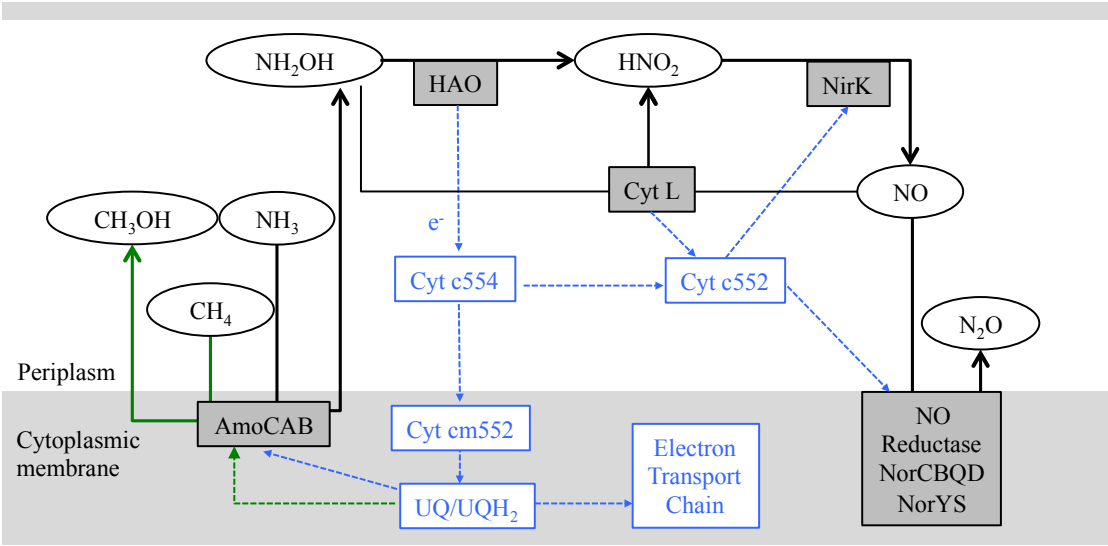

Figure 5.1. Nitrogen metabolism and electron flows in AOB. (Adapted from Chandran et al, 2011[37]). Open circles and gray blocks represent nitrogen species and enzymes, respectively, participated in the oxidation cascade. The blue block represents the electron pool and blue lines indicate electron flows. Methane to methanol oxidation is catalyzed by AMO and required electrons are from the UQ/UQH_2 electron pool.

AOB and MOB play important roles in global nitrogen and methane cycles [22, 151]. Though both AOB and MOB are capable of ammonia and methane oxidation, it was implicated that the contribution of AOB to methane cycle seems to be very minor [131, 152]. Nevertheless, recent studies have proposed to take advantage of the cometabolic methane oxidation activity as a sustainable and environment-friendly strategy for

methanol production [18, 19]. In this study, *N. eutropha* rather than *N. europaea* was used to expand the understanding on methane cometabolism in diverse AOB. Furthermore, *N. eutropha* was cultivated in the presence of ammonia and methane in chemostat reactors to gain a more comprehensive view of the impacts of methane cometabolism on *N. eutropha*. The physiological activities including ammonia and hydroxylamine oxidation, cell growth, and oxygen uptake were monitored. In addition, the expressions of functional genes related to redox nitrogen transformation in *N. eutropha* in response to methane exposure were also tracked.

5.2 Materials and methods

5.2.1 Maintenance of chemostat *Nitrosomonas eutropha* culture

N. eutropha cells were cultivated in Bio Flo115 fermenter systems (Eppendorf North America, Hauppauge, NY) using medium containing 280 mg NH_3-N L^{-1} as previously described [153] with minor adjustment (Table S5.1). Lab air was filtered through 0.2 μm millipore cellulose filter at a rate of 1 L min^{-1} for oxygen supply. The water-jacketed reactors were maintained at 30 °C and pH was automatically controlled at 7.50 ± 0.05 using 50 g L^{-1} $NaHCO_3$ solution. During reactors startup, *N. eutropha* cells from parent batch culture were inoculated into the fermenters with medium containing 280 mg NH_3-N L^{-1} and the working volume was 2.2-liter. Cells were grown in batch mode and continuous ammonia-N feed (dilution rate = 0.45 d^{-1}) were applied when the ammonia-N in the reactors were depleted. The reactors were maintained under current operational condition until proceed to co-feeding experiment.

5.2.2 Ammonia and methane co-feeding experiment

Three phases were included in the ammonia and methane co-feeding experiment: pre-exposure phase (to establish baseline for subsequent comparisons), methane exposure phase, and post-exposure phase (to evaluate the recoverability from methane exposure). During pre-exposure phase, 0.9 L min^{-1} lab air and 0.1 L min^{-1} nitrogen (Tech Air, White Plains, NY) were supplied until steady state operation was achieved [154]. After steady state was achieved, nitrogen was switched to 0.1 L min^{-1} methane (Tech Air, White Plains, NY) to evaluate the impacts of methane on *N. eutropha*. After 4 days of exposure, methane was replaced by 0.1 L min^{-1} nitrogen and reactors were operated under the same condition as pre-exposure phase. Total gas flow rates (1 L min^{-1}) and other operational parameters remained constant throughout the experiment.

5.2.3 Analytical methods

Reactor performance was monitored by measuring concentrations of total ammonia (ammonia + ammonium, S_{NH3}) (Hach Method 10031, Hach, Loveland, CO), hydroxylamine (intermediate of ammonia oxidation, S_{NH2OH})[68], and nitrite (S_{NO2}) (Dionex ICS2100 with AS18 column, Fisher Scientific, CA). Cell concentrations were monitored by direct cell count (brightline hemocytometer, Hausser Scientific, Horsham, PA) under phase contrast microscope (Canon). Methanol concentrations (S_{CH3OH}) were measured using MXT-1 column (Restek, Bellefonte, PA) and gas chromatography equipped with flame ignition detector (GC8610C, SRI Instrument,

Torrance, CA) to assess the co-oxidation of methane.

5.2.4 Determination of specific rates for ammonia oxidation, biomethanol production, and oxygen uptake

The specific rates of ammonia oxidation and biomethanol production were calculated based on the mass balance equation:

$$\frac{dS}{dt}V = rXV + Q(S_{in} - S)$$

where V = 2.2 L, S = S_{NH3} or S_{CH3OH}, X = cell concentration (cell mL^{-1}), Q = influent flow rate = 0.99 L d^{-1}, S_{in} = influent ammonia-N concentration (280 mg NH_3-N L^{-1}) or influent methanol concentration (0 mg COD L^{-1}).

The in situ specific oxygen uptake rates (sOUR) were calculated based on volumetric mass transfer coefficient (KLa) and dissolved oxygen profile [155]. The KLa was determined for each dissolved oxygen probe in the absence of biomass and the gas supply during the adsorption of oxygen was 0.9 L min^{-1} air plus 0.1 L min^{-1} nitrogen to simulate the gas composition of co-feeding experiment. The KLa was used in the mass balance equation for oxygen:

$$\frac{dS_{O2}}{dt} = OTR - OUR = KLa' (S^*_{O2} - S_{O2}) - X' sOUR$$

where dS_{O2}/dt = the rate of oxygen accumulation in the liquid phase, OTR = rate of oxygen transfer from gas to liquid, which is equal to the product of KLa and the oxygen gradient, OUR = oxygen uptake rate, which can be expressed by the product of cell concentration (X) and specific oxygen uptake rate (sOUR), S_{O2} = dissolved oxygen concentration, S_{O2}* = saturated dissolved oxygen concentration under the

experimental condition (6.8 mg O_2 L^{-1} at 30 °C).

5.2.5 Monitoring the expression of genes involved in nitrogen metabolism

To evaluate the expression of target genes during different operational conditions, cells were harvested from 20 - 100 mL biomass (~10^9 cells) and treated with RNAprotect reagent (Qiagen, Valencia, CA) before stored in -80 °C freezer until being extracted using QIAcube (Qiagen, Valencia, CA) according to the manufacter's instructions. Approximately 1 μg of total RNA was reverse transcribed to cDNA using QuantiTect Reverse Transcription kit (Qiagen, Valencia, CA). Primers (Table S5.2) targeting on genes involved in nitrogen metabolisms including ammonia monooxygenase subunit A (*amoA*), hydroxylamine oxidoreductase (*hao1*), nitrite reductase (*nirK*), nitric oxide reductase subunit C of cNOR (*norC*), nitric oxide reductase subunit Y of sNOR (*norY*) were used in qPCR with SYBR Green chemistry. The expression levels were normalized with respective16S rRNA gene expression for each sample. Gene expression fold changes were calculated using average expression level from pre-exposure phase (n = 2) as denominator and target gene expression levels as numerator.

5.3 Results

5.3.1 Ammonia oxidation and cell growth were negatively and reversibly affected by the presence of methane

Changes in concentrations of nitrogenous compounds, methanol, and cell

concentrations were plotted in Figure 5.2 (and Fig S5.1). During pre-exposure period, S_{NH3} and S_{NO2} were 5.23 ± 0.38 mg NH_3-N L^{-1} (n = 8) and 244 ± 16 mg NO_2-N L^{-1} (n = 8), respectively (Fig 5.2A). However, an initial decrease was observed for S_{NH2OH} and S_{NH2OH} eventually stabilized at 0.014 ± 0.005 mg NH_2OH-N L^{-1} (n = 5).

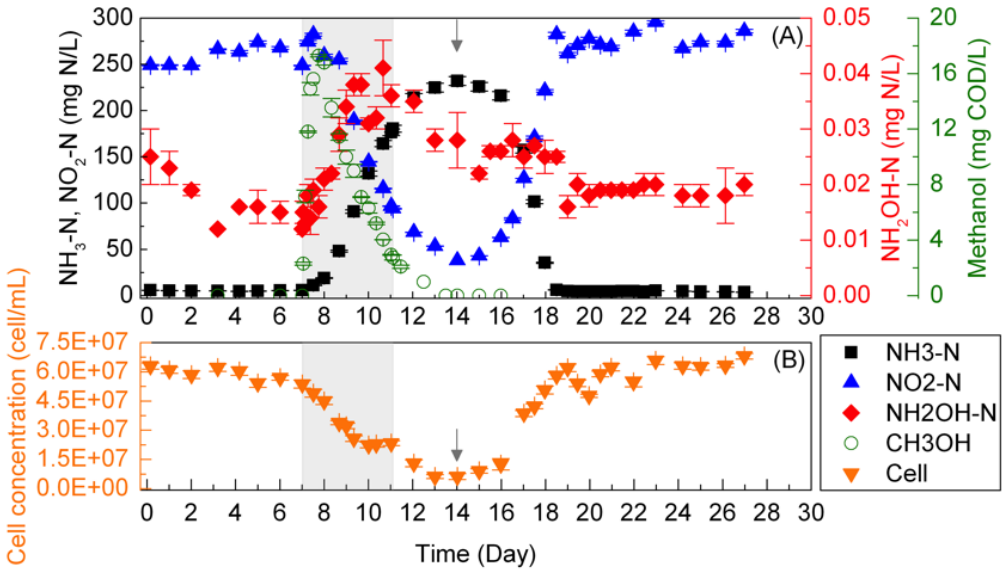

Figure 5.2. Nitrogen, methanol (A) and cell concentration (B) profiles. Gray area indicated the 4-day methane exposure phase.

The coefficient of sequential variation (ω, ≤0.2 indicates steady state) [154] was 0.00 based on S_{NH3} data (Fig 5.2A, Day 0 to Day 7). After methane was introduced to the reactors, S_{NH3} increased to 11.1 ± 0.2 mg NH_3-N L^{-1} within 12 hours of exposure and reached 180 ± 4 mg NH_3-N L^{-1} in 4 days while S_{NO2} decreased to 93.9 ± 0.3 mg NO_2-N L^{-1} at the end of exposure phase (Fig 5.2A, gray area). Similar to S_{NH3} profile, an increase in S_{NH2OH} were observed during early methane exposure phase, however, S_{NH2OH} were stabilizing at 0.036 ± 0.008 mg NH_2OH-N L^{-1} (n = 6) for about 1.5 days before methane supply was terminated (Fig 5.2A).

After methane was replaced by nitrogen, a transient increase in S_{NH3}, up to 232 ± 5 mg NH_3-N L^{-1} (Fig 5.2A, indicated by the arrow) and the corresponding decrease in S_{NO2} were observed. S_{NH3} decreased from peak S_{NH3} to 4.70 ± 0.10 mg NH_3-N L^{-1} within 5 days and S_{NH3} and S_{NO2} were stabilized at 4.45 ± 0.38 mg NH_3-N L^{-1} (n = 11) and 274 ± 11 mg NO_2-N L^{-1} (n = 11), respectively, until the end of experiment (Fig 5.2A). The coefficient of sequential variation was 0.14 based on S_{NH3} data (Fig 5.2A, Day 19 to Day 27). On the other hand, S_{NH2OH} started to decrease when methane supply was terminated and remained at 0.026 ± 0.008 mg NH_2OH-N L^{-1} (n = 9) as S_{NH3} were decreasing. A further decrease in S_{NH2OH} was observed concurrently when S_{NH3} returned to pre-exposure level and then S_{NH2OH} was stabilized at 0.019 ± 0.007 mg NH_2OH-N L^{-1} (n = 13) (Fig 5.2A).

With regard to cell growth, cell concentrations were stabilized at $5.87 \times 10^7 \pm 6.29 \times 10^6$ cell mL^{-1} (n = 8) prior to methane exposure (Fig 5.2B). Cell concentraitons were decreasing during early methane exposure phase and, similar to S_{NH2OH} profile, stabilizing at $2.36 \times 10^7 \pm 3.16 \times 10^6$ cell mL^{-1} (n = 4) for ~1.5 days before methane supply was stopped. Cell concentrations started to increase at the same time when S_{NH3} began to decrease (Fig 5.2B, indicated by the arrow) and returned to pre-exposure level at $6.02 \times 10^7 \pm 8.16 \times 10^6$ cell mL^{-1} (n = 11).

5.3.2 Increasing in situ specific rates for ammonia oxidation and oxygen uptake during methane exposure

Based on profiles of dissolved oxygen concentrations and S_{NH3}, in situ specific rates

of ammonia and oxygen consumption were determined and depicted in Figure 5.3 (and Fig S5.2). During pre-exposure phase, specific ammonia oxidation rates (r_{nh}) and specific oxygen uptake rates (sOUR) in the reactor were $2.15 \times 10^{-9} \pm 2.45 \times 10^{-9}$ mg NH_3-N $cell^{-1}d^{-1}$ (n = 6) and $7.60 \times 10^{-9} \pm 8.81 \times 10^{-10}$ mg O_2 $cell^{-1}d^{-1}$ (n = 8), respectively (Fig 5.3). Oxygen and NH_3-N were consumed with a stoichiometry of 1.58 ± 0.04 mol O_2 consumed per mol NH_3-N oxidized (n = 6).

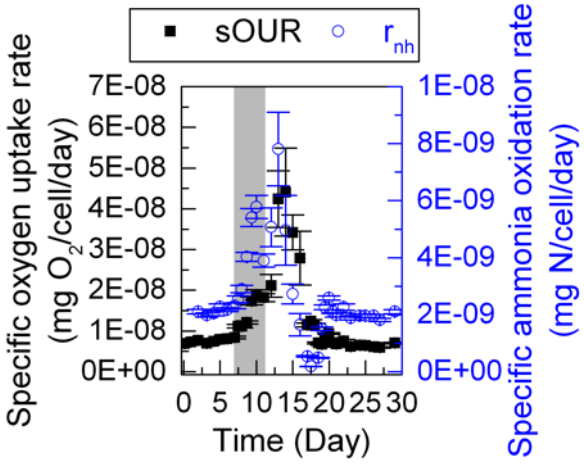

Figure 5.3. Specific rates of oxygen uptake (A) and ammonia oxidation (B) at reactor level. Gray area indicated the 4-day methane exposure phase. Error bars represent one standard deviation calculated from S_{NH3}, oxygen profile and cell concentrations.

Both r_{nh} and sOUR showed increasing trends, up to $5.78 \times 10^{-9} \pm 4.00 \times 10^{-10}$ mg NH_3-N $cell^{-1}d^{-1}$ (~2.7-fold higher than pre-exposure level) and $1.89\ 10^{-8} \pm 1.25 \times 10^{-9}$ mg O_2 $cell^{-1}d^{-1}$ (~2.5-fold higher than pre-exposure level) respectively, in the presence of methane. When *N. eutropha* were relieved from methane exposure, transient increase in r_{nh} and sOUR were observed. The decreasing r_{nh} and sOUR were captured in parallel with decreasing S_{NH3}. While sOUR and S_{NH3} returned to the respective

pre-exposure levels approximately at the same time, r_{nh} dropped to ~2×10^{-10} mg O_2 $cell^{-1}d^{-1}$ before returned to ~2×10^{-9} mg O_2 $cell^{-1}d^{-1}$. After reactors returned to steady state, the r_{nh} and sOUR were $2.03 \times 10^{-9} \pm 3.68 \times 10^{-10}$ mg NH_3-N $cell^{-1}d^{-1}$ (n = 11) and $6.96 \times 10^{-9} \pm 1.19 \times 10^{-9}$ mg O_2 $cell^{-1}d^{-1}$ (n = 11), respectively.

5.3.3 High-rate biomethanol production during early methane exposure phase

Figure 5.4 illustrated the changes in S_{CH3OH} and the rates of methanol production based on data from both biological replicates. The timeline was adjusted to focus on methane exposure phase (Day 0 of exposure phase corresponded to Day 7 of the ammonia and methane co-feeding experiment). While no methanol was detected (detection limit = 1.72 mg COD L^{-1}) in the absence of methane supply, the increase in S_{CH3OH} to a concentration of 6.23 ± 1.36 mg COD L^{-1} within 3 hours of methane exposure were detected (Fig 5.4). S_{CH3OH} were increasing during the first 18 hours of ammonia and methane co-feeding, up to 17.3 ± 0.1 mg COD L^{-1}, and gradually decreased to 3.14 ± 0.59 mg COD L^{-1} at the end of methane supply. The residual methanol dropped below detection limit within 36 hours after methane supply was stopped. Specific methanol production rates (r_{CH3OH}) peaked at 2.81 ± 0.16 mg-CH_3OH-COD mg-biomass-$COD^{-1}d^{-1}$ within 12 hours after methane was introduced. Decreasing from peak r_{CH3OH}, r_{CH3OH} were maintained at ~0.8 mg-CH_3OH-COD mg-biomass-$COD^{-1}d^{-1}$ for ~1.5 day (Fig 5.4, Exposure phase Day 1.5 to Day 3) before further decreased to 0.31 ± 0.07 mg-CH_3OH-COD mg-biomass-$COD^{-1}d^{-1}$.

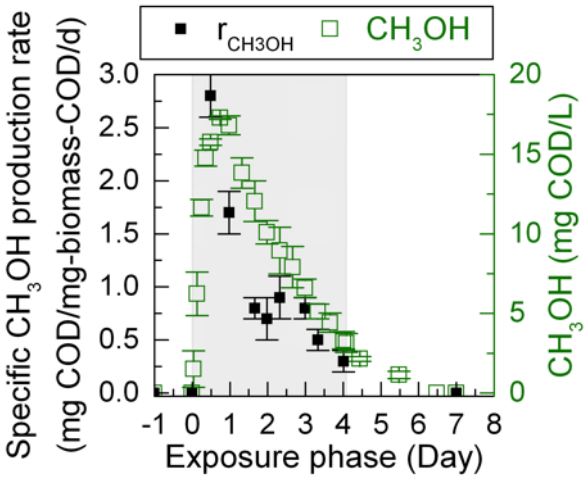

Figure 5.4. Specific biomethanol production rates. Gray area indicated the 4-day methane exposure phase. Error bars represent one standard deviation calculated from S_{CH3OH} and cell concentrations.

5.3.4 Reduction of *amoA* and *hao1* genes expression and transient induction of *nirK* and *norY* genes expression in response to methane exposure

The expression of *amoA* and *hao1*, which were central to AOB catabolism, decreased rapidly in response to methane exposure and *amoA* gene expression was more responsive than the expression of *hao1*. Within 24 hours of exposure, the expression levels of *amoA* and *hao1* genes were 13.2 % ± 4.2 % and 34.4 % ± 8.5 %, respectively, of pre-exposure levels and both remained at ~10 % of pre-exposure level from Day 1.5 to Day 4 of exposure phase (Fig 5.5A). While cell concentrations were increasing during recovery phase, amoA and hao1 expression were partially recovered and fluctuated below the pre-exposure level. Unexpectedly, the expression of *amoA* and *hao1* showed decreasing trends, as low as ~30 % of pre-exposure levels (Fig 5.5B), even when the systems had returned to steady state (ω based on S_{NH3}) at reactor level (Fig 5.2A).

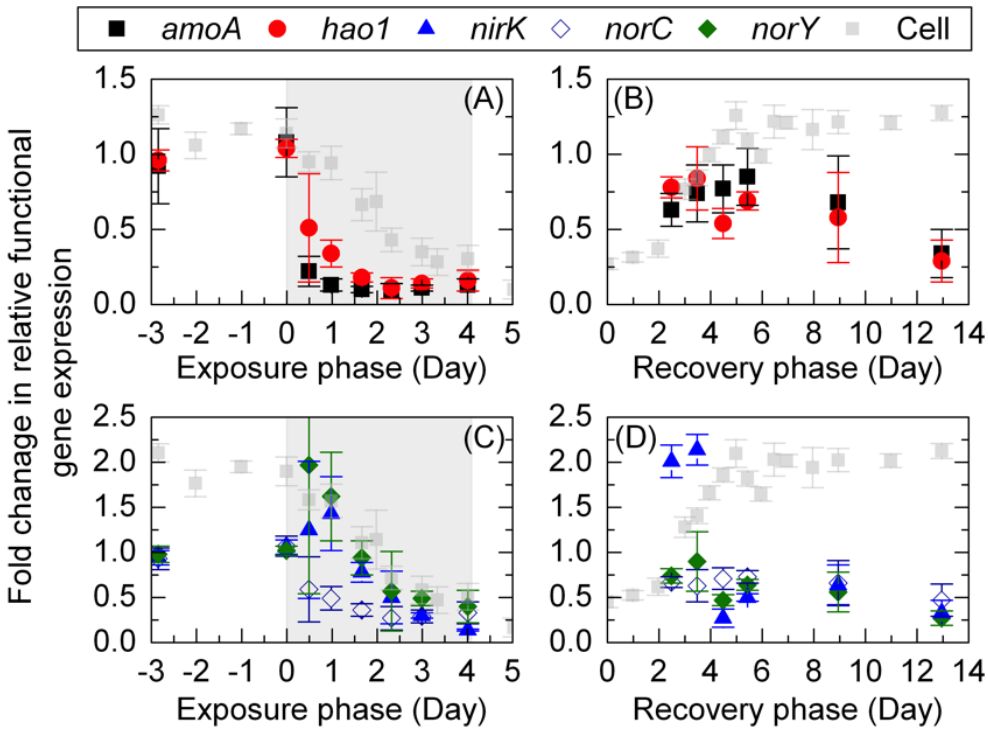

Figure 5.5. Expression of genes related to oxidation/reduction of nitrogenous compounds during (A) methane exposure phase and (B) recovery phase of chemostat operation. Cell concentrations are used as a reference of reactor operation; the scale for cell concentration is not shown. Error bars represent standard deviation from triplicate qPCR analysis and duplicate biological replicates.

The expression of three genes participated in further nitrogen metabolism were also analyzed. While *norC* expression followed similar trends as *amoA* and *hao1* expression, expression of *nirK* and *norY* were induced during early methane exposure phase. During the first day of exposure, expression of *nirK* and *norY* were sustained at ~1.5-fold of pre-exposure levels. Nevertheless, subsequent decrease in the expression of *nirK* to ~14% of pre-exposure levels, and *norY* and *norC* to ~35% of pre-exposure levels were observed as methane exposure continued (Fig 5.5C). During early recovery phase, high expression levels of *nirK*, up to 2-fold of pre-exposure levels, were observed.

As cell concentrations approached steady state level, expression of *nirK* dropped

below ~30% of pre-exposure level. Expression of *norY* partially recovered to 89.9 % ± 32.6 % of pre-exposure levels and dropped to ~50% of pre-exposure level concurrently with the decrease in *nirK* expression. The expression of *norC* were stable at ~70% of pre-exposure level during early recovery phase (Fig 5.5D). As cell concentrations returned to pre-exposure level, the decrease in *nirK*, *norC* and *norY* genes expression, similar to the changes in *amoA* and *hao1*, were observed as chemostat operation continued (Fig 5.5D).

5.4 Discussion

5.4.1 Physiological responses of *N. eutropha* to methane supply

Methane has been categorized as a competitive inhibitor with ammonia for the AMO binding site[16]. The energy metabolism in AOB, which is normally initiated by ammonia oxidation, would be affected when methane is available for AMO. Both the competition between ammonia and methane and the oxidation of methane reduce the electrons available for downstream electron transport chain (ETC) (Fig 5.1.). Our results of the increasing S_{NH2OH} (Fig 5.2), r_{nh} and sOUR (Fig 5.3) indicated a trend toward higher electron flux during methane exposure compared with the absence of methane, possibly to compensate for the deficiency in electrons. Additionally, the decreasing cell concentrations (Fig 5.2A) indicated a lower anabolic activity during methane exposure, which further implied the ability of *N. eutropha* to regulate the partition of electrons for catabolism or anabolism during the presence of an alternative electron-consuming substrate (methane). The capability for bacteria to

manage balances between catabolism and anabolism under energy limitation had been reviewed previously[156]. The stabilized S_{NH2OH}, cell concentrations (Fig 5.2), and r_{nh} (Fig 5.3) during late exposure phase also implied the tendency of *N. eutropha* to adapt to methane exposure.

5.4.2 Relationships between reactor performance, specific rates, and genes expression

In this study, we employed various tools to capture the responses of *N. eutropha* to the exposure and recovery from methane supply. The changes in *amoA* and *hao1* genes expression aligned better with ex situ batch $sOUR_{NH3}$ compared with in situ sOUR, suggesting the functional genes expression might not reflect the in situ bacterial activity. On the other hand, though the depletion of *amoA* and *hao1* mRNA during starvation and induction of *amoA* and *hao1* genes expression by ammonium in *N. europaea* has been demonstrated [42], our results suggested that the presence of ammonium did not necessarily induce *amoA* and *hao1* gene expressions (Fig 5.2 and Fig 5.6). The lower gene expression levels after reactor returned to steady state might reflect a lag for the establishment of steady state at the transcription level after the environment disturbance, which was observed in *N. europaea* previously [114].

5.4.3 Roles of *nirK* and *norY* genes in *N. eutropha* metabolism

The copper-containing nitrite reductase encoded by *nirK* in AOB catalyzes the reduction of nitrite (NO_2^-) to nitric oxide (NO) and the expression is related to

increasing NO_2^- concentrations [40, 139]. Moreover, the need for NirK to prevent formation of nitrosating compounds and the supportive role of NirK activity for the growth of *N. europaea* has been discussed [157]. The functional partner of NirK is previously identified as cNOR [139, 143], which consists of NorCBQD subunits [33]. However, increasing evidence suggests that an alternative NO reductase, sNOR, is present in AOB, [149] but the related mechanisms remain unclear [44, 134, 144]. In this study, we tracked the expression of *nirK*, *norC* (encodes subunit of cNOR) and *norY* (encodes subunit of sNOR) and found similar expression patterns of *nirK* and *norY* during and post methane exposure, which revealed the functional relationships between *nirK* and *norY* genes in *N. eutropha* (Fig 5.6C and 5.6D). On the other hand, the pattern of *norC* expression was similar with *amoA* and *hao1* expression (Fig 5.6). Our qPCR results also demonstrated the requirement of *nirK* expression during the rehabilitation of *N. eutropha* culture in the chemostat reactors (Fig 5.6D), which was consistent with its proposed roles. The elevated *nirK* expression levels during early recovery phase also suggested that S_{NO2} is not the only inducing factor for *nirK* expression. Considering the assimilatory roles of NirK and sNOR within AOB, we further propose that the expression of *nirK* and *norY* are related to the electron flows in AOB. When an additional electron sink existed, transient *nirK* and *norY* expression increased in support of higher rates of ammonia and hydroxylamine oxidation. However, when the balance between catabolism and anabolism changed, the use of electrons for NO/N_2O reduction became unfavorable, because more electrons were needed for AMO or downstream ETC. During the recovery phase when both growing

substrate and energy were not limited, NirK and sNOR were utilized to manage the imbalance between electron production and consumption as demonstrated previously[158].

5.4.4 Ammonia and methane co-oxidation in *N. eurtopha*

Previous studies have shown methanol production during short-term batch incubations (from 1 hour to 24 hours) and the maximum r_{CH3OH} ranged from 0.09 to 0.82 mg-CH_3OH-COD mg-biomass-$COD^{-1}d^{-1}$ [15, 19]. In this study, we observed peak r_{CH3OH} up to 2.81 ± 0.16 mg-CH_3OH-COD mg-biomass-$COD^{-1}d^{-1}$ within 12 hours of methane exposure (Fig 5.4). Unlike the batch systems, in which the decrease in r_{CH3OH} could result from depletion of ammonia-N or increasing S_{CH3OH} [19], the changes in r_{CH3OH} during methane exposure in the chemostat reactors could also be related to increasing S_{NH3} (Fig 5.2A). While the increasing r_{nh} indicate a higher electron flux was directed back to AMO, and methane oxidation should benefit from the additional electrons, the competitive effect of ammonia to methane would be manifest as an increased S_{NH3}. While the stable r_{CH3OH} during exposure phase Day 1.5 to Day 3 indicated a temporary balance for the partitioning of electrons between ammonia oxidation, methane oxidation, and downstream ETC, the further decrease in r_{CH3OH} (Fig 5.4, Day 3 to Day 4) suggested that a new steady state was not achieved yet.

The rapid responses of *N. europaea* to trichloroethylene (TCE), also a competitive inhibitor of ammonia oxidation in AOB, and recovery in AMO activity during co-existence of ammonia and TCE have been demonstrated and modeled in a

fed-batch system [159]. While TCE and 1-1, DCE were categorized as class III cometabolic substrates for AOB, which transformation would cause substantial cellular injury [147], an alternative explanation for the decrease in mixed culture AOB activity when exposed to methanol other than noncompetitive inhibition of ammonia by methanol [19] should be considered. Hyman et al (1995)[160] also demonstrated that *N. europaea* was able to recover from TCE exposure, which requires de novo protein synthesis. In addition, Hyman et al (1995)[160] proposed that the rate of TCE oxidation could be improved through balancing the extent of inactivation of AMO activity and the rate of protein synthesis. In this study, we further showed the potential of sustained ammonia and methane co-oxidation through re-partitioning of the electrons flux in *N. eutropha* (as discussed in previous paragraphs), which is crucial for the application of AOB cometabolism for bioremediation [161] or biofuel production [15].

5.5 Conclusion and implications

In this study, we investigated the responses of methane cometabolism in *N. eutropha* at macroscopic (reactor) level and microscopic (transcription) level. Our results suggested that *N. eutropha* adapted to methane exposure by regulating the balance between catabolism and anabolism. We also demonstrated the expression of genes involved in nitrogen metabolism in *N. eutropha* during chemostat operation and offered new evidences for the regulation and potential roles of *amoA* and *nirK* genes in *N. eutropha*. Our results of methane cometabolism in the chemostat reactors also provide insights for the application of AOB cometabolism for bioremediation or

biofuel production.

5.6 Supporting information

The supporting information includes (1) Medium recipe for *N. eutropha* cultivation (2) primers used in this study (3) biological replicate of nitrogen, methanol and cell concentration profiles (4) biological replicate of specific rates of oxygen uptake and ammonia oxidation at reactor level.

Table S5.1. Medium recipe for *N. eutropha* cultivation.

Chemical	Mass Per Liter	
(NH4)2SO4	1.32	g
MgSO4*7H2O	0.2	g
CaCl2*2H2O	0.02	g
K2HPO4	0.087	g
EPPS	2.52	g
NaHCO3	0.5	g
EDTA-Fe3+	1	mg
CuSO4*5H2O	0.25	mg
Na2MoO4*2H2O	100	mg
MnCl2*4H2O	172	mg
ZnSO4*7H2O	100	mg
CoCl2*6H2O	4	mg

Table S5.2. Primers used in *N. eutropha* experiments.

Target Gene	Primer Set	Sequence (5'-3')	PCR product size (bp)	Annealing temp (°C)	Reference
amoA	amoAFq4	AAATCCCAGTCACCTGCCAACAAC	145	56	This study
	amoARq4	AAGAGATCCTGAAAGCGGCCAAGA			
hao1	haoFq4	TGGAGAAGGCGTCTTTCAGACGAA	80	58	This study
	haoRq4	TATGTCCAAGCATGGCAAACTGGC			
nirK	nirKFq4	ATCGCCTGGCCCAATTGTATAGGA	134	56	This study
	nirKRq4	ACTTTGTCAACGCTGGACCCAATG			
norC	norCFq2	TGGGCTCTCATCCAGGCCTTTAAT	84	56	This study
	norCRq2	ACTGGGTAATGTTTGGGTCCGCTA			
norY	norYFq1	GGTACCGGGTCATTTTCATTTCT	68	56	[162]
	norYRq1	AGTAGGCAAATCCGATGAGCAT			
EUB16S	1055F	ATGGCTGTCGTCAGCT	353	55.5	[98]
	1392R	ACGGGCGGTGTGTAC			

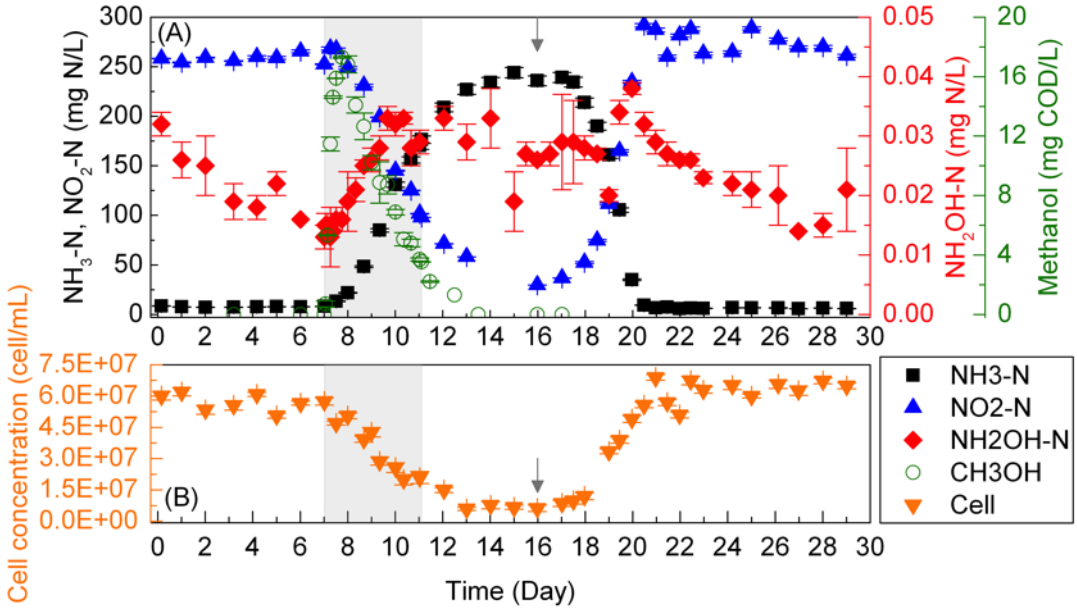

Figure S5.1. Biological replicate of nitrogen, methanol (A) and cell concentration (B) profiles. Gray area indicated the 4-day methane exposure phase.

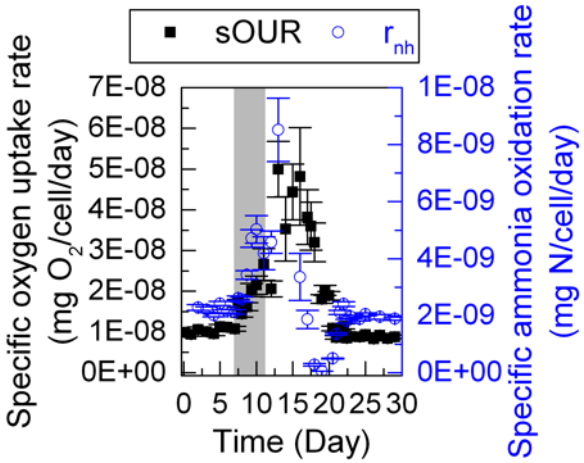

Figure S5.2. Biological replicate of specific rates of oxygen uptake (A) and ammonia oxidation (B) at reactor level. Error bars represent one standard deviation calculated from S_{NH3}, oxygen profile and cell concentrations.

CHAPTER 6

Comparative transcriptomics of methane cometabolism in *Nitrosomonas europaea* ATCC 19718 and *Nitrosomonas eutropha* C91

This chapter is the basis of the paper:

Yu-Chen Su and Kartik Chandran*

Comparative transcriptomics of methane cometabolism in *Nitrosomonas europaea* ATCC 19718 and *Nitrosomonas eutropha* C91 (In preparation)

Affiliation:

Department of Earth and Environmental Engineering, Columbia University

500 West 120th Street, Room 1045 Mudd Hall, New York, NY 10027

Abstract

The broad substrate specificity of ammonia monooxygenase contributes to the ability of chemolithoautotrophic ammonia oxidizing bacteria (AOB) to co-metabolically oxidize selected alternate organic compounds. However, little information exists regarding the actual molecular underpinnings of co-metabolism. In this study, we investigated the conversion of methane to methanol using axenic chemostat cultures of *Nitrosomonas europaea* ATCC 19718 and *Nitrosomonas eutropha* C91. Upon methane exposure and conversion to methanol, at the global transcriptional level, the impacts of methane exposure were more evident for *N. europaea* ATCC 19718 than for *N. eutropha* C91. Despite the comparable genome sizes (~2.8 Mbp), a total of 503 genes were differentially expressed in *N. europaea* ATCC 19718 compared to only 243 genes in *N. eutropha* C91. A decrease in *amoCAB* expression and increasing *amoC3* transcript levels were observed in both strains. However, changes in hydroxylamine oxidoreductase transcription were divergent. For functional genes involved in the electron transport chain (ETC) downstream of hydroxylamine oxidation, the induction of genes for regulatory proteins (*ncyA* and *nsrR*) were detected in *N. europaea* ATCC 19718 whereas increasing transcript levels of genes encoding intermediate electron carriers (mostly c-type cytochrome) in *N. eutropha* C91 were observed. On the other hand, both strains reduced the expression of genes related to NADH synthesis during methane exposure, which might have resulted in lack of energy sources for anabolic activities. Decrease in transcript levels of gene clusters involved in cell division and cell wall biosynthesis were also observed in both

strains. In summary, the global transcriptomic analysis permitted a detailed delineation of methane metabolism in AOB and revealed considerable differences between *N. europaea* ATCC 19718 and *N. eutropha* C91 during methane oxidation.

6.1 Introduction

Chemolithoautotrophic ammonia oxidizing bacteria (AOB) play a critical role in the nitrification process in both natural and engineered systems. AOB oxidize ammonia to hydroxylamine using ammonia monooxygenase (AMO). Hydroxylamine is further oxidized to nitrite by hydroxylamine oxidoreductase (HAO). The electrons are extracted from hydroxylamine by HAO and transferred through the electron transport chain, during which the electrons are directed back to AMO for subsequent ammonia oxidation or used to generate proton motive force for energy synthesis in AOB[20].

$$NH_3 + O_2 + 2e^- \xrightarrow{AMO} NH_2OH + H_2O \quad (1)$$

$$NH_2OH + H_2O \xrightarrow{HAO} NO_2^- + 5H^+ + 4e^- \quad (2)$$

The ability of AOB to catalyze the oxidation of a wide range of substrates in addition to ammonia has been well documented [22], which is referred to as cometabolism [163]. It is believed that the evolutionarily relationship and peptide similarity between AMO and the particulate methane monooxygenase (pMMO) in methane oxidizing bacteria (MOB) might have resulted in the observed overlapping substrate pools in AOB and MOB [21, 35]. The co-oxidation of organic substrates including methane, (halogenated) alkanes and alkenes, and aromatic compounds[103] has led to researches on bioremediation[161, 164] or liquid fuel production[15, 16, 18] using AOB. Nevertheless, the physiological impacts of cometabolism on AOB remain poorly understood. For example, methane competes with ammonia for AMO [23-26] and consumes reducing equivalents, which can be otherwise used for ammonia oxidation or energy synthesis in AOB. Also, no known enzymes for catabolic methanol metabolism are found in

AOB genomes, which suggest that reducing equivalents cannot be replenished to support AMO activity during cometabolic methane oxidation. However, little efforts have been made to understand the relationship between cometabolism and energy metabolism in AOB.

$$CH_4 + O_2 + 2H^+ + 2e^- \xrightarrow{AMO} CH_3OH + H_2O \quad (3)$$

Cometabolic methane oxidation has been considered as an attractive platform for methanol production[15] and the development of the bioprocess using AOB in the mixed culture nitrifying consortia further highlights the potential for field application[19]. Though previous studies have described the kinetics of methane oxidation in AOB[17, 24-26], other physiological responses in addition to AMO and HAO activities remain unclear, especially at the systems biology and metabolic regulations levels. On the other hand, while previous reports have demonstrated the transcriptional responses of *Nitrosomonas. europaea* to chloroform/chloromethane [138], toulene/benzene [27], and phenol/toulene [165] cometabolism, no studies have addressed the impacts of cometabolic substrates on other AOB at transcriptional level. In order to understand the underlying metabolic regulations of methane cometabolism in AOB, *Nitrosomonas europaea* ATCC 19718 [33] and *Nitrosomonas eutropha* C91 [34], two closely related AOB, were cultivated in chemostat reactors and exposed to methane. Comparative transcriptome analysis was performed using biomass samples fed with ammonia as the sole substrate or with ammonia and methane for 24 hours. Reactor level AOB activities (ammonia oxidation activity, cell growth, methanol production) were monitored (as described in Chapter 4 and Chapter 5) to give complementary

information on methane cometabolism in AOB.

6.2 Materials and Methods

6.2.1 Bacterial cultivation, methane exposure, and sample collection

The cultivation of *N. europaea* ATCC 19178 and *N. eutropha* C91 in the absence and presence of methane have been described previously (refer to Chapter 4 and Chapter 5). In brief, both strains were cultivated separately in 2.2 water-jacketed chemostat reactors (BioFlo115, Eppendorf) and fed with 10 mM $(NH_4)_2SO_4$ at a dilution rate of 0.45 d^{-1}. The pH was controlled automatically at 7.50 ± 0.05 using 1M $NaHCO_3$ and the temperature was maintained at 30 °C. During pre-exposure phase, oxygen was supplied using 0.9 $Lmin^{-1}$ lab air and 0.1 $Lmin^{-1}$ nitrogen (Techair) which were filtered through 0.22 □m filter (Millipore). During methane exposure phase, the total gas flow rate was maintained at 1 $Lmin^{-1}$ using 0.1 $Lmin^{-1}$ methane (Techair) plus 0.9 $Lmin^{-1}$ lab air. Reactor performance has been demonstrated in previous chapters (Fig 4.1 for *N. europaea* ATCC 19718 and Fig 5.2 for *N. eutropha* C91). Biomass samples (approximately 10^9 cells) were collected at the end of pre-exposure phase and after 24 hours of methane exposure. The cells were treated with RNA protect reagent (Qiagen) immediately after sampling and stored in -80 °C freezer until further processing.

6.2.2 RNA isolation and whole transcriptome sequencing

Total RNA was extracted using Qiacube (Qiagen) following the manufacturer's manual. The quality and concentration of the total RNA was measured using

NanoDrop (Fisher Scientific) Total RNA samples were then processed based on Ion Torrent PGM platform workflow (Life Technology). All kits were purchased from Life Technology unless otherwise noted. Approximately 1 - 2 μg total RNA was mixed with ERCC RNA Spike-In Control before proceed to rRNA removal step using Ribo-Zero Magnetic Kit for Bacteria (Illumina). Whole transcriptome cDNA libraries were constructed following the protocol of Ion Total RNA-Seq Kit v2 and each library was barcoded using Ion Xpress RNA-Seq Barcode Kit. Sequencing templates on the Ion Sphere Particles (ISP) were prepared using Ion PGM Hi-Q OT2 Kit - 400 and the Ion OneTouch 2 System. Enriched ISPs were loaded and sequenced following Ion PGM Hi-Q Sequencing Kit protocol on Ion 318 chips with 850 flows. UBAM files with the raw sequencing data were stored in the Torrent Suite (v5.0.4) server and used for subsequent analysis.

6.2.3 RNA-Seq data analysis

In this study, we used Bowtie2 [166] to remove remaining rRNA-related fragments and for read alignment against *N. europaea* ATCC 19718 or *N. eutropha* C91 genomes. SILVA rRNA database (v128) [106] and annotated genomes for *N. europaea* ATCC 19718 /*N. eutropha* C91 [167] were used to build the indexes for Bowtie2. UBAM files exported from the server were converted to fastq files using BEDTools [168] and trimmed (Phred score of 20 and minimum length of 25 bp) using mothur [105] for additional quality control. The trimmed fasta files and the indexes created from SILVA rRNA database were used as input for Bowtie2 to remove rRNA-related

fragments. The resulting fasta files should be free of rRNA-related fragments and contain only mRNA-related sequences. These fasta files and indexes created from *N. europaea* ATCC 19718 or *N. eutropha* C91 genomes were further used as the input for Bowtie2 to map the sequencing reads to specific genes. The output files from Bowtie2 containing genes information and read numbers of each replicate, from both strains, were merged based on a custom-made *N. europaea* ATCC 19718 and *N. eutropha* C91 corresponding genome inventory for comparative analysis. Reference genome databases for *N. europaea* ATCC 19718 and *N. eutropha* C91 were downloaded from National Center for Biotechnology Information (NCBI). Two genomes were compiled primarily based on KEGG orthology (KO) number with minor manual modification. The complete count table was used for differential gene expression analysis using edgeR package [169]. For statistical analysis, p-values are adjusted using the Benjamini-Hochberg method [170] and present as false discovery rate (FDR) in edgeR.

6.3 Results

6.3.1 Whole transcriptomic responses of *N. europaea* ATCC 19718 and *N. eutropha* C91 to methane exposure.

Exposure of *N. europaea* ATCC 19718 and *N. eutropha* C91 to methane negatively affected ammonia oxidation and cell growth for both strains as previously described (Fig 4.1 and Fig 5.1) and the impacts were reversible when methane supply was discontinued. Comparative transcriptome analysis of *N. europaea* ATCC 19718 and *N. eutropha* C91 cultures grown with only ammonia or with concurrent ammonia and

methane feed was performed after 24 hours of methane exposure. Results showed that *N. europaea* ATCC 19718 was more responsive to methane exposure than *N. eutropha* C91. A total of 503 genes were differentially expressed in *N. europaea* ATCC 19718 whereas only 243 genes were differentially expressed in *N. eutropha* C91 (criteria: FDR $\leq$ 0.01 and |gene expression fold change| $\geq$ 2) (Table S6.1). The mRNA transcript levels (based on Reads Per Kilobase Million, RPKM) of *amoCAB*, gene encodes cytochrome c552 (Table 6.1), *cspD2* (cold shock protein), and *cbbLS* (data not shown) were among the highest during pre-exposure phase for both *N. europaea* ATCC 19718 and *N. eutropha* C91.

Methane exposure induced the expression of stress response genes related to ATP-dependent protease, chaperones, and heat shock proteins in *N. europaea* ATCC 19718 (1.6 to 141-fold induction, FDR $\leq$ 0.01 unless otherwise noted) and *N. eutropha* C91 (1.5 to 8.9-fold induction) (Table S6.2). Interestingly, methane exposure induced the expression of *mer* operon in *N. europaea* ATCC 19718 (11.0 to 153-fold induction except for *merR*), however, no significant differences were observed for all 3 copies of *mer* operon in *N. eutropha* C91 (Table S6.2). The discrepancy was also noticed for genes involved in fatty acid biosynthesis pathway (*fab* gene cluster *fabDFGHZ*, 1.5 to 3.1-fold reduction) and aromatic amino acid biosynthesis (up to 3.1-fold reduction) were downregulated in *N. europaea* ATCC 19718 but remained stable in *N. eutropha* C91 (Table S6.2 and Table S6.3). On the other hand, AMP-dependent synthetase/ligase (NE1549, NE2235, Neut_0702) for fatty acid biosynthesis were significantly downregulated (-1.6 to -2.5-fold) in both strains and

only *accA*, which encode a carboxyl transferase, was upregulated in *N. eutropha* C91 (Table S6.2).

6.3.2 Nitrogen metabolism, electron transport chain, and energy molecules synthesis

Due to the reported competition between ammonia and methane for the same binding site of AMO [75] and the requirement of reducing equivalents for methane oxidation, we expected that the presence of methane would negatively affect AOB catabolism. Therefore, we next examined the transcriptional responses of AOB catabolic pathway module.

AOB derive energy for growth and other cellular functions from ammonia oxidation, which involve a series of enzymes and intermediate electron carriers. Figure 6.1 shows the plot for all the functional partners involved in nitrogen metabolism, ETC, and terminal oxidases and Table 6.1 lists those genes that were differentially expressed in response to methane exposure. It was expected that the transcript levels of genes encode AMO and HAO would be stable or upregulated since that ammonia was being fed continuously. However, a decreasing trend for *amoCAB* expression (-1.3 to -2.9-fold) was observed while *amoC3*, the divergent copy of *amoC* that was proposed to be part of the stress response system [171], was upregulated (2.3 to 6.1-fold) in both strains. The expression of *amoED* (1.6 to 2.3-fold) was upregulated in *N. europaea* ATCC 19718 while the downregulation of *amoD* (-1.5-fold) in *N. eutropha* C91 was observed (Table 6.1). As for genes involve in hydroxylamine oxidation,

~1.5-fold induction of *haoA* expression, the purported active subunit for hydroxylamine oxidation [172], was observed in *N. europaea* ATCC 19718 but no significant changes for the genes expression of the electron carriers (*cycA*, *cycB*, NE0810, *petC*) immediately downstream. For *N. eutropha* C91, the expression of *haoAB-cycAB* gene cluster showed no significant differences however the transcript levels of genes related to the downstream cytochrome bc1 complex (Neut_1111 and Neut_1112) were increasing (1.6 to 1.7-fold) (Table 6.1). Results also showed that genes related to cytochrome c552 (2.5 to 3.1-fold), and *nirK* gene cluster (3.2 to 219-fold) were upregulated in both strains while the expression *norQD* (-3.0 to -3.4-fold) and *cytL* (-4.2-fold) was decreasing in *N. europaea* ATCC 19718 (Fig 6.1). It was noted that the RPKM values for *nirK* gene cluster in *N. europaea* ATCC 19718 (68 to 131) were much lower than *N. eutropha* C91 (833 to 1356) during pre-exposure period. On the contrary, the RPKM values for *norCBQD* and senC-*norYS* gene clusters were higher in *N. europaea* ATCC 19718 when ammonia was the only substrate (Table 6.1). While the complete *senC-norYS* gene cluster, which encodes sNOR-type NO reductase, in *N. eutropha* C91 was induced (2.5 to 5.8-fold), only *norY* (1.7-fold) was induced in *N. europaea* ATCC 19718 (Table 6.1) during methane exposure. In other word, for participants involved in the ETC following hydroxylamine oxidation, the induction of genes for regulatory proteins (*nsrR* and *ncyA*) were observed in *N. europaea* whereas increasing transcript levels of genes encode intermediate electron carriers (mostly c-type cytochrome) in *N. eutropha* C91 were observed in response to methane exposure. Additionally, increasing transcript

levels of the nearly complete *ccm* gene cluster encoding cytochrome c maturation system (NE0764, NE0766-NE0771, NE2389/ Neut_1635-Neut_1639, Neut_1643) were observed in both strains (Table S6.4). At the end of ETC, the expressions of genes encode the aa3-type cytochrome c oxidase were relatively stable except *ctaG* in *N. europaea* ATCC 19718 (1.8-fold reduction) and *coxB* in *N. eutropha* C91 (1.9-fold induction). Furthermore, the transcription of genes for two of the bo3-type cytochrome c oxidase subunits (-2.1 to -2.8-fold) and all four subunits for cbb3-type cytochrome c oxidase (-2.2 to -3.0-fold) were decreasing in *N. eutropha* C91 (Table 6.1).

Based on the chemiosmotic model for oxidative phosphorylation, electrons are channeled from the electron donor to the terminal electron acceptor down the electron transport chain, resulting in the development of a transmembrane proton gradient, which eventually contributes to ATP or NADH production. During the presence of methane, both *N. europaea* ATCC 19718 and *N eutropha* C91 increased the expression of genes related to ATP synthase and reduced the expression of genes for NADH-quinone oxidoreductase. A 1.5 to 2.5-fold upregulation of all genes encodes the membrane-bound ATP synthase Fo subcomplex (*atpBFE*) and 1.7 to 2.7-fold downregulation of genes for NADH-quinone oxidoreductase membrane subunits (*nuoMNJKH*) were observed (Table 6.2). Additionally, the expression of *atpAHC* genes (3 out of 5 genes related to ATP synthase F1 subcomplex) also showed ~1.5-fold increase (FDR $\leq$ 0.05) in *N. eutropha* C91.

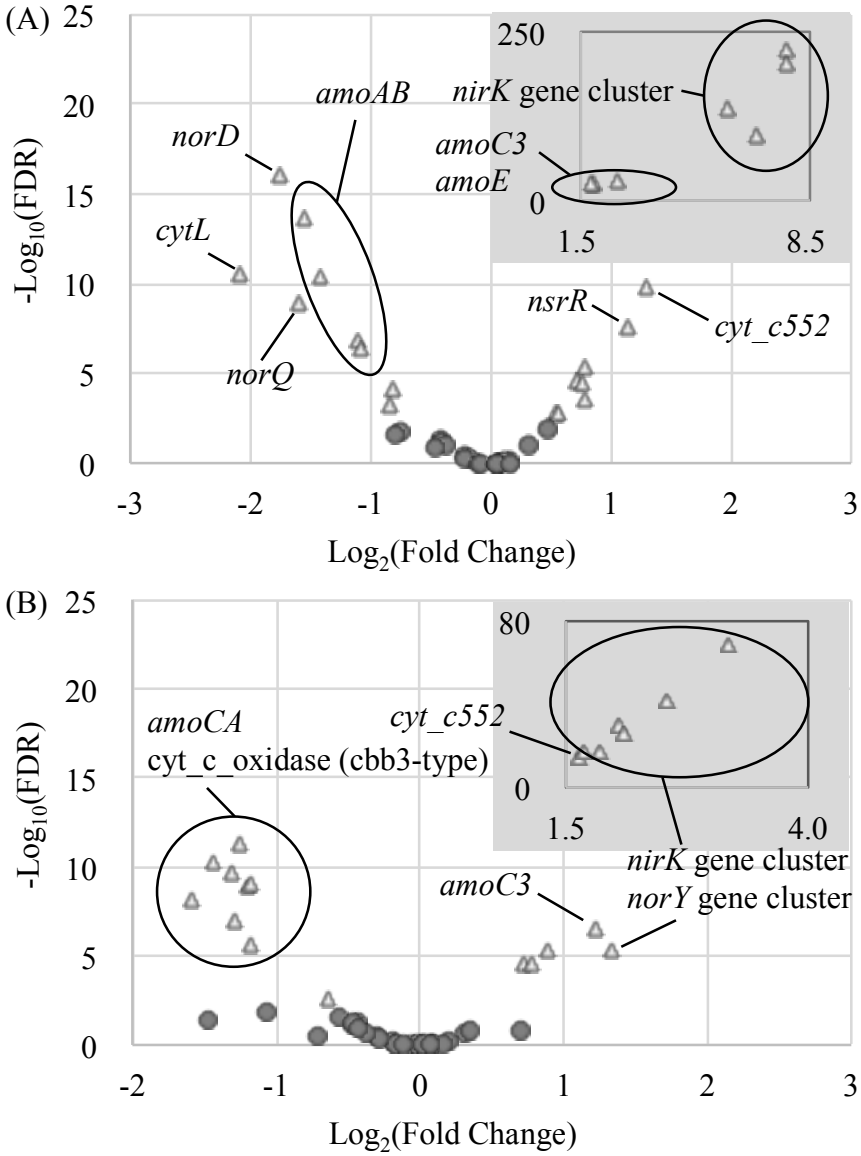

Figure 6.1. Volcano plot of genes involve in nitrogen metabolism, electron transport chain, and terminal oxidase in (A) *N. europaea* ATCC 19718 and (B) *N. eutropha* C91. Circles represent FDR > 0.01 and triangles represent FDR ≤ 0.01. Labels indicate |gene expression fold changes| ≥ 2, i.e. |log2 (Fold Change)| ≥ 1.

Table 6.1. Differentially expressed genes involve in nitrogen metabolism, electron transport chain, and terminal oxidases.

Gene product	Gene name[1]	*N. europaea* ATCC 19718			*N. eutropha* C91		
		Locus tag[2]	RPKM[3]	FC[4]	Locus tag[2]	RPKM[3]	FC[4]
Ammonia monooxygenase C	*amoC*	NE0945	28501	-1.3	Neut_2078	56304	**-2.3**
Ammonia monooxygenase A	*amoA*	NE0944	7414	**-2.9**	Neut_2077	9173	**-2.5**
Ammonia monooxygenase B	*amoB*	NE0943	19953	**-2.1**	Neut_2076	14654	-1.4
Ammonia monooxygenase E	*amoE*	NE0942	1090	**3.8**	Neut_2075	442	1.0
Ammonia monooxygenase D	*amoD*	NE0941	385	**1.7**	Neut_2074	776	-1.4
Ammonia monooxygenase C3	*amoC3*	NE1411	604	**6.1**	Neut_1520	1266	**2.3**
Hydroxylamine oxidoreductase (*hao* gene cluster)	*haoA*	NE0962	2422	**1.5**	Neut_2335	2183	1.1
Hypothetical protein (*hao* gene cluster)	*haoB*	NE0961	1108	**-1.8**	Neut_2334	903	-1.1
Cytochrome b (cytochrome bc1 complex)	NE0810	NE0810	1292	1.0	Neut_1111	1755	**1.6**
Cytochrome c1 (cytochrome bc1 complex)	*petC*	NE0811	1614	1.0	Neut_1112	2099	**1.7**
Cytochrome c-552 precursor	*cyt_c552*	NE0102	11365	**2.5**	Neut_2242	18140	**3.1**
Multicopper oxidase type 1 (*nirK* gene cluster)	*ncgB, pan1*	NE0927	68	**219.1**	Neut_1406	833	**9.1**
Cytochrome c, class I (*nirK* gene cluster)	*ncgC*	NE0926	59	**215.0**	Neut_1405	837	**4.2**
cytochrome c oxidase cbb3-type subunit III	*ncgA*	NE0925	51	**120.3**	Neut_1404	936	**4.3**
Nitrite reductase (*nirK* gene cluster)	*nirK, aniA*	NE0924	131	**61.7**	Neut_1403	1356	**3.2**
Nitric oxide reductase (cNOR gene cluster)	*norQ*	NE2005	502	**-3.0**	Neut_0520	117	1.0
von Willebrand factor type A domain (cNOR gene cluster)	*norD*	NE2006	411	**-3.4**	Neut_0521	94	1.6
Cytochrome P460	*cyp, cytL*	NE0011	1014	**-4.2**	Neut_0132	749	1.1
SCO1/SenC (sNOR gene cluster)	*senC*	NE0682	966	-1.4	Neut_1876	280	**2.5**
Cytochrome c oxidase, subunit I (sNOR gene cluster)	*norY*	NE0683	3919	**1.7**	Neut_1875	619	**3.6**

cytochrome c oxidase subunit II (sNOR gene cluster)	*norS*	NE0684	3149	1.3	Neut_1874	425	**5.8**
Nitrosocyanin	*ncyA*	NE0143	7670	**1.7**	Neut_2173	18969	1.2
Nitrite-sensitive transcription repressor	*nsrR*	NE0928	384	**2.2**	Neut_1407	706	1.1
Cytochrome c oxidase (aa3-type)	*coxB*	NE1017	2273	-1.2	Neut_2395	2165	**1.9**
	coxA	NE1016	3733	-1.1	Neut_2394	2892	1.3
	ctaG	NE1015	3668	**-1.8**	Neut_2393	1757	1.0
	coxC	NE1013	3849	-1.2	Neut_2392	2720	-1.2
Quinol oxidase (bo3-type)	Neut_0694	N/A			Neut_0694	88	-2.8
	Neut_0695	N/A			Neut_0695	125	-2.1
	Neut_0696	N/A			Neut_0696	118	-1.3
	Neut_0697	N/A			Neut_0697	211	-1.4
Cytochrome c oxidase (cbb3-type)	*fixN*	N/A			Neut_1582	696	**-2.4**
	fixO	N/A			Neut_1583	654	**-2.4**
	fixP	N/A			Neut_1584	465	**-2.2**
	Neut_1585	N/A			Neut_1585	343	**-3.0**

1 Gene names are primarily based on genes present in *N. europaea* ATCC 19718 genome except for quinol oxidase (bo3-type) and cytochrome c oxidase (cbb3-type).

2 Locus tags are based on KEGG nomenclature.

3 RPKM values are the average RPKM of two biological replicates during pre-exposure phase.

4 Fold changes (FC) of gene expression during exposure phase and pre-exposure phase are calculated using edgeR. Detail is described in Materials and Methods. Values in bold indicate the significant differences (FDR ≤ 0.01) in gene expression between methane exposure phase and pre-exposure phase. Underlined values indicate the significant differences (FDR ≤ 0.05) in gene expression between methane exposure phase and pre-exposure phase.

5 Due to the sequence similarities of the two *amoCABE* gene clusters and the *haoAB* genes (refer to section 6.5.1 for more information), values from one of the copies were shown.

Table 6.2. Structural genes of ATP synthase and NADH-quinone oxidoreductase.

Gene product	Gene name	*N. europaea* ATCC 19718		*N. eutropha* C91	
		Locus tag[1]	FC[2]	Locus tag[1]	FC[2]
ATP synthase F1 subcomplex alpha subunit	*atpA*	NE0204	1.3	Neut_0275	1.4
ATP synthase F1 subcomplex beta subunit	*atpD*	NE0206	-1.3	Neut_0277	1.3
ATP synthase F1 subcomplex delta subunit	*atpH*	NE0203	1.2	Neut_0274	1.5
ATP synthase F1 subcomplex epsilon subunit	*atpC*	NE0207	1.0	Neut_0278	1.4
ATP synthase F1 subcomplex gamma subunit	*atpG*	NE0205	-1.1	Neut_0276	1.0
ATP synthase F0 subcomplex A subunit	*atpB*	NE0200	**1.6**	Neut_0271	**1.9**
ATP synthase F0, B subunit	*atpF*	NE0202	**1.5**	Neut_0273	**1.6**
ATP synthase F0, C subunit	*atpE*	NE0201	**1.9**	Neut_0272	**2.5**
NADH-quinone oxidoreductase subunit L	*nuoL*	NE1766	**-2.3**	Neut_0799	**1.7**
NADH-quinone oxidoreductase subunit M	*nuoM*	NE1765	**-2.7**	Neut_0934	**-2.0**
NADH-quinone oxidoreductase subunit N	*nuoN*	NE1764	**-2.6**	Neut_0935	**-1.7**
NADH-quinone oxidoreductase subunit A	*nuoA*	NE1777	**2.2**	Neut_0922	1.4
NADH-quinone oxidoreductase subunit J	*nuoJ*	NE1768	**-2.4**	Neut_0931	-1.2
NADH-quinone oxidoreductase subunit K	*nuoK*	NE1767	**-2.1**	Neut_0932	**-2.2**
NADH-quinone oxidoreductase subunit H	*nuoH*	NE1770	**-2.0**	Neut_0929	-1.6
NADH-quinone oxidoreductase subunit D	*nuoD*	NE1774	1.2	Neut_0925	1.1
NADH-quinone oxidoreductase subunit C	*nuoC*	NE1775	**1.8**	Neut_0924	1.3
NADH-quinone oxidoreductase subunit I	*nuoI*	NE1769	**-1.9**	Neut_0930	-1.1
NADH-quinone oxidoreductase subunit B	*nuoB*	NE1776	**2.1**	Neut_0923	1.4
NADH-quinone oxidoreductase subunit E	*nuoE*	NE1773	1.4	Neut_0926	-1.2
NADH-quinone oxidoreductase subunit F	*nuoF*	NE1772	-1.0	Neut_0927	-1.1
NADH-quinone oxidoreductase subunit G	*nuoG*	NE1771	-1.3	Neut_0928	-1.3

1 Locus tags are based on KEGG nomenclature.

2 Fold changes (FC) of gene expression during exposure phase and pre-exposure phase are calculated using edgeR. Detail is described in Materials and Methods. Values in bold indicate the significant differences (FDR ≤ 0.01) in gene expression between methane exposure phase and pre-exposure phase. Underlined values indicate the significant differences (FDR ≤ 0.05) in gene expression between methane exposure phase and pre-exposure phase.

6.3.3 Carbon fixation and cell growth

All known autotrophic AOB utilize ribulose biphosphate carboxylase/oxygenase (RuBisCO), encodes by the *cbb* operon (Fig 6.2), for CO_2 fixation. The *cbb* operon in *N. europaea* ATCC 19718 is regulated by the *cbbR* gene locates upstream the gene cluster *cbbLSQON* [43]. A 5.8-fold decrease in *cbbR* expression and upregulation (1.6-fold to 7.4 -fold) of the entire *cbb* gene cluster was observed in *N. europaea* ATCC 19718 during methane exposure (Fig 6.2). A similar organization of *cbbR* and *cbb* operon is present in *N. eutropha* C91 with additional genes encoding carboxysome locate between *cbbS* and *cbbQ* [34]. In contrast to the expression of *cbb* operon in *N. europaea* ATCC 19718, reduced transcript levels of *cbbQO* (-1.7 to -1.8-fold) and genes for carboxysome shell protein (*csoS1A/S1B*, ~1.5-fold reduction) in *N. eutropha* C91 were noticed (Fig 6.2). A further examination of the genes relate carbon fixation (based on KEGG pathway neu00710 and net00710) showed that the disturbance caused by methane exposure was more evident in *N. europaea* ATCC 19718 than in *N. eutropha* C91 (Table 6.3). In *N. europaea* ATCC 19718, two genes that encode proteins function preceding RuBisCO (*cbbP*, -2.2-fold) and succeeding RuBisCO (*cbbG*, -2.0-fold) were downregulated and three genes were upregulated (*cbbF*, *cbbJ*, *xfp*, ~2-fold). On the other hand, while *cbbF* transcript level *in N. eutropha* C91 also demonstrated a 2.2-fold increase, *cbbK* and *cbbT* transcript levels were increasing and no genes were downregulated (Table 6.3).

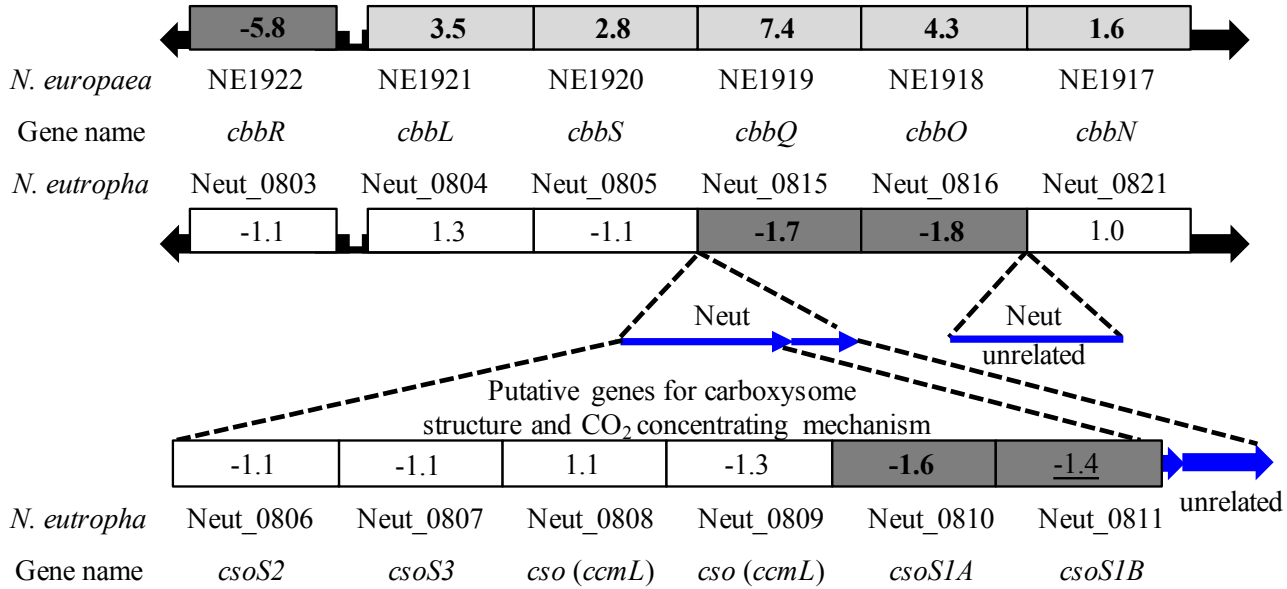

Figure 6.2. Genes involve in *cbb* operon (adapted from Stein et al., 2007[34]). Numbers represent expression fold change (normalized with gene expression during pre-exposure phase) of each gene during methane exposure phase. Values in bold indicate the significant differences with FDR ≤ 0.01 and underlined values indicate the significant differences with FDR ≤ 0.05. Blocks in dark gray or light gray indicate down-regulation or up-regulation, respectively.

Table 6.3. Genes relate to carbon fixation (based on KEGG pathways neu00710 and net00710). Genes for *cbb* operon and carboxylsome are illustrated in Figure 6.2.

Gene product	Gene name	*N. europaea* ATCC 19718		*N. eutropha* C91	
		Locus tag[1]	FC[2]	Locus tag[1]	FC[2]
Phosphoglycerate kinase	*cbbK, pgk*	NE0326	-1.1	Neut_1579	**1.5**
Glyceraldehyde 3-phosphate dehydrogenase	*cbbG*	NE0327	**-2.0**	Neut_1578	1.3
				Neut_0333	-1.2
Fructose-bisphosphate aldolase	*cbbA, fba*	NE0324	-1.3	Neut_1996	-1.0
				Neut_1581	1.4
Fructose-1,6-bisphosphatase/sedoheptulose-1,7-bisphosphatase	*cbbF, fbp*	NE0521	**2.0**	Neut_1176	**2.2**
Transketolase	*cbbT, tkl*	NE0328	1.3	Neut_1577	**2.0**
Ribose 5-phosphate isomerase	*cbbI,ppi,*	NE1743	1.3	Neut_1829	1.1
Phosphoribulokinase	*cbbP, prk*	NE1474	**-2.2**	Neut_0772	1.1
Triosephosphate isomerase	*cbbJ, tpiA*	NE1779	**1.9**	Neut_0920	1.2
Fructose-6-phosphate phosphoketolase	*xfp*	NE2135	**1.9**	Neut_2087	1.1
Ribulose-phosphate 3-epimerase	*cbbE*	NE2148	1.3	Neut_2096	1.2
Phosphoglycolate phosphatase	*cbbZ, pgp*	NE2149	1.1	Neut_2097	-1.0

1 Locus tags are based on KEGG nomenclature.

2 Fold changes (FC) of gene expression between methane exposure phase and pre-exposure phase. Values in bold indicate the significant differences (FDR ≤ 0.01) in gene expression between methane exposure phase and pre-exposure phase.

Table 6.4. Genes involved in ell division (*fts* genes) and peptidoglycan elongation.

Gene product	Gene name	*N. europaea* ATCC 19718		*N. eutropha* C91	
		Locus tag[1]	FC[2]	Locus tag[1]	FC2
Cell division checkpoint GTPase YihA	*yihA*	NE2458	**1.6**	Neut_0234	**1.8**
DNA translocase FtsK	*ftsK*	NE1051	**-2.5**	Neut_2488	**-1.8**
Cell division protein FtsZ	*ftsZ*	NE0997	1.3	Neut_0240	**-1.8**
Cell division protein FtsA	*ftsA*	NE0996	-1.1	Neut_0241	**-1.9**
Cell division protein FtsQ	*ftsQ*	NE0995	-1.6	Neut_0242	**-2.1**
Cell division protein FtsB	*ftsB*	NE1043	**-2.4**	Neut_2481	1.2
Cell division protein FtsL	*ftsL*	NE0984	-1.6	Neut_0253	-1.4
Cell division-specific peptidoglycan biosynthesis regulator FtsW	*ftsW*	NE0990	**-5.9**	Neut_0247	**-2.9**
Peptidoglycan synthetase FtsI	*ftsI*	NE0985	**-1.7**	Neut_0252	**-1.9**
Signal recognition particle-docking protein FtsY	*pilA*	NE1415	1.1	Neut_1529	1.0
Cell division protein FtsX	*ftsX*	NE1413	**-1.6**	Neut_1527	-1.0
Cell division ATP-binding protein FtsE	*ftsE*	NE1414	-1.3	Neut_1528	-1.0
UDP-N-acetylglucosamine 1-carboxyvinyltransferase	*murA*	NE1852	1.2	Neut_1556	1.1
UDP-N-acetylmuramate dehydrogenase	*murB*	NE0993	**-4.6**	Neut_0244	**-6.9**
UDP-N-acetylmuramate--L-alanine ligase	*murC*	NE0992	**-5.6**	Neut_0245	**-3.1**
UDP-N-acetylmuramoylalanine--D-glutamate ligase	*murD*	NE0989	**-4.6**	Neut_0248	**-2.7**
UDP-N-acetylmuramoylalanyl-D-glutamate--2, 6-diaminopimelate ligase	*murE*	NE0986	**-2.8**	Neut_0251	**-2.6**
D-alanine--D-alanine ligase	*ddlB*	NE0994	**-7.4**	Neut_0243	**-2.9**
UDP-N-acetylmuramoyl-tripeptide--D-alanyl-D-alanine ligase	*murF*	NE0987	**-4.5**	Neut_0250	**-2.8**
Phospho-N-acetylmuramoyl-pentapeptide-transferase	*mraY*	NE0988	**-3.8**	Neut_0249	**-2.7**
UDP-N-GlcNAc--lipid intermediate I N-acetylglucosamine transferase	*murG*	NE0991	**-6.2**	Neut_0246	**-2.8**

1 Locus tags are based on KEGG nomenclature.

2 Fold changes (FC) of gene expression during exposure phase and pre-exposure phase. Values in bold indicate the significant differences with FDR ≤ 0.01 and underlined values indicate the significant differences with FDR ≤ 0.05 in response to methane exposure.

Table 6.5. Candidate genes involved in methanol metabolism.

Gene product	*N. europaea* ATCC 19718			*N. eutropha* C91		
	Locus tag[2]	RPKM[3]	FC[4]	Locus tag[2]	RPKM[3]	FC[4]
Alcohol dehydrogenase, zinc-binding domain protein	NE0907[5]	283	**2.77**	Neut_1385[5]	468	**1.49**
S-formylglutathione hydrolase	NE0908[5]	336	**2.27**	Neut_1386[5]	574	**2.30**
Formate and nitrite transporters[1]	NE0680	589	1.40	Neut_1877	123	**2.55**
Putative transmembrane protein[1]	NE0681	837	-1.43	Neut_1878	147	**3.67**
Zinc-containing alcohol dehydrogenase superfamily	NE0742	408	-1.27	N/A		
Iron-containing alcohol dehydrogenase	NE0620	171	1.26	N/A		
Zinc-containing alcohol dehydrogenase superfamily	NE0820	224	-1.10	N/A		
Alcohol dehydrogenase, zinc-binding domain protein	N/A			Neut_1071	126	-1.40

1 Gene products for NE0680 and Neut_1878 are formate/nitrite transporter. Gene product for NE0681 and Neut_1877 are putative transmembrane protein.

2 Locus tags are based on KEGG nomenclature.

3 RPKM values are the average RPKM of two biological replicates during pre-exposure phase.

4 Fold changes (FC) of gene expression during exposure phase and pre-exposure phase are calculated using edgeR. Detail is described in Materials and Methods. Values in bold indicate the significant differences (FDR ≤ 0.01) in gene expression between methane exposure phase and pre-exposure phase.

5 Based on KEGG pathways neu00680 and net00680.

While cell washout was observed during methane exposure for both strains, the expression of genes involve in carbon fixation only showed moderate reduction (Fig 6.2 and Table 6.3). As we further examined the metabolic pathways involve in cell replication, we found that the expressions of genes for cell division and peptidoglycan biosynthesis, which are largely clustered together in *N. europaea* ATCC 19718 and *N. eutropha* C91 (NE0984-NE0997 and Neut_0240-Neut_0253), were negatively affected in response to methane (Table 6.4). For both *N. europaea* ATCC 19718 and *N. eutropha* C91, ~1.7-fold upregulation of *yihA* expression, a crucial gene for proper cell division [173], were noted while other partner genes for cell division showed either no significant changes or up to 5.9-fold downregulation (Table 6.3). Moreover, 8 out of 9 genes participate in peptidoglycan elongation were downregulated in *N. europaea* ATCC 19718 (-2.8 to -7.4-fold) and *N. eutropha* C91 (-2.6 to -6.9-fold) (Table 6.3).

6.3.4 Candidate genes related to further methanol metabolism

The oxidation of methane to methanol by AMO in AOB has been well documented and widely discussed [174]. However, the further oxidation or metabolism of methanol remains unclear. The alcohol dehydrogenase and the immediately downstream gene (NE0907-NE0908 and Neut_1385-Neut_1386) are candidates involve in methanol metabolism (based on KEGG neu00680 and net00680) and our results showed that these genes are upregulated in *N. europaea* ATCC 19718 (2.3 to 2.8-fold) and *N. eutropha* C91 (1.5 to 2.3-fold) during methane exposure. No significant changes were observed for other possible alcohol dehydrogenase superfamily genes present in *N.*

europaea ATCC 19718 or *N. eutropha* C91 (Table 6.5). Furthermore, the transcript levels of genes encode formate/nitrite transpoter gene cluster in *N. eutropha* C91 (Neut_1877-Neut_1878) also showed up to 3.7-fold increase in response to methane exposure but not in *N. europaea* ATCC 19718 (NE0680-NE0681).

6.4 Discussion

6.4.1 Transcriptional regulation of *amoA* in response to elevated ammonia concentrations caused by methane exposure

The expression of *amoA* has been used as an indicator for AOB activity [175]. It has been proposed that ammonia could be the signaling molecule that induces *amoA* expression in *N. europaea* ATCC 19718 [42, 176]. However, other studies have demonstrated that high ammonia concentrations did not necessarily lead to elevated *amoA* expression in *N. europaea* ATCC 19718 [114] and decrease in *amoA* expression was observed during instantaneous spikes of ammonia into chemostat *N. eutropha* C91 culture (Ma et al., unpublished data). Our results also showed that the expression of *amoA* was reduced after 24 hour of methane exposure (Table 6.1), during which ammonia concentrations were increasing from < 8 mg NH_3-NL^{-1} to > 20 mg NH_3-NL^{-1} in both strains (refer to previous chapters). An intriguing hypothesis proposed by Perez-Garcia et al. (2014)[158], in combination with the observation by Yu et al. (2010)[114], is that during high ammonia concentrations, the specific AMO activity approaches the maximum activity, which results in overproduction of electrons and NO/N_2O production. The transcriptional results further suggest that reducing *amoA*

expression could be part of the strategy to manage overproduction of electrons.

6.4.2 Re-balanced electron flows and the impact on NADH synthesis

During normal physiological state (pre-exposure period), the electron fluxes toward AMO (for NH_3 oxidation) : Complex III/IV (for proton motive force generation) : Complex I (for NADH synthesis) should be approximately 1.00 : 0.88 : 0.12 [177]. The presence of methane could lead to an unexpected "leak" of electrons used for methane oxidation, which consumes part of the electrons that are directed to AMO and induces the signal to re-balance the electron flux. Furthermore, the balance seems to be tightly regulated since that the disturbance was not relieved during the rapid increase in ammonia concentration which supposed to outcompete methane which has lower AMO affinity than ammonia [16, 24]. Our results showed that both strains reduced the expressions of NADH-quinone oxidoreductase subunits genes (Table 6.2), which indicate less electrons are to be directed to Complex I. The elevated transcript levels of genes encode cytochrome bc1 complex in *N. eutropha* C91 and genes relate to cytochrome c552, *nirK* gene cluster, and sNOR gene cluster in both strains (Table 6.1) also imply a higher demand for these intermediate electron carries or alternative electron acceptors. On the other hand, the upregulation of genes for cytchomr bc1 complex in *N. eutropha* C91 might indicate the tendency to attract more electrons toward Complex III. This re-balanced partitioning of electrons should not be confused with the responses to electron overflow discussed in previous section.

What are other possible regulators for the partitioning of electron flux? The

highly responsive *ncyA* expression to changes in cellular energy status in *Nitrosococcus oceani*, a marine AOB, suggested that NcyA, which is encoded by *ncyA*, as a regulatory switch for electrons flow into and out of the quinone pool [134]. Nitrosocyanin has been found only in AOB and is suggested to be important for ammonia catabolism. During chemostat operation when ammonia was the only substrate, the high RPKM values of *ncyA* (top 1% in both strains) also suggested their critical roles in AOB (Table 6.1). Nevertheless, it has been proposed previously that NcyA might be involved in mediating NOx toxicity [149] but no direct evidence shows how nitrosocyanin actually participates in AOB metabolism. While we observed the induction of *ncyA* expression in *N. europaea* ATCC 19718, the transcript level of *ncyA* in *N. eutropha* C91 remained unchanged during methane exposure. Also as the results showed that the expression levels of cNOR-related genes were downregulated in *N. europaea* ATCC 19718 (Table 6.1), NcyA might serve as an alternative for cNOR. Therefore, the function of NcyA remains unresolved.

6.4.3 Energy molecules and organic molecules synthesis

As the downregulation of genes involved in NADH-quinone oxidoreductase indicate the negative impact of methane exposure on NADH production, *N. eutropha* C91 (6/14 NADH-related genes were affected at FDR $\leq$ 0.05) was less affected than *N. europaea* ATCC 19718 (10/14 NADH-related genes were affected at FDR $\leq$ 0.05) (Table 6.2). On the other hand, the upregulation of genes involved in ATP synthase subunits were more evident in *N. eutropha* C91 (6/8 genes at FDR $\leq$ 0.05) than *N.*

europaea ATCC 19718 (3/8 genes at FDR ≤ 0.05) (Table 6.2). Furthermore, the reduced transcript levels of genes encode cbb3-type and bo3-type terminal oxidase in *N. eutorpha* indicate the tendency to use aa3-type cytochrome c oxidase, which has higher proton pump activity than other terminal oxidases [178], for proton motive force generation (Table 6.1).

Carbon fixation via the carbon cycle is an energy-demanding process and the expression of *cbb* operon appears to be responsive to the energy state of the cells [179]. It has been demonstrated that he transcription of *cbb* operon is dependent on cellular energy status in *N. europaea* ATCC 19718 as indicated by the detection of *cbbLS* transcripts only when energy source (ammonia or hydroxylamine) was provided [43]. In that case, our transcription data of stable *cbbLS* expression in *N. eutropha* C91 or increasing *cbbLS* transcript levels in *N. europaea* ATCC 19718 suggest that the cells were not under energy-deficient condition (Fig 6.2), despite that genes related to NADH production were downregulated (Table 6.2). On the other hand, although carbon fixation appears to be active during methane exposure, the genes involved in biosynthesis of key organic molecules such as peptidoglycan were downregulated in both strains (Table 6.4). For *N. europaea* ATCC 19718, the genes for aromatic amino acids and lipids biosynthesis were also downregulated (Table S6.2 and Table S6.3). It could be possible that the synthesis organic molecules in AOB are regulated by the variation of ATP but not NADH. As *N. eutropha* C91 switches the dependency toward aa3-type cytochrome c oxidase, a more efficient PMF can be generated and contribute to ATP production, thus quickly adapt to the presence of methane and sustain organic

molecules synthesis. However, this hypothesis requires further experimental examination. Also, the contradictory mRNA trends between stable or increasing expression of genes related to CO_2 fixation and downregulation of genes synthesis involved in cellular macromolecules synthesis suggest that indicators in addition to genes or enzymes relate to CO_2 fixation (*cbb* operon or carbonic anhydrase [53, 54]) should be considered when interrogating AOB anabolism.

6.4.4 Possible methanol metabolism in AOB

In addition to methane oxidation ability, other genes involved in methane metabolism are categorized in KEGG pathway (neu00680 and net00680). While the methane to methanol conversion is catalyzed by AMO, two enzymes might be catalyzing the downstream methanol metabolism (NE0907/NE0908, Neut_1385/Neut_1386) have been identified. Previous reports also showed the detection of formaldehyde and formate when *N. europaea* was incubated with methanol [28]. Alcohol dehydrogenase (ADH, NE0907 and Neut_1385) possibly catalyze methanol to formaldehyde conversion, then glutathione (GSH) and formaldehyde can form S-(Hydroxymethyl)-glutathione spontaneously. S-(Hydroxymethyl)-glutathione can be further converted to formate by ADH and S-formylglutathione hydrolase (NE0908 and Neut_1386). The upregulation of a formate/nitrite transporter gene and its potential functional partner in *N. eutropha* C91 further indicate methanol might be converted to formate and being exported (Table 6.5). Though increasing transcript levels were observed for these genes, it should be noted that NE0907/NE0908 and

Neut_1385/Neut_1386 also participate in other carbon metabolic pathways. Therefore, other direct measurements such as aqueous formaldehyde or formate concentrations should be considered in order to conclude methanol metabolic pathway in AOB.

6.5 Conclusions

The primary focus of this study is to determine the global transcriptional responses of two common AOB during methane exposure. To our knowledge, this is the first study to investigate AOB cometabolism in continuous flow reactors. While accumulating studies have been working on AMO-catalyzed cometabolic enzymatic reactions and biokinetics characterization [159, 180], we would like to extend our knowledge of cometabolism using systems biology approach and further understand the underlying mechanisms. The key findings from this study are that (1) *N. europaea* ATCC 19718 is more sensitive to methane exposure than the closely related *N. eutropha* C91; (2) *N. europaea* ATCC 19718 and *N. eutropha* C91 regulate their ETC differently during methane exposure but appear to apply similar strategy to control ATP/NADH synthesis; (3) *N. eutropha* C91 depends more on aa3-type cytochrome c oxidase during methane exposure; (4) a systematic decrease in the transcription of division/cell wall (dcw) gene cluster is observed during methane exposure for both strains. The whole transcriptome analysis offers a comprehensive and detailed view regarding methane metabolism in AOB and reveals considerable differences for *N. europaea* ATCC 19718 and *N. eutropha* C91 in response to methane.

6.6 Supporting information

The supporting information include (1) Comparisons of *N. europaea* ATCC 19718 and *N. eutropha* C91 genome inventories relate to nitrogen metabolism and regulation, electron transport chain, and terminal oxidase (2) Summary table for comparative transcriptome analysis of *N. europaea* ATCC 19718 and *N. eutropha* C91 (3) Summary table for enes related to stress response mechanisms, mer operon, and fatty acid biosynthesis (4) Summary table for genes involve in cytochrome c maturation (ccm) system.

6.6.1 Comparison of genes involved in nitrogen metabolism and electron transport chain between *N. europaea* ATCC 19718 and *N. eutropha* C91.

AOB which survive in s specific niche in the environment possess multiple copies of *amo* operon and *hao* gene cluster to extract reducing equivalents form ammonia for energy synthesis. The genome information has revealed the location and orientation of the genes on the chromosome and allowed side by side comparison of structural genes in different copies. Table S6.5 summarizes the gene inventory related to ammonia oxidation, N-oxide metabolism, and terminal oxidases in both strains [181]. Gene clusters related to AMO (two *amoCABED* copies and a single *amoC3* gene) and HAO (two *haoAB-cycAB* copies and one *haoAB-ycyA* cluster) are highly similar between *N. europaea* ATCC 19718 and *N. eutropha* C91 [34]. Table S6.6 compares the sequences of *amoCABED* and *haoAB* genes in *N. europaea* ATCC 19718 and *N. eutropha* C91 separately in order to properly present the RNA-seq data in Table 6.1.

Table S6.1. Summary of transcriptome changes during methane exposure phase (with pre-exposure phase as baseline).

Name	*N. europaea* ATCC 19718	*N. eutropha* C91
Number of coding sequences	2623	2687
Up-regulation	273	144
No change	2038	2211
Down-regulation	230	99

* Up- or down-regulation are defined as |gene expression fold change| ≥ 2 and FDR ≤ 0.01.

Table S6.2. Genes related to stress response mechanisms and *mer* operon, and fatty acid biosynthesis.

	Gene product	Gene name	*N. europaea* ATCC 19718		*N. eutropha* C91	
			Locus tag	FC	Locus tag	FC
Stress response	Protein GrpE (HSP-70 cofactor)	*grpE*	NE1950	**35.1**	Neut_0411	**7.9**
	PpiC-type peptidyl-prolyl cis-trans isomerase	*ppiD*	NE2206	1.3	Neut_0662	**1.5**
	Heat shock protein HtpG	*htpG*	NE1762	**32.3**	Neut_0937	**2.3**
	Chaperone protein DnaK (HSP70)	*dnaK*	NE1949	**87.8**	Neut_0412	**6.6**
	60 kDa chaperonin (Protein Cpn60)	*groEL*	NE0028	**23.6**	Neut_0206	**8.9**
	Heat shock hsp20 (Alpha crystallin) proteins family	*hsp20*	NE2074	**113.2**	Neut_1596	**5.9**
	DnaJ N-terminal domain:DnaJ C terminal domain	*dnaJ*	NE1155	**-1.8**	Neut_1445	1.4
	ATP-dependent zinc metalloprotease FtsH	*hflB*	NE0528	**7.3**	Neut_0998	**2.1**
	ATP-dependent zinc metalloprotease FtsH	*ftsH*	NE0906	**3.8**	Neut_1384	-1.2
	ClpA, ATP dependent protease, chaperonin	*clpA*	NE1733	**2.6**	Neut_2048	**1.6**
	ATP-dependent Clp protease ATP-binding subunit ClpX	*clpX*	NE0032	**3.9**	Neut_0202	**1.7**
	ATP-dependent Clp protease proteolytic subunit	*clpP*	NE0031	**2.5**	Neut_0203	**1.9**
	Chaperone protein ClpB	*clpB*	NE2402	**59.2**	Neut_0734	**8.8**
	ATP-dependent protease ATPase subunit HslU	*hslU*	NE2261	1.2	Neut_0611	1.2
	ATP-dependent protease subunit HslV (EC 3.4.25.2)	*hslV*	NE2260	**2.0**	Neut_0612	**1.9**
	Lon protease (ATP-dependent protease La)	*lon*	NE0033	**2.4**	Neut_0201	1.2
	Lon protease (ATP-dependent protease La)	*lonA*	NE1278	**141.3**	Neut_0970	**4.2**
	Serine proteases, subtilase family	NE1183	NE1183	**1.6**	N/A	

	Htra-like serine protease signal peptide protein	NE1508	NE1508	1.1	N/A	
	Serine proteases, trypsin family	*mucD*	NE0379	**-1.8**	Neut_1783	**1.5**
	MucD serine protease MucD	*mucD*	NE2329	**3.1**	Neut_1783	**1.5**
	Carboxy-terminal processing protease	NE1782	NE1782	**2.2**	Neut_0917	1.3
	Protease HtpX homolog	*htpX*	NE1421	**38.0**	Neut_1535	**4.2**
mer operon	Bacterial regulatory proteins, MerR family	*merR*	NE0843	1.9	Neut_1305	1.67
	MerT mercuric transport protein	*merT*	NE0842	**11.8**	Neut_1306	1.88
	Mercury scavenger protein:Heavy-metal-associated domain	*merP*	NE0841	**152.9**	Neut_1307	2.25
	Putative mercury transport protein	*merC*	NE0840	**39.1**	Neut_1308	-2.31
	Mercuric reductase	*merA*	NE0839	**12.7**	Neut_1309	-1.09
	Bacterial regulatory proteins, MerR family	*merD*	NE0838	**11.0**	Neut_1310	ND
	Mercuric reductase	*merA*	N/A		Neut_2567	-1.21
	MerC mercury resistance protein	*merC*	N/A		Neut_2568	-1.47
	Mercuric transport protein MerT	*merT*	N/A		Neut_2570	2.07
	Bacterial regulatory proteins, MerR family	*merR*	N/A		Neut_2571	1.53
	Bacterial regulatory proteins, MerR family	*merR*	N/A		Neut_0034	2.39
	Mercuric transport protein MerT	*merT*	N/A		Neut_0033	2.72
	Mercuric transport protein periplasmic component	*merP*	N/A		Neut_0032	2.66
	MerC mercury resistance protein	*merC*	N/A		Neut_0031	-12.86
	Mercuric reductase	*merA*	N/A		Neut_0030	-1.76
	Bacterial regulatory proteins, MerR family	*merD*	N/A		Neut_0029	1.08

Fatty acid synthesis	Carboxyl transferase, alpha subunit	*accA*	NE1021	-1.1	Neut_2398	**2.1**
	Biotin carboxyl carrier protein of acetyl-CoA carboxylase	*accB1*	NE0652	1.3	Neut_1900	-1.1
	Biotin carboxylase protein	*accC1*	NE0653	-1.3	Neut_1899	-1.2
	Acetyl-CoA carboxylase carboxyl transferase beta subunit	*accD*	NE0695	-1.3	Neut_1154	1.2
	Malonyl CoA-acyl carrier protein transacylase	*fabD*	NE1647	**-1.8**	Neut_0469	-1.4
	3-oxoacyl-[acyl-carrier-protein] synthase III	*fabH*	NE1646	**-1.5**	Neut_0470	-1.1
	Beta-ketoacyl synthase	*fabF*	NE1650	**-2.5**	Neut_0466	1.1
	3-oxoacyl-[acyl-carrier protein] reductase	*fabG*	NE1648	**-2.3**	Neut_0468	-1.2
	Bacterial thioester dehydrase	*fabZ*	NE1708	**-3.1**	Neut_2025	-1.3
	Enoyl-[acyl-carrier protein] reductase I		NE2205	-1.0	Neut_0663	1.3
	AMP-dependent synthetase and ligase		NE1549	**-2.5**	Neut_0702	**-1.8**
	AMP-dependent synthetase and ligase		NE2235	**-1.6**	N/A	

1 Gene names are primarily based on genes present in *N. europaea* ATCC 19718 genome.

2 Locus tags are based on KEGG nomenclature.

3 Fold changes (FC) of gene expression during exposure phase and pre-exposure phase. Values in bold indicate the significant differences (FDR ≤ 0.01) in response to methane exposure.

4 N/A: no corresponding gene in the genome. ND: not detected.

Table S6.3. Genes involved in aromatic amino acids biosynthesis.

Gene product	Gene name	*N. europaea* ATCC 19718		*N. eutropha* C91	
		Locus tag	FC[1]	Locus tag	FC[1]
HIT (Histidine triad) family	*hitA*	NE0640	1.2	Neut_1912	1.1
Phosphoribosyl-ATP pyrophosphohydrolase	*hisE*	NE0641	1.3	Neut_1911	1.3
Phosphoribosyl-AMP cyclohydrolase	*hisI*	NE0642	1.0	Neut_1910	-1.3
Imidazoleglycerol-phosphate synthase	*hisF*	NE0643	**-3.3**	Neut_1909	-1.2
Phosphoribosylformimino-5-aminoimidazole carboxamide ribotide isomerase	*hisA*	NE0644	**-1.7**	Neut_1908	1.2
Glutamine amidotransferase class-I	*hisH*	NE0645	**-1.6**	Neut_1907	-1.1
Imidazoleglycerol-phosphate dehydratase	*hisB*	NE0646	**-1.5**	Neut_1906	1.0
Aminotransferases class-I	*hisC*	NE0647	-1.3	Neut_1905	-1.1
ATP phosphoribosyltransferase	*hisG*	NE0871	-1.4	Neut_1205	-1.2
Histidinol dehydrogenase	*hisD*	NE0872	**-2.5**	Neut_1206	-1.3
Aminotransferases class-I	*hisC2*	NE0336	**-1.6**	Neut_1569	1.0
3-dehydroquinate synthase	*aroB*	NE1981	**-1.8**	Neut_0381	-1.2
Dehydroquinase class II	*aroQ1*	NE0651	**-1.6**	Neut_1901	-1.1
Shikimate / quinate 5-dehydrogenase	*aroE1*	NE1627	**-2.1**	Neut_0496	-1.3
Shikimate kinase	*aroK*	NE1980	-1.1	Neut_0382	1.0
EPSP synthase (3-phosphoshikimate 1-carboxyvinyltransferase)	*aroA*	NE1964	**-2.8**	Neut_0398	-1.1
Chorismate synthase	*aroC*	NE1877	1.4	Neut_1957	1.2

Prephenate dehydratase	*aroQ/pheA*	NE0335	**-2.0**	Neut_1570	-1.1
Prephenate dehydrogenase	*tyrA*	NE0337	**-2.2**	Neut_1568	-1.1
panthranilate synthase component II	*trpG*	NE0014	**2.5**	Neut_0135	**1.6**
Anthranilate synthase component I	*trpE*	NE2150	**2.1**	Neut_2098	1.5
phosphoribosylanthranilate transferase	*trpD*	NE0013	**-1.9**	Neut_0134	-1.2
N-(5'phosphoribosyl)anthranilate isomerase	*trpF*	NE0692	1.1	Neut_1151	**1.8**
Indole-3-glycerol phosphate synthase	*trpC*	NE0012	**-1.6**	Neut_0133	1.5
Tryptophan synthase, beta chain	*trpB*	NE0693	1.3	Neut_1152	**1.6**
Tryptophan synthase (alpha chain) protein	*trpA*	NE0694	-1.2	Neut_1153	1.3

1 Fold changes (FC) of gene expression during exposure phase and pre-exposure phase. Values in bold indicate the significant differences (FDR ≤ 0.01) in response to methane exposure.

Table S6.4. Genes involve in cytochrome c maturation (ccm) system.

Gene product	Gene name	*N. europaea* ATCC 19718		*N. eutropha* C91	
		Locus tag	FC[1]	Locus tag	FC[1]
ABC superfamily, heme exporter protein A	*ccmA*	NE0764	**1.6**	Neut_0063	3.2
ABC transporter, permease domain, heme exporter protein B	*ccmB*	NE0765	1.4	Neut_0062	-3.1
ABC transporter, permease domain, heme exporter protein C	*ccmC*	NE0766	**2.0**	Neut_0061	-1.7
CcmE/CycJ proteins	*ccmE*	NE0767	**7.5**	Neut_0060	-8.4
Cytochrome c-type biogenesis protein CcmF	*ccmF*	NE0768	**4.5**	Neut_0059	1.4
Periplasmic protein thiol:disulfide oxidoreductase DsbE	*ccmG*	NE0769	**2.5**	Neut_0058	-2.1
Putative cytochrome C-type biogenesis protein CcmH	*ccmH*	NE0770	**1.9**	Neut_0056	-1.5
Cytochrome C biogenesis protein TPR repeat	*ccmI*	NE0771	**1.8**	Neut_0057	2.5
Thioredoxin:Cyt c biogenesis protein transmembrane region	*dsbD*	NE2389	**2.8**	Neut_0846	1.1
Heme exporter protein CcmA	*ccmA*	N/A		Neut_1643	**1.9**
Heme exporter protein CcmB	*ccmB*	N/A		Neut_1642	1.5
Heme exporter protein CcmC	*ccmC*	N/A		Neut_1641	1.3
CcmE/CycJ protein	*ccmE*	N/A		Neut_1639	**4.5**
Cytochrome c-type biogenesis protein CcmF	*ccmF*	N/A		Neut_1638	**2.2**
Periplasmic protein thiol:disulfide oxidoreductase DsbE	*ccmG*	N/A		Neut_1637	**1.7**
Cytochrome C biogenesis protein	*ccmH*	N/A		Neut_1636	**1.5**
Tetratricopeptide TPR_2 repeat protein	*ccmI*	N/A		Neut_1635	**1.7**

1 Fold changes (FC) of gene expression during exposure phase and pre-exposure phase. Values in bold indicate the significant differences

(FDR ≤ 0.01) in gene expression between methane exposure phase and pre-exposure phase.

Table S6.5. Gene inventory with implications in ammonia oxidation, N-oxide metabolism and terminal oxidase in *N. europaea* ATCC 19718 and *N. eutropha* C91 genome (adopted from Arp et al., 2007 [181] and Kozlowski et al., 2016 [39]).

Enzyme and its associated partners	*N. europaea* ATCC 19718	*N. eutropha* C91
Ammonia monooxygenase	*amoCAB*ED (NE945-940, NE2064-2060) *amoC3* (NE1411)	*amoCAB-orf4,5* (Neut_2078-2074, Neut_2319-2315) *amoC3* (Neut_1520)
Hydroxylamine oxidoreductase	*haoAB-cycAB* (NE0962-0959, NE2339-2336) haoAB-cycA (NE2044-2042)	*haoAB-cycAB* (Neut_2335-2332, Neut_1793-1790) haoAB-cycA (Neut_1672-1670)
Nitrite reductase	*ncgBCA-nirK* (NE0927-0924)	ncgBCA-*nirK* (Neut_1406-1403)
Nitric oxide reductases (cNOR)	*norCBQD* (NE2003-2006)	*norCBQD* (Neut_0518-0521)
Cytochrome c'-beta	*cytS* (NE0824)	Neut_1345
Cytochrome P460	*cyp* or *cytL* (NE0011)	Neut_0132
Cytochrome c oxidase aa_3 (NO reductase, sNOR)	senC (NE0682) norY (NE0683), norS (NE0684)	senC (Neut_1876) norY (Neut_1875), norS (Neut_1874)
Nitrosocyanin	ncyA (NE0143)	Neut_2173
Nitrite-sensitive transcription repressor (nirK gene cluster regulator)	*nsrR* (NE0928)[2]	*nsrR* (Neut_1407)
NO-responsive transcriptional regulator	nnrS (NE1722)[1,3]	Neut_1938[3]
Cytochrome c oxidase (aa_3-type)	coxA (NE1016), coxB (NE1017)	Neut_2394, Neut_2395

	coxC (NE1013), ctaG (NE1015)	Neut_2392, Neut_2393
Quinol oxidase (bo_3-type)	N/A	Neut_694-697
Cytochrome c oxidase (cbb_3-type)	N/A	Neut_1582-1585

1 Based on Kozlowski et al (2016).

2 Based on Beaumont et al (2004).

3 Both Neut_1938 (Stein et al, 2007) and NE1722 (Chain et al, 2003) belong to Fur (ferric uptake regulator) family. Assigned to NE0926 in Kozlowski et al (2016)

Table S6.6. Sequence comparison of *amoCABED* and *haoAB* genes in *N. europaea* ATCC 19718 and *N. eutropha* C91.

Gene	*N. europaea* ATCC 19718		*N. eutropha* C91	
	Locus tag	Identity	Locus tag	Identity
amoC	0945/2064	805/816 (98.7%)	2078/2319	816/816 (100%)
amoA	0944/2063	831/831 (100%)	2077/2318	831/831 (100%)
amoB	0943/2062	1263/1263 (100%)	2076/2317	1265/1266 (99.9%)
amoE	0942/2061	636/636 (100%)	2075/2316	567/573 (99.0%)
amoD	0941/2060	553/555 (99.6%)	2074/2315	581/588 (98.8%)
haoA	0962/2044/2339	1713/1713/1713 (100%)	2335/1793/1672	1708/1705/1713 (> 99.5%)
haoB	0961/2043/2338	1110/1110/1110 (100%)	2334/1792/1671	1115/1113/1122 (> 99.1%)

CHAPTER 7

Concluding Remarks

In this research, we build upon previous axenic and mixed culture batch studies and extend the knowledge of methane cometabolism in AOB using molecular biology tools and process engineering approaches. The physiological basis of methane cometabolism in AOB and a platform for continuous biomethanol production using mixed culture nitrifying consortia have been presented.

7.1 Exploitation of AOB cometabolism for biomethanol production

The wide substrate range of AMO allows AOB to oxidize not just ammonia, but also methane, (halogenated) alkanes and alkenes, and aromatic compounds[103]. In this study, we demonstrate a biomethanol production process technology, which takes advantage of the AMO activity for biomethanol production and shows the impacts of HRT and nitrogen sources (as electron donors) on maximum and steady state specific biomethanol production rates. The results indicate that using resources (AOB, ammonia, and methane) available within the WRRFs, biomethanol production is viable. The process model developed from the biomethanol production process is expected to provide information for operational strategies. For example, based on the model prediction (with initial conditions such as AOB, NOB concentrations and HRT being specified), the influent S_{NH3} should be controlled at 10 - 20 mg-NH_3-N L^{-1} in order to have an effluent S_{NH3} at ~1 mgNH_3-N L^{-1}. Concurrently, using the developed process, accumulation of 10 mg-COD-CH_3OH L^{-1} in the production reactor can be

achieved, which can substitute ~11% - 22% of methanol requirement for denitrification (the mg-COD-CH_3OH to mg-NO_3-N ratio can range from 4.1 to 4.8[61, 182] for methanol-based denitrification).

To complement the primary focus of the biomethanol production process using AOB as a catalyst, characterization of AOB during long-term methane exposure was also conducted, to enable further optimization of the biomethanol production process. From the perspective of microbial physiology, our results showed that although methane as a cometabolic substrate competes with the primary energy source (ammonia) for AMO binding site, AOB are capable of regulating the anabolic and catabolic activities in response to the additional electron demand exerted by methane. The increases in specific ammonia oxidation rates observed in *N. eutropha* experiments (~2.7-fold increase) and long-term methane exposure experiments (~2-fold increase) indicate that AOB increase the rates of reducing equivalents generation during methane exposure, possibly to compensate for the additional electron demand exerted by co-oxdiation of methane by AMO. From the perspective of process engineering, the adaptation of AOB leads to the questions such as: what operation parameters should be considered to maintain an active AOB community within the mixed culture nitrifying consortia while optimizing biomethanol production process during long-term methane exposure? One possible factor would be controlling NH_3-to-CH_4 ratio in the reactors (discussed in section 3.4.2) due to the competitive effects between the two substrates. Furthermore, can we improve biomethanol production rates and yields by using adapted AOB in the continuous

process? These questions are possible directions for future studies.

7.2 An integrated platform for concurrent biomethanol production and biological nitrogen removal in WRRFs

In this research, we propose the integration of the biomethanol production process with current BNR processes, possibly by building a methanol production CSTR or by transforming nitrification reactors for simultaneous nitrification and biomethanol production. Assuming all the 4 moles of electrons released during each mole of hydroxylamine oxidation are transferred back to AMO for subsequent ammonia or methane conversion, oxidation of 1 mole of ammonia (14 mg-N) can sustain 1 mole of methanol (48 mg-COD) production. Based on these calculations, integration of the biomethanol production process into conventional BNR schemes can result in up to 20% offsets in external methanol demand based on COD:N ratios for nitrate reduction to N_2 [61, 182]). Recalling also that NOB growth was more significantly impaired by methane exposure, which was not expected (discussed in section 5.5), offers the possibility for partial nitrification, which can further reduce the carbon requirement. Furthermoe, with some reports concerning methane emission from wastewater treatment process[183-185], which contribute up to 13.5% of the total carbon footprint in a case study in the Netherland[186], the biomethanol production platform is expected to reduce methane emission and also recover the nutrient carbon in CH_4 and capture it as methanol. These arguments illustrate the multiple benefits of integrating our biomethanol process for resource recovery and *in-situ* reuse into the current WRRF

model.

7.3 Systems biology associated with nitrogen and carbon metabolism in mixed and pure cultures

While some previous studies[17, 23-25, 28] have established the basis for methane oxidation by AMO, the application of high-throughput sequencing technology for global proteome survey allows us to uncover the metabolic pathways associated with methane cometabolism in AOB. The proteomic analysis showed that *N. europaea* maintains the key proteins involved in nitrogen metabolism (AmoCAB and HAO) at high relative abundance during the presence of methane, an alternative substrate that consumes electrons but not contributes to electron regeneration. At proteomic level, the impacts of methane metabolism on nitrogen metabolism appear to be on the downstream processes. The increasing relative abundances of alternative electron acceptors and decrease in carbon fixation proteins might explain the impacts of methane on AOB growth. At transcription level, the upregulation of genes involved in electron transport chain and ATP production implied that AOB tend to harvest more energy in the form of ATP during methane exposure. However, the downregulation of genes involved in NADH production, organic molecules synthesis, and cell division might have resulted in the negative impacts on AOB anabolism.

From experiments using mixed culture nitrifying consortia, the changes in microbial community revealed by 16S rRNA sequencing provides valuable information about nitrogen- and carbon- associated organisms. The changes in nitrifying communities

(stable AOB fraction and decreasing NOB fraction) are similar between the targeted qPCR data and whole community analysis, and the stabilized S_{NH3} and elevated S_{NO2} in the long-term methane exposure experiment agree with the results. On the other hand, the increasing relative abundances of the potential methanol and other carbon-utilization denitrifying bacteria were not expected. This also implies that methanol produced and excreted by AOB could be further metabolized to support organisms that do not consume methanol directly but that perhaps grew on endogenous metabolites from the methylotrophs. However, we did not observe significant nitrogen loss in our experiment. The reason could be that the operational conditions are not appropriate for the facultative denitrifying bacteria to carry out denitrification. With the information acquired from 16S rRNA sequencing, it is possible to revise the reactor design either to prevent methanol consumption during biomethanol production process or to create an environment appropriate for simultaneous nitrification, biomethanol production, and denitrification.

7.4 Summary

This research was aimed at significantly enhancing past work on cometabolic conversion of organic substrates by AOB. On the fundamental side, this study truly opens up the 'black-box' of AOB cometabolism using systems biology approaches in two model chemolithoautotrophic bacteria. Using the systems approaches, we elucidate the impacts of organic carbon metabolism on catabolism, anabolism, and electron transport pathways in these AOB.

On the practical engineering side, we extend previous proof-of-concept batch reactor technologies for producing biomethanol from methane through the development of continuous reactor technologies. We further examined the factors controlling biomethanol production and evaluated the impacts of long-term methane exposure on mixed culture nitrifying consortia. The high-throughput sequencing technologies for proteome identification or community analysis provided rich information on fundamental microbial physiology and threads for potential use in further process engineering and optimization of AOB-mediated biomethanol production. The information can be used to further optimize the biomethanol production process and to develop more resource-efficient wastewater treatment process.

As the wastewater treatment industry truly transitions towards water resource recovery, it is crucial to go beyond using conventional roles and capabilities of microorganisms in activated sludge processes to perhaps explore ‘what else they can do’. The use of next generation high-throughput sequencing technologies along with a fundamental understanding of microbial systems and metabolism allows us to transcend the limits of conventional scientific understanding and engineering practices to truly harness the true potential of engineered microbial processes and technologies.

References

1. USEPA, Nutrient control design manual. **2010**.
2. Zhu, I.; Getting, T., A review of nitrate reduction using inorganic materials. *Environmental Technology Reviews* **2012,** *1*, (1), 46-58.
3. Guest, J. S.; Skerlos, S. J.; Barnard, J. L.; Beck, M. B.; Daigger, G. T.; Hilger, H.; Jackson, S. J.; Karvazy, K.; Kelly, L.; Macpherson, L.; Mihelcic, J. R.; Pramanik, A.; Raskin, L.; Van Loosdrecht, M. C.; Yeh, D.; Love, N. G., A new planning and design paradigm to achieve sustainable resource recovery from wastewater. *Environmental science & technology* **2009,** *43*, (16), 6126-30.
4. USEPA, Opportunities for Combined Heat and Power at Wastewater Treatment Facilities Market Analysis and Lessons from the Field. **2011**.
5. Kleerebezem, R.; van Loosdrecht, M. C., Mixed culture biotechnology for bioenergy production. *Current opinion in biotechnology* **2007,** *18*, (3), 207-12.
6. Gavazza dos Santos, S.; Amâncio Varesche, M. B.; Zaiat, M.; Foresti, E., Comparison of Methanol, Ethanol, and Methane as Electron Donors for Denitrification. *Environmental Engineering Science* **2004,** *21*, (3), 313-320.
7. Osaka, T.; Ebie, Y.; Tsuneda, S.; Inamori, Y., Identification of the bacterial community involved in methane-dependent denitrification in activated sludge using DNA stable-isotope probing. *FEMS microbiology ecology* **2008,** *64*, (3), 494-506.
8. Waki, M.; Yasuda, T.; Yokoyama, H.; Hanajima, D.; Ogino, A.; Suzuki, K.; Yamagishi, T.; Suwa, Y.; Tanaka, Y., Nitrogen removal by co-occurring methane oxidation, denitrification, aerobic ammonium oxidation, and anammox. *Applied Microbiology and Biotechnology* **2009,** *84*, (5), 977-985.
9. Thalasso, F.; Vallecillo, A.; García-Encina, P.; Fdz-Polanco, F., The use of methane as a sole carbon source for wastewater denitrification. *Water research* **1997,** *31*, (1), 55-60.
10. Ettwig, K. F.; van Alen, T.; van de Pas-Schoonen, K. T.; Jetten, M. S.; Strous, M., Enrichment and molecular detection of denitrifying methanotrophic bacteria of the NC10 phylum. *Applied and environmental microbiology* **2009,** *75*, (11), 3656-62.
11. Kits, K. D.; Klotz, M. G.; Stein, L. Y., Methane oxidation coupled to nitrate reduction under hypoxia by the GammaproteobacteriumMethylomonas denitrificans, sp. nov. type strain FJG1. *Environmental Microbiology* **2015,** *17*, (9), 3219-3232.
12. Raghoebarsing, A. A.; Pol, A.; van de Pas-Schoonen, K. T.; Smolders, A. J.; Ettwig, K. F.; Rijpstra, W. I.; Schouten, S.; Damste, J. S.; Op den Camp, H. J.; Jetten, M. S.; Strous, M., A microbial consortium couples anaerobic methane oxidation to denitrification. *Nature* **2006,** *440*, (7086), 918-21.
13. Modin, O.; Fukushi, K.; Yamamoto, K., Denitrification with methane as external carbon source. *Water research* **2007,** *41*, (12), 2726-2738.
14. Corder, R. E.; Johnson, E. R.; Vega, J. L.; Clausen, E. C.; Gaddy, J. L., Biological Production of Methanol from Methane. *Abs Pap Am Chem Soc* **1988,** *196*, 231-234.
15. Ge, X.; Yang, L.; Sheets, J. P.; Yu, Z.; Li, Y., Biological conversion of methane to liquid fuels: status and opportunities. *Biotechnology advances* **2014,** *32*, (8), 1460-75.
16. Hyman, M. R.; Wood, P. M., Methane oxidation by Nitrosomonas europaea. *The*

Biochemical journal **1983,** *212*, (1), 31-7.
17. Hyman, M. R.; Murton, I. B.; Arp, D. J., Interaction of Ammonia Monooxygenase from Nitrosomonas europaea with Alkanes, Alkenes, and Alkynes. *Applied and environmental microbiology* **1988,** *54*, (12), 3187-90.
18. Wang, L.; Tabata, K.; Kamachi, T.; Okura, I., Effect of Electron Donor on Methanol Production by Ammonia-oxidizing Bacterium Nifrosomonas europaea. *Journal of the Japan Petroleum Institute* **2010,** *53*, (6), 319-326.
19. Taher, E.; Chandran, K., High-rate, high-yield production of methanol by ammonia-oxidizing bacteria. *Environmental science & technology* **2013,** *47*, (7), 3167-73.
20. Whittaker, M.; Bergmann, D.; Arciero, D.; Hooper, A. B., Electron transfer during the oxidation of ammonia by the chemolithotrophic bacterium Nitrosomonas europaea. *Biochimica et biophysica acta* **2000,** *1459*, (2-3), 346-55.
21. Holmes, A. J.; Costello, A.; Lidstrom, M. E.; Murrell, J. C., Evidence that particulate methane monooxygenase and ammonia monooxygenase may be evolutionarily related. *FEMS microbiology letters* **1995,** *132*, (3), 203-8.
22. Kowalchuk, G. A.; Stephen, J. R., Ammonia-oxidizing bacteria: a model for molecular microbial ecology. *Annual review of microbiology* **2001,** *55*, 485-529.
23. Keener, W. K.; Arp, D. J., Kinetic Studies of Ammonia Monooxygenase Inhibition in Nitrosomonas europaea by Hydrocarbons and Halogenated Hydrocarbons in an Optimized Whole-Cell Assay. *Applied and environmental microbiology* **1993,** *59*, (8), 2501-10.
24. Jones, R. D.; Morita, R. Y., Methane Oxidation by Nitrosococcus oceanus and Nitrosomonas europaea. *Applied and environmental microbiology* **1983,** *45*, (2), 401-10.
25. Suzuki, I.; Kwok, S. C.; Dular, U., Competitive inhibition of ammonia oxidation in Nitrosomonas europaea by methane, carbon monoxide or methanol. *FEBS letters* **1976,** *72*, (1), 117-20.
26. Ward, B. B., Kinetic studies on ammonia and methane oxidation by Nitrosococcus oceanus. *Archives of Microbiology* **1987,** *147*, 126-133.
27. Radniecki, T. S.; Dolan, M. E.; Semprini, L., Physiological and Transcriptional Responses ofNitrosomonas europaeato Toluene and Benzene Inhibition. *Environmental science & technology* **2008,** *42*, (11), 4093-4098.
28. Voysey, P. A.; Wood, P. M., Methanol and Formaldehyde Oxidation by an Autotrophic Nitrifying Bacterium. *Journal of General Microbiology* **1987,** *33*, 283-290.
29. Hooper, A. B.; Terry, K. R., Specific inhibitors of ammonia oxidation in Nitrosomonas. *Journal of bacteriology* **1973,** *115*, (2), 480-5.
30. Nancy, A. M.; Ward, N.; Larsen, Ø.; Sakwa, J.; Bruseth, L.; Khouri, H.; Durkin, A. S.; Dimitrov, G.; Jiang, L.; Scanlan, D.; Kang, K. H.; Lewis, M.; Nelson, K. E.; Methé, B.; Wu, M.; Heidelberg, J. F.; Paulsen, I. T.; Fouts, D.; Ravel, J.; Tettelin, H.; Ren, Q.; Read, T.; DeBoy, R. T.; Seshadri, R.; Salzberg, S. L.; Jensen, H. B.; Birkeland, N. K.; Nelson, W. C.; Dodson, R. J.; Grindhaug, S. H.; Holt, I.; Eidhammer, I.; Jonasen, I.; Vanaken, S.; Utterback, T.; Feldblyum, T. V.; Fraser, C. M.; Lillehaug,

J. R.; Eisen, J. A., Genomic Insights into Methanotrophy: The Complete Genome Sequence of Methylococcus capsulatus (Bath). *PLoS Biology* **2004,** *2*, (10), e303.
31. Meiklejohn, J., The isolation of Nitrosomonas europaea in pure culture. *J Gen Microbiol* **1950,** *4*, (2), 185-91.
32. Watson, S. W.; Mandel, M., Comparison of the morphology and deoxyribonucleic acid composition of 27 strains of nitrifying bacteria. *Journal of bacteriology* **1971,** *107*, (2), 563-9.
33. Chain, P.; Lamerdin, J.; Larimer, F.; Regala, W.; Lao, V.; Land, M.; Hauser, L.; Hooper, A.; Klotz, M.; Norton, J.; Sayavedra-Soto, L.; Arciero, D.; Hommes, N.; Whittaker, M.; Arp, D., Complete genome sequence of the ammonia-oxidizing bacterium and obligate chemolithoautotroph Nitrosomonas europaea. *Journal of bacteriology* **2003,** *185*, (9), 2759-73.
34. Stein, L. Y.; Arp, D. J.; Berube, P. M.; Chain, P. S. G.; Hauser, L.; Jetten, M. S. M.; Klotz, M. G.; Larimer, F. W.; Norton, J. M.; Op den Camp, H. J. M.; Shin, M.; Wei, X., Whole-genome analysis of the ammonia-oxidizing bacterium, Nitrosomonas eutropha C91: implications for niche adaptation. *Environmental Microbiology* **2007,** *9*, (12), 2993-3007.
35. Norton, J. M.; Alzerreca, J. J.; Suwa, Y.; Klotz, M. G., Diversity of ammonia monooxygenase operon in autotrophic ammonia-oxidizing bacteria. *Archives of Microbiology* **2001,** *177*, (2), 139-149.
36. Bergmann, D. J.; Hooper, A. B.; Klotz, M. G., Structure and Sequence Conservation of hao Cluster Genes of Autotrophic Ammonia-Oxidizing Bacteria: Evidence for Their Evolutionary History. *Applied and environmental microbiology* **2005,** *71*, (9), 5371-5382.
37. Chandran, K.; Stein, L. Y.; Klotz, M. G.; van Loosdrecht, M. C., Nitrous oxide production by lithotrophic ammonia-oxidizing bacteria and implications for engineered nitrogen-removal systems. *Biochemical Society transactions* **2011,** *39*, (6), 1832-7.
38. Stein, L. Y., Heterotrophic nitrification and nitrifier denitrification. In *Nitrification*, Ward, B. B.; Arp, D. J.; Klotz, M. G., Eds. ASM Press: Washington, DC, 2011; pp 95-114.
39. Kozlowski, J. A.; Kits, K. D.; Stein, L. Y., Comparison of Nitrogen Oxide Metabolism among Diverse Ammonia-Oxidizing Bacteria. *Frontiers in Microbiology* **2016,** *7*.
40. Beaumont, H. J. E.; Lens, S. I.; Reijnders, W. N. M.; Westerhoff, H. V.; Van Spanning, R. J. M., Expression of nitrite reductase in Nitrosomonas europaea involves NsrR, a novel nitrite-sensitive transcription repressor. *Molecular Microbiology* **2004,** *54*, (1), 148-158.
41. Cua, L. S.; Stein, L. Y., Effects of nitrite on ammonia-oxidizing activity and gene regulation in three ammonia-oxidizing bacteria. *FEMS microbiology letters* **2011,** *319*, (2), 169-175.
42. Sayavedra-Soto, L. A.; Hommes, N. G.; Russell, S. A.; Arp, D. J., Induction of ammonia monooxygenase and hydroxylamine oxidoreductase mRNAs by ammonium in Nitrosomonas europaea. *Molecular Microbiology* **1996,** *20*, (3), 541-548.

43. Wei, X.; Sayavedra-Soto, L. A.; Arp, D. J., The transcription of the cbb operon in Nitrosomonas europaea. *Microbiology* **2004,** *150*, (6), 1869-1879.
44. Kartal, B.; Wessels, H. J. C. T.; van der Biezen, E.; Francoijs, K. J.; Jetten, M. S. M.; Klotz, M. G.; Stein, L. Y., Effects of Nitrogen Dioxide and Anoxia on Global Gene and Protein Expression in Long-Term Continuous Cultures of Nitrosomonas eutropha C91. *Applied and environmental microbiology* **2012,** *78*, (14), 4788-4794.
45. Wei, X.; Yan, T.; Hommes, N. G.; Liu, X.; Wu, L.; McAlvin, C.; Klotz, M. G.; Sayavedra-Soto, L. A.; Zhou, J.; Arp, D. J., Transcript profiles ofNitrosomonas europaeaduring growth and upon deprivation of ammonia and carbonate. *FEMS microbiology letters* **2006,** *257*, (1), 76-83.
46. Dangel, A. W.; Tabita, F. R.; Margolin, W., CbbR, the Master Regulator for Microbial Carbon Dioxide Fixation. *Journal of bacteriology* **2015,** *197*, (22), 3488-3498.
47. Shively, J. M.; Ball, F.; Brown, D. H.; Saunders, R. E., Functional Organelles in Prokaryotes: Polyhedral Inclusions (Carboxysomes) of Thiobacillus neapolitanus. *Science* **1973,** *182*, (4112), 584-586.
48. Cameron, Jeffrey C.; Wilson, Steven C.; Bernstein, Susan L.; Kerfeld, Cheryl A., Biogenesis of a Bacterial Organelle: The Carboxysome Assembly Pathway. *Cell* **2013,** *155*, (5), 1131-1140.
49. Cannon, G. C.; Shively, J. M., Characterization of a homogenous preparation of carboxysomes from Thiobacillus neapolitanus. *Archives of Microbiology* **1983,** *134*, (1), 52-59.
50. Holthuijzen, Y. A.; van Breemen, J. F. L.; Konings, W. N.; van Bruggen, E. F. J., Electron microscopic studies of carboxysomes of Thiobacillus neapolitanus. *Archives of Microbiology* **1986,** *144*, (3), 258-262.
51. Holthuijzen, Y. A.; Kuenen, J. G.; Konings, W. N., Activity of ribulose-1,5-bisphosphate carboxylase in intact and disrupted carboxysomes ofThiobacillus neapolitanus. *FEMS microbiology letters* **1987,** *42*, (2-3), 121-124.
52. Cannon, G. C.; Bradburne, C. E.; Aldrich, H. C.; Baker, S. H.; Heinhorst, S.; Shively, J. M., Microcompartments in Prokaryotes: Carboxysomes and Related Polyhedra. *Applied and environmental microbiology* **2001,** *67*, (12), 5351-5361.
53. Jiang, D.; Khunjar, W. O.; Wett, B.; Murthy, S. N.; Chandran, K., Characterizing the Metabolic Trade-Off inNitrosomonas europaeain Response to Changes in Inorganic Carbon Supply. *Environmental science & technology* **2015,** *49*, (4), 2523-2531.
54. Mellbye, B. L.; Giguere, A.; Chaplen, F.; Bottomley, P. J.; Sayavedra-Soto, L. A.; Parales, R. E., Steady-State Growth under Inorganic Carbon Limitation Conditions Increases Energy Consumption for Maintenance and Enhances Nitrous Oxide Production in Nitrosomonas europaea. *Applied and environmental microbiology* **2016,** *82*, (11), 3310-3318.
55. Zheng, Y.; Huang, R.; Wang, B. Z.; Bodelier, P. L. E.; Jia, Z. J., Competitive interactions between methane- and ammonia-oxidizing bacteria modulate carbon and nitrogen cycling in paddy soil. *Biogeosciences* **2014,** *11*, (12), 3353-3368.
56. El Diwani, G.; El Rafie, S.; El Ibiari, N. N.; El-Aila, H. I., Recovery of ammonia

nitrogen from industrial wastewater treatment as Struvite slow releasing fertilizer. *Desalination* **2007,** *214*, (1-3), 200-214.
57. Desmidt, E.; Ghyselbrecht, K.; Zhang, Y.; Pinoy, L.; Van der Bruggen, B.; Verstraete, W.; Rabaey, K.; Meesschaert, B., Global Phosphorus Scarcity and Full-Scale P-Recovery Techniques: A Review. *Critical Reviews in Environmental Science and Technology* **2015,** *45*, (4), 336-384.
58. Kargbo, D. M., Biodiesel Production from Municipal Sewage Sludges. *Energy Fuels* **2010,** *24*, 2791-2794.
59. Rodgers, M.; Wu, G., Production of polyhydroxybutyrate by activated sludge performing enhanced biological phosphorus removal. *Bioresource Technology* **2010,** *101*, (3), 1049-1053.
60. Taher, E.; Chandran, K., High-Rate, High-Yield Production of Methanol by Ammonia-Oxidizing Bacteria. *Environmental Science & Technology* **2013,** *47*, (7), 3167-3173.
61. Cherchi, C.; Onnis-Hayden, A.; El-Shawabkeh, I.; Gu, A. Z., Implication of Using Different Carbon Sources for Denitrification in Wastewater Treatments. *Water Environment Research* **2009,** *81*, (8), 788-799.
62. Holmes, A. J.; Costello, A.; Lidstrom, M. E.; Murrell, J. C., Evidence that participate methane monooxygenase and ammonia monooxygenase may be evolutionarily related. *FEMS Microbiology Letters* **1995,** *132*, (3), 203-208.
63. Prosser, J. I., Autrotrophic Nitrification in Bacteria. *Adv. Microb. Physiol.* **1989,** *30*, 125-181.
64. Hanson, R. S.; Hanson, T. E., Methanotrophic bacteria. *Microbiological reviews* **1996,** *60*, (2), 439-71.
65. Ge, X.; Yang, L.; Sheets, J. P.; Yu, Z.; Li, Y., Biological conversion of methane to liquid fuels: Status and opportunities. *Biotechnology Advances* **2014,** *32*, (8), 1460-1475.
66. Chain, P.; Lamerdin, J.; Larimer, F.; Regala, W.; Lao, V.; Land, M.; Hauser, L.; Hooper, A.; Klotz, M.; Norton, J.; Sayavedra-Soto, L.; Arciero, D.; Hommes, N.; Whittaker, M.; Arp, D., Complete Genome Sequence of the Ammonia-Oxidizing Bacterium and Obligate Chemolithoautotroph Nitrosomonas europaea. *Journal of Bacteriology* **2003,** *185*, (9), 2759-2773.
67. Wang, L.; Tabata, K.; Kamachi, T.; Okura, I., Effect of Electron Donor on Methanol Production by Ammonia-oxidizing Bacterium Nitrosomonas europaea. *Journal of the Japan Petroleum Institute* **2010,** *53*, (6), 319-326.
68. Frear, D. S.; Burrell, R. C., Spectrophotometric Method for Determining Hydroxylamine Reductase Activity in Higher Plants. *Analytical Chemistry* **1955,** *27*, (10), 1664-1665.
69. APHA; AWWA; WEF, Standard Methods for the Examination of Water and Wastewater. In 20th Edition ed.; 1999.
70. Ferris, M. J.; Muyzer, G.; Ward, D. M., Denaturing gradient gel electrophoresis profiles of 16S rRNA-defined populations inhabiting a hot spring microbial mat community. *Appl. Environ. Microbiol.* **1996,** *62*, (2), 340-346.
71. Rotthauwe, J. H.; Witzel, K. P.; Liesack, W., The ammonia monooxygenase

structural gene amoA as a functional marker: Molecular fine-scale analysis of natural ammonia-oxidizing populations. *Appl. Environ. Microbiol.* **1997,** *63*, (12), 4704-4712.
72. Kindaichi, T.; Kawano, Y.; Ito, T.; Satoh, H.; Okabe, S., Population dynamics and in situ kinetics of nitrifying bacteria in autotrophic nitrifying biofilms as determined by real-time quantitative PCR. *Biotechnol. Bioeng.* **2006,** *94*, (6), 1111-1121.
73. Graham, D. W.; Knapp, C. W.; Van Vleck, E. S.; Bloor, K.; Lane, T. B.; Graham, C. E., Experimental demonstration of chaotic instability in biological nitrification. *Isme Journal* **2007,** *1*, (5), 385-393.
74. Henze, M.; Gujer, W.; Mino, T.; Loosdrecht, M. V., *Activated sludge models ASM1, ASM2, ASM2d and ASM3*. IWA Pub.: London, 2000; p vi, 121 p.
75. Arp, D. J.; Stein, L. Y., Metabolism of inorganic N compounds by ammonia-oxidizing bacteria. *Crit Rev Biochem Mol* **2003,** *38*, (6), 471-495.
76. Hauduc, H.; Rieger, L.; Oehmen, A.; van Loosdrecht, M. C. M.; Comeau, Y.; Heduit, A.; Vanrolleghem, P. A.; Gillot, S., Critical review of activated sludge modeling: State of process knowledge, modeling concepts, and limitations. *Biotechnol. Bioeng.* **2013,** *110*, (1), 24-46.
77. Grady, C. P. L.; Diagger, G. T.; Lim, H. C., *Biological Wastewater Treatment*. Marcel Dekker: New York, 1999.
78. Munz, G.; Lubello, C.; Oleszkiewicz, J. A., Factors affecting the growth rates of ammonium and nitrite oxidizing bacteria. *Chemosphere* **2011,** *83*, (5), 720-725.
79. Marsili-Libelli; Ratini P; Spagni A; Bortone G, Implementation, study and calibration of a modified ASM2d for the simulation of SBR processes. *Water Science and Technology* **2001,** *43*, (3), 69-76.
80. Ahn, J. H.; Yu, R.; Chandran, K., Distinctive microbial ecology and biokinetics of autotrophic ammonia and nitrite oxidation in a partial nitrification Bioreactor. *Biotechnol. Bioeng.* **2008,** *100*, (6), 1078-1087.
81. Manser, R.; Gujer, W.; Siegrist, H., Consequences of mass transfer effects on the kinetics of nitrifiers. *Water Res.* **2005,** *39*, (19), 4633-4642.
82. Sin, G.; Kaelin, D.; Kampschreur, M. J.; Takacs, I.; Wett, B.; Gernaey, K. V.; Rieger, L.; Siegrist, H.; van Loosdrecht, M. C. M., Modelling nitrite in wastewater treatment systems: a discussion of different modelling concepts. *Water Science and Technology* **2008,** *58*, (6), 1155-1171.
83. Munz, G.; Mori, G.; Vannini, C.; Lubello, C., Kinetic parameters and inhibition response of ammonia- and nitrite-oxidizing bacteria in membrane bioreactors and conventional activated sludge processes. *Environmental Technology* **2010,** *31*, (14), 1557-1564.
84. Kampschreur, M. J.; Picioreanu, C.; Tan, N.; Kleerebezem, R.; Jetten, M. S. M.; van Loosdrecht, M. C. M., Unraveling the source of nitric oxide emission during nitrification. *Water Environment Research* **2007,** *79*, (13), 2499-2509.
85. Jones, R. M.; Dold, P.; Takacs, I.; Chapman, K.; Wett, B.; Murthy, S.; O'Shaughnessy, M., Simulation for Operation and Control of Reject Water Treatment Processes. In *WEFTEC 2007*, Water Environment Federation: San Diego, CA, 2007.
86. Sathyamoorthy, S.; Chandran, K.; Ramsburg, C. A., Biodegradation and cometabolic modeling of selected beta blockers during ammonia oxidation. *Environ*

Sci Technol **2013,** *47*, (22), 12835-43.
87. McCuen, R. H.; Knight, Z.; Cutter, A. G., Evaluation of the Nash-Sutcliffe efficiency index. *Journal of Hydrologic Engineering* **2006,** *11*, (6), 597-602.
88. Sathyamoorthy, S.; Vogel, R. M.; Chapra, S. C.; Ramsburg, C. A., Uncertainty and sensitivity analyses using GLUE when modeling inhibition and pharmaceutical cometabolism during nitrification. *ENVIRON MODELL SOFTW* **2014,** *60*, (0), 219-227.
89. McKay, M. D.; Beckman, R. J.; Conover, W. J., A Comparison of Three Methods for Selecting Values of Input Variables in the Analysis of Output from a Computer Code. *Technometrics* **1979,** *21*, (2), 239-245.
90. Keener, W. K.; Arp, D. J., Kinetic Studies of Ammonia Monooxygenase Inhibition in Nitrosomonas Europaea by Hydrocarbons and Halogenated Hydrocarbons in an Optimized Whole Cell Assay. *Appl. Environ. Microbiol.* **1993,** *59*, (8), 2501-2510.
91. Suzuki, I.; Kwok, S. C.; Dular, U., Competitive Inhibition of Ammonia Oxidation in Nitrosomonas Europaea by Methane, Cabron Monoxide or Methanol. *Febs Letters* **1976,** *72*, (1), 117-120.
92. Hyman, M. R.; Murton, I. B.; Arp, D. J., Interaction of ammonia monooxygenase from Nitrosomas europaea with alkanes, alkenes, and alkynes. *Appl. Environ. Microbiol.* **1988,** *54*, 3187.
93. Khin, T.; Annachhatre, A. P., Nitrogen removal in a fluidized bed bioreactor by using mixed culture under oxygen-limited conditions. *Water science and technology : a journal of the International Association on Water Pollution Research* **2004,** *50*, (6), 313-20.
94. Metcalf & Eddy, I.; Tchobanogolous, G.; Burton, L.; D.H., S., *Wastewater Engineering: Treatment and Reuse*. McGraw-Hill: 2003.
95. Constantine, T. A., North American Experience with Centrate Treatment Technologies for Ammonia and Nitrogen Removal. In *WEFTEC 2006*, Water Environment Federation: Dallas, TX, 2006.
96. Weissenbacher, N.; Takacs, I.; Murthy, S.; Fuerhacker, M.; Wett, B., Gaseous Nitrogen and Carbon Emissions from a Full-Scale Deammonification Plant. *Water Environment Research* **2010,** *82*, (2), 169-175.
97. Graham, D. W.; Knapp, C. W.; Van Vleck, E. S.; Bloor, K.; Lane, T. B.; Graham, C. E., Experimental demonstration of chaotic instability in biological nitrification. *The ISME Journal* **2007,** *1*, (5), 385-393.
98. Ferris, M. J.; Muyzer, G.; Ward, D. M., Denaturing gradient gel electrophoresis profiles of 16S rRNA-defined populations inhabiting a hot spring microbial mat community. *Applied and environmental microbiology* **1996,** *62*, (2), 340-6.
99. Rotthauwe, J. H.; Witzel, K. P.; Liesack, W., The ammonia monooxygenase structural gene amoA as a functional marker: molecular fine-scale analysis of natural ammonia-oxidizing populations. *Applied and environmental microbiology* **1997,** *63*, (12), 4704-12.
100. Wang, L.; Tabata, K.; Kamachi, T.; Okura, I., Effect of Electron Donor on Methanol Production by. Ammonia-oxidizing Bacterium Nitrosomonas europaea.

Journal of the Japan Petroleum Institute **2010,** *53*, (6), 8.
101. Burnham, K. P.; Anderson, D. R.; Burnham, K. P., Model selection and multimodel inference a practical information-theoretic approach. In 2nd ed.; Springer,: New York, 2002.
102. Park, D.; Lee, J., Biological conversion of methane to methanol. *Korean Journal of Chemical Engineering* **2013,** *30*, (5), 977-987.
103. Hooper, A. B.; Vannelli, T.; Bergmann, D. J.; Arciero, D. M., Enzymology of the oxidation of ammonia to nitrite by bacteria. *Antonie van Leeuwenhoek* **1997,** *71*, (1/2), 59-67.
104. Ahn, J. H.; Kwan, T.; Chandran, K., Comparison of Partial and Full Nitrification Processes Applied for Treating High-Strength Nitrogen Wastewaters: Microbial Ecology through Nitrous Oxide Production. *Environmental science & technology* **2011,** *45*, (7), 2734-2740.
105. Schloss, P. D.; Westcott, S. L.; Ryabin, T.; Hall, J. R.; Hartmann, M.; Hollister, E. B.; Lesniewski, R. A.; Oakley, B. B.; Parks, D. H.; Robinson, C. J.; Sahl, J. W.; Stres, B.; Thallinger, G. G.; Van Horn, D. J.; Weber, C. F., Introducing mothur: Open-Source, Platform-Independent, Community-Supported Software for Describing and Comparing Microbial Communities. *Applied and environmental microbiology* **2009,** *75*, (23), 7537-7541.
106. Quast, C.; Pruesse, E.; Yilmaz, P.; Gerken, J.; Schweer, T.; Yarza, P.; Peplies, J.; Glockner, F. O., The SILVA ribosomal RNA gene database project: improved data processing and web-based tools. *Nucleic Acids Research* **2012,** *41*, (D1), D590-D596.
107. Lu, H.; Nuruzzaman, F.; Ravindhar, J.; Chandran, K., Alcohol dehydrogenase expression as a biomarker of denitrification activity in activated sludge using methanol and glycerol as electron donors. *Environmental Microbiology* **2011,** *13*, (11), 2930-2938.
108. Heylen, K.; Lebbe, L.; De Vos, P., Acidovorax caeni sp. nov., a denitrifying species with genetically diverse isolates from activated sludge. *International Journal of Systematic and Evolutionary Microbiology* **2008,** *58*, (1), 73-77.
109. Lu, H.; Chandran, K., Diagnosis and Quantification of Glycerol Assimilating Denitrifying Bacteria in an Integrated Fixed-Film Activated Sludge Reactor via13C DNA Stable-Isotope Probing. *Environmental science & technology* **2010,** *44*, (23), 8943-8949.
110. Chistoserdova, L.; Chen, S. W.; Lapidus, A.; Lidstrom, M. E., Methylotrophy in Methylobacterium extorquens AM1 from a genomic point of view. *Journal of bacteriology* **2003,** *185*, (10), 2980-7.
111. Su, Y.-C.; Sathyamoorthy, S.; Chandran, K., Concurrent Nitrification and Methanol Production Using Nitrifying Activated Sludge in a Continuous Flow Process. *Proceedings of the Water Environment Federation* **2015,** *2015*, (7), 5666-5667.
112. Daebeler, A.; Bodelier, P. L. E.; Yan, Z.; Hefting, M. M.; Jia, Z.; Laanbroek, H. J., Interactions between Thaumarchaea, Nitrospira and methanotrophs modulate autotrophic nitrification in volcanic grassland soil. *The ISME Journal* **2014,** *8*, (12), 2397-2410.

113.Harper, W. F.; Takeuchi, Y.; Riya, S.; Hosomi, M.; Terada, A., Novel abiotic reactions increase nitrous oxide production during partial nitrification: Modeling and experiments. *Chemical Engineering Journal* **2015,** *281*, 1017-1023.
114.Yu, R.; Kampschreur, M. J.; van Loosdrecht, M. C.; Chandran, K., Mechanisms and specific directionality of autotrophic nitrous oxide and nitric oxide generation during transient anoxia. *Environmental science & technology* **2010,** *44*, (4), 1313-9.
115.Badger, J. H.; Kumar, P. S.; Brooker, M. R.; Dowd, S. E.; Camerlengo, T., Target Region Selection Is a Critical Determinant of Community Fingerprints Generated by 16S Pyrosequencing. *PLoS ONE* **2011,** *6*, (6), e20956.
116.Tremblay, J.; Singh, K.; Fern, A.; Kirton, E. S.; He, S.; Woyke, T.; Lee, J.; Chen, F.; Dangl, J. L.; Tringe, S. G., Primer and platform effects on 16S rRNA tag sequencing. *Frontiers in Microbiology* **2015,** *6*.
117.Ginige, M. P.; Keller, J.; Blackall, L. L., Investigation of an Acetate-Fed Denitrifying Microbial Community by Stable Isotope Probing, Full-Cycle rRNA Analysis, and Fluorescent In Situ Hybridization-Microautoradiography. *Applied and environmental microbiology* **2005,** *71*, (12), 8683-8691.
118.Hiraishi, A.; Khan, S. T., Application of polyhydroxyalkanoates for denitrification in water and wastewater treatment. *Applied Microbiology and Biotechnology* **2003,** *61*, (2), 103-109.
119.Van Aken, B., Methylobacterium populi sp. nov., a novel aerobic, pink-pigmented, facultatively methylotrophic, methane-utilizing bacterium isolated from poplar trees (Populus deltoidesxnigra DN34). *International Journal of Systematic and Evolutionary Microbiology* **2004,** *54*, (4), 1191-1196.
120. Dedysh, S. N., Methane utilization by Methylobacterium species: new evidence but still no proof for an old controversy. *International Journal of Systematic and Evolutionary Microbiology* **2004,** *54*, (6), 1919-1920.
121. Yang, N.; Lü, F.; He, P.; Shao, L., Response of methanotrophs and methane oxidation on ammonium application in landfill soils. *Applied Microbiology and Biotechnology* **2011,** *92*, (5), 1073-1082.
122. Bodelier, P. L. E.; Laanbroek, H. J., Nitrogen as a regulatory factor of methane oxidation in soils and sediments. *FEMS microbiology ecology* **2004,** *47*, (3), 265-277.
123. King, G. M.; Schnell, S., Ammonium and Nitrite Inhibition of Methane Oxidation by Methylobacter albus BG8 and Methylosinus trichosporium OB3b at Low Methane Concentrations. *Applied and environmental microbiology* **1994,** *60*, (10), 3508-13.
124. Steudler, P. A.; Bowden, R. D.; Melillo, J. M.; Aber, J. D., Influence of nitrogen fertilization on methane uptake in temperate forest soils. *Nature* **1989,** *341*, (6240), 314-316.
125. Hermansson, A.; Lindgren, P. E., Quantification of Ammonia-Oxidizing Bacteria in Arable Soil by Real-Time PCR. *Applied and environmental microbiology* **2001,** *67*, (2), 972-976.
126. Poly, F.; Wertz, S.; Brothier, E.; Degrange, V. r., First exploration of Nitrobacter diversity in soils by a PCR cloning-sequencing approach targeting

functional gene nxrA. *FEMS microbiology ecology* **2008,** *63*, (1), 132-140.
127. Melcer, H.; Dold, P. O.; Jones, R. M.; Bye, C. M.; Stensel, H. D.; Wilson, A. W.; Sun, P. A.; Bury, S. *Methods for Wastewater Characterization in Activated Sludge Modelling*; Water Environment and Reuse Foundation: Alexandria, VA, 2004.
128. Grady, C. P. L. J.; Daigger, G. T.; Lim, H. C., *Biological Wastewater Treatment*. Marcel Dekker: New York, 1999.
129. Aakra, A.; Utaker, J. B.; Nes, I. F., RFLP of rRNA genes and sequencing of the 16S-23S rDNA intergenic spacer region of ammonia-oxidizing bacteria: a phylogenetic approach. *International Journal of Systematic Bacteriology* **1999,** *49*, (1), 123-130.
130. Starkenburg, S. R.; Chain, P. S. G.; Sayavedra-Soto, L. A.; Hauser, L.; Land, M. L.; Larimer, F. W.; Malfatti, S. A.; Klotz, M. G.; Bottomley, P. J.; Arp, D. J.; Hickey, W. J., Genome Sequence of the Chemolithoautotrophic Nitrite-Oxidizing Bacterium Nitrobacter winogradskyi Nb-255. *Applied and environmental microbiology* **2006,** *72*, (3), 2050-2063.
131. Jiang, Q. Q.; Bakken, L. R., Nitrous oxide production and methane oxidation by different ammonia-oxidizing bacteria. *Applied and environmental microbiology* **1999,** *65*, (6), 2679-84.
132. Berg, I. A., Ecological Aspects of the Distribution of Different Autotrophic CO2 Fixation Pathways. *Applied and environmental microbiology* **2011,** *77*, (6), 1925-1936.
133. Onnis-Hayden, A.; Gu, A. Z., Comparisons of Organic Sources for Denitrification: Biodegradability, Denitrification Rates, Kinetic Constants and Practical Implication for Their Application in WWTPs. *WEFTEC Proceedings* **2008**.
134. Stein, L. Y.; Campbell, M. A.; Klotz, M. G., Energy-mediated vs. ammonium-regulated gene expression in the obligate ammonia-oxidizing bacterium, Nitrosococcus oceani. *Front Microbiol* **2013,** *4*, 277.
135. Wilhelm, R.; Abeliovich, A.; Nejidat, A., Effect of long-term ammonia starvation on the oxidation of ammonia and hydroxylamine by Nitrosomonas europaea. *Journal of biochemistry* **1998,** *124*, (4), 811-5.
136. Hommes, N. G.; Sayavedra-Soto, L. A.; Arp, D. J., Mutagenesis and expression of amo, which codes for ammonia monooxygenase in Nitrosomonas europaea. *Journal of bacteriology* **1998,** *180*, (13), 3353-9.
137. Wei, X.; Sayavedra-Soto, L. A.; Arp, D. J., The transcription of the cbb operon in Nitrosomonas europaea. *Microbiology* **2004,** *150*, (Pt 6), 1869-79.
138. Gvakharia, B. O.; Permina, E. A.; Gelfand, M. S.; Bottomley, P. J.; Sayavedra-Soto, L. A.; Arp, D. J., Global transcriptional response of Nitrosomonas europaea to chloroform and chloromethane. *Applied and environmental microbiology* **2007,** *73*, (10), 3440-5.
139. Beaumont, H. J. E.; Hommes, N. G.; Sayavedra-Soto, L. A.; Arp, D. J.; Arciero, D. M.; Hooper, A. B.; Westerhoff, H. V.; van Spanning, R. J. M., Nitrite reductase of Nitrosomonas europaea is not essential for production of gaseous nitrogen oxides and confers tolerance to nitrite. *Journal of bacteriology* **2002,** *184*, (9), 2557-+.

140. Beyer, S.; Gilch, S.; Meyer, O.; Schmidt, I., Transcription of Genes Coding for Metabolic Key Functions in Nitrosomonas europaea during Aerobic and Anaerobic Growth. *J Mol Microb Biotech* **2009,** *16*, (3-4), 187-197.
141. Jason, J.; Cantera, L.; Stein, L. Y., Role of nitrite reductase in the ammonia-oxidizing pathway of Nitrosomonas europaea. *Archives of Microbiology* **2007,** *188*, (4), 349-354.
142. Jiang, D.; Khunjar, W. O.; Wett, B.; Murthy, S. N.; Chandran, K., Characterizing the metabolic trade-off in Nitrosomonas europaea in response to changes in inorganic carbon supply. *Environmental science & technology* **2015,** *49*, (4), 2523-31.
143. Beaumont, H. J.; van Schooten, B.; Lens, S. I.; Westerhoff, H. V.; van Spanning, R. J., Nitrosomonas europaea expresses a nitric oxide reductase during nitrification. *Journal of bacteriology* **2004,** *186*, (13), 4417-21.
144. Cho, C. M. H.; Yan, T. F.; Liu, X. D.; Wu, L. Y.; Zhou, J. Z.; Stein, L. Y., Transcriptome of a Nitrosomonas europaea mutant with a disrupted nitrite reductase gene (nirK). *Applied and environmental microbiology* **2006,** *72*, (6), 4450-4454.
145. Kozlowski, J. A.; Price, J.; Stein, L. Y., Revision of N2O-Producing Pathways in the Ammonia-Oxidizing Bacterium Nitrosomonas europaea ATCC 19718. *Applied and environmental microbiology* **2014,** *80*, (16), 4930-4935.
146. Geets, J.; Boon, N.; Verstraete, W., Strategies of aerobic ammonia-oxidizing bacteria for coping with nutrient and oxygen fluctuations. *FEMS microbiology ecology* **2006,** *58*, (1), 1-13.
147. Rasche, M. E.; Hyman, M. R.; Arp, D. J., Factors Limiting Aliphatic Chlorocarbon Degradation by Nitrosomonas europaea: Cometabolic Inactivation of Ammonia Monooxygenase and Substrate Specificity. *Applied and environmental microbiology* **1991,** *57*, (10), 2986-94.
148. Duncan, A. J.; Bott, C. B.; Terlesky, K. C.; Love, N. G., Detection of GroEL in activated sludge: a model for detection of system stress. *Letters in applied microbiology* **2000,** *30*, (1), 28-32.
149. Klotz, M. G.; Stein, L. Y., Nitrifier genomics and evolution of the nitrogen cycle. *FEMS microbiology letters* **2008,** *278*, (2), 146-56.
150. Chandran, K.; Love, N. G., Physiological state, growth mode, and oxidative stress play a role in Cd(II)-mediated inhibition of Nitrosomonas europaea 19718. *Applied and environmental microbiology* **2008,** *74*, (8), 2447-53.
151. Conrad, R., The global methane cycle: recent advances in understanding the microbial processes involved. *Environmental Microbiology Reports* **2009,** *1*, (5), 285-292.
152. Bodelier, P. L.; Frenzel, P., Contribution of methanotrophic and nitrifying bacteria to CH4 and NH4+ oxidation in the rhizosphere of rice plants as determined by new methods of discrimination. *Applied and environmental microbiology* **1999,** *65*, (5), 1826-33.
153. Yu, R.; Chandran, K., Strategies of Nitrosomonas europaea 19718 to counter low dissolved oxygen and high nitrite concentrations. *BMC microbiology* **2010,** *10*, 70.

154. Keen, G. A.; Prosser, J. I., Steady state and transient growth of autotrophic nitrifying bacteria. *Archives of Microbiology* **1987,** *147*, (1), 73-79.
155. Garcia-Ochoa, F.; Gomez, E., Bioreactor scale-up and oxygen transfer rate in microbial processes: An overview. *Biotechnology advances* **2009,** *27*, (2), 153-176.
156. Russell, J. B.; Cook, G. M., Energetics of bacterial growth: balance of anabolic and catabolic reactions. *Microbiological reviews* **1995,** *59*, (1), 48-62.
157. Cantera, J. J. L.; Stein, L. Y., Role of nitrite reductase in the ammonia-oxidizing pathway of Nitrosomonas europaea. *Archives of Microbiology* **2007,** *188*, (4), 349-354.
158. Perez-Garcia, O.; Villas-Boas, S. G.; Swift, S.; Chandran, K.; Singhal, N., Clarifying the regulation of NO/N2O production in Nitrosomonas europaea during anoxic–oxic transition via flux balance analysis of a metabolic network model. *Water research* **2014,** *60*, 267-277.
159. Ely, R. L.; Hyman, M. R.; Arp, D. J.; Guenther, R. B.; Williamson, K. J., A cometabolic kinetics model incoroporating enzyme inhibition, inactivation, and recovery: II. Trichloroethylene degradaation experiments. *Biotechnology and Bioengineering* **1995,** *46*, (3), 232-245.
160. Hyman, M. R.; Russell, S. A.; Ely, R. L.; Williamson, K. J.; Arp, D. J., Inhibition, Inactivation, and Recovery of Ammonia-Oxidizing Activity in Cometabolism of Trichloroethylene by Nitrosomonas europaea. *Applied and environmental microbiology* **1995,** *61*, (4), 1480-7.
161. Sayavedra-Soto, L. A.; Gvakharia, B.; Bottomley, P. J.; Arp, D. J.; Dolan, M. E., Nitrification and degradation of halogenated hydrocarbons—a tenuous balance for ammonia-oxidizing bacteria. *Applied Microbiology and Biotechnology* **2010,** *86*, (2), 435-444.
162. Ishii, S.; Song, Y.; Rathnayake, L.; Tumendelger, A.; Satoh, H.; Toyoda, S.; Yoshida, N.; Okabe, S., Identification of key nitrous oxide production pathways in aerobic partial nitrifying granules. *Environmental Microbiology* **2014,** *16*, (10), 3168-3180.
163. Horvath, R. S., Microbial co-metabolism and the degradation of organic compounds in nature. *Bacteriological reviews* **1972,** *36*, (2), 146-55.
164. Yang, L.; Chang, Y.; Chou, M., Feasibility of bioremediation of trichloroethylene contaminated sites by nitrifying bacteria through cometabolism with ammonia. *Journal of hazardous materials* **1999,** *69*, (1), 111-26.
165. Lauchnor, E. G.; Radniecki, T. S.; Semprini, L., Inhibition and gene expression of Nitrosomonas europaea biofilms exposed to phenol and toluene. *Biotechnology and Bioengineering* **2011,** *108*, (4), 750-757.
166. Langmead, B.; Salzberg, S. L., Fast gapped-read alignment with Bowtie 2. *Nature Methods* **2012,** *9*, (4), 357-359.
167. Kersey, P. J.; Allen, J. E.; Armean, I.; Boddu, S.; Bolt, B. J.; Carvalho-Silva, D.; Christensen, M.; Davis, P.; Falin, L. J.; Grabmueller, C.; Humphrey, J.; Kerhornou, A.; Khobova, J.; Aranganathan, N. K.; Langridge, N.; Lowy, E.; McDowall, M. D.; Maheswari, U.; Nuhn, M.; Ong, C. K.; Overduin, B.; Paulini, M.; Pedro, H.; Perry, E.; Spudich, G.; Tapanari, E.; Walts, B.; Williams, G.; Tello–Ruiz, M.; Stein, J.; Wei, S.;

Ware, D.; Bolser, D. M.; Howe, K. L.; Kulesha, E.; Lawson, D.; Maslen, G.; Staines, D. M., Ensembl Genomes 2016: more genomes, more complexity. *Nucleic Acids Research* **2016,** *44*, (D1), D574-D580.
168. Quinlan, A. R.; Hall, I. M., BEDTools: a flexible suite of utilities for comparing genomic features. *Bioinformatics* **2010,** *26*, (6), 841-842.
169. Robinson, M. D.; McCarthy, D. J.; Smyth, G. K., edgeR: a Bioconductor package for differential expression analysis of digital gene expression data. *Bioinformatics* **2009,** *26*, (1), 139-140.
170. Benjamini, Y.; Hochberg, Y., Controlling the False Discovery Rate: A Practical and Powerful Approach to Multiple Testing. *Journal of the Royal Statistical Society. Series B (Methodological)* **1995,** *57*, (1), 289-300.
171. Berube, P. M.; Stahl, D. A., The divergent AmoC3 subunit of ammonia monooxygenase functions as part of a stress response system in Nitrosomonas europaea. *Journal of bacteriology* **2012,** *194*, (13), 3448-56.
172. Logan, M. S.; Hooper, A. B., Suicide inactivation of hydroxylamine oxidoreductase of Nitrosomonas europaea by organohydrazines. *Biochemistry* **1995,** *34*, (28), 9257-64.
173. Dassain, M.; Leroy, A.; Colosetti, L.; Carole, S.; Bouche, J. P., A new essential gene of the 'minimal genome' affecting cell division. *Biochimie* **1999,** *81*, (8-9), 889-95.
174. Stein, L. Y.; Roy, R.; Dunfield, P. F., Aerobic Methanotrophy and Nitrification: Processes and Connections. **2012**.
175. Kapoor, V.; Li, X.; Elk, M.; Chandran, K.; Impellitteri, C. A.; Santo Domingo, J. W., Impact of Heavy Metals on Transcriptional and Physiological Activity of Nitrifying Bacteria. *Environmental science & technology* **2015,** *49*, (22), 13454-13462.
176. Hyman, M. R.; Arp, D. J., Effects of Ammonia on the De-Novo Synthesis of Polypeptides in Cells of Nitrosomonas-Europaea Denied Ammonia as an Energy-Source. *Journal of bacteriology* **1995,** *177*, (17), 4974-4979.
177. Poughon, L.; Dussap, C. G.; Gros, J. B., Energy model and metabolic flux analysis for autotrophic nitrifiers. *Biotechnol Bioeng* **2001,** *72*, (4), 416-33.
178. Arai, H., Regulation and Function of Versatile Aerobic and Anaerobic Respiratory Metabolism in Pseudomonas aeruginosa. *Frontiers in Microbiology* **2011,** *2*.
179. Kusian, B.; Bowien, B., Organization and regulation of cbb CO2 assimilation genes in autotrophic bacteria. *FEMS microbiology reviews* **1997,** *21*, (2), 135-55.
180. Ely, R. L.; Williamson, K. J.; Hyman, M. R.; Arp, D. J., Cometabolism of chlorinated solvents by nitrifying bacteria: Kinetics, substrate interactions, toxicity effects, and bacterial response. *Biotechnology and Bioengineering* **1997,** *54*, (6), 520-534.
181. Arp, D. J.; Chain, P. S. G.; Klotz, M. G., The Impact of Genome Analyses on Our Understanding of Ammonia-Oxidizing Bacteria. *Annual review of microbiology* **2007,** *61*, (1), 503-528.
182. Christensson, M.; Lie, E.; Welander, T., A comparison between ethanol and

methanol as carbon sources for denitrification. *Water Science and Technology* **1994,** *30*, (6), 83.
183. Czepiel, P. M.; Crill, P. M.; Harriss, R. C., Methane emissions from municipal wastewater treatment processes. *Environmental science & technology* **1993,** *27*, (12), 2472-2477.
184. Wang, J.; Zhang, J.; Xie, H.; Qi, P.; Ren, Y.; Hu, Z., Methane emissions from a full-scale A/A/O wastewater treatment plant. *Bioresource technology* **2011,** *102*, (9), 5479-85.
185. Daelman, M. R.; van Voorthuizen, E. M.; van Dongen, U. G.; Volcke, E. I.; van Loosdrecht, M. C., Methane emission during municipal wastewater treatment. *Water research* **2012,** *46*, (11), 3657-70.
186. Daelman, M. R.; van Voorthuizen, E. M.; van Dongen, L. G.; Volcke, E. I.; van Loosdrecht, M. C., Methane and nitrous oxide emissions from municipal wastewater treatment - results from a long-term study. *Water science and technology : a journal of the International Association on Water Pollution Research* **2013,** *67*, (10), 2350-5.

List of publications

Core dissertation publications and conference presentations

1. Y-C Su, S. Sathyamoorthy, and K. Chandran, Methanol Production using Ammonia Oxidizing Bacteria in a Continuous Flow Process (In preparation)
2. Y-C Su and K. Chandran, Physiological characterization and community analysis of nitrifying enrichment consortium in a coupled nitrification and biomethanol production process (In preparation)
3. Y-C Su, S. Sathyamoorthy, and K. Chandran, Proteomic and transcriptional responses of methane cometabolism in *Nitrosomonas europaea* (In preparation)
4. Y-C Su, L. Arellano-García, and K. Chandran, Physiological and transcriptional analysis of genes related to nitrogen metabolism in response to methane exposure in *Nitrosomonas eutropha* (In preparation)
5. Y-C Su and K. Chandran, Comparative transcriptomic analysis for methane cometabolism in *Nitrosomonas europaea* and *Nitrosomonas eutropha* (In preparation)
6. Y-C Su, L. Arellano-Garcia, and K. Chandran (2017) Physiological and molecular characterization of continuous cometabolic methanol production by a nitrifying enrichment consortium. 90th WEFTEC
7. Y-C Su, L. Arellano-Garcia, S. Sathyamoorthy and K. Chandran (2017) Characterization and implications of cometabolic bio-methanol production by ammonia oxidizing bacteria. 253rd ACS National Meeting
8. Y-C Su, L. Arellano-Garcia, R. Lebrero, J.L. Yong, C. Aguiar and K. Chandran (2017) Simultaneous Nitrification and Methanol Production Process for Biological Nitrogen Removal. 89th NYWEA Annual Meeting
9. Y-C Su, S. Sathyamoorthy, K. Chandran (2015) Concurrent Nitrification and Methanol Production Using Nitrifying Activated Sludge in a Continuous Flow Process. 88th WEFTEC AEESP Session
10. Y-C Su, S. Sathyamoorthy, K. Chandran (2015) Physiological and proteomic responses of methane and ammonia cometabolism in Nitrosomonas europaea. 4th International Conference on Nitrification and Related Processes
11. Y-C Su, S. Sathyamoorthy, K. Chandran (2014) Factors Affecting Bio-methanol Production Using A Mixed Culture Nitrifying Community. 1st New England Graduate Student Water Symposium

Participated research

1. C. Ma, Y-C Su et al., (2017) Understanding N_2O production mechanisms in *Nitrosomonas eutropha* by linking $^{15}N/^{18}O$ stable isotope-labelling technique with functional gene transcription (In preparation)
2. L. Arellano-Garcia, R. Lebrero, Y-C Su, K Chandran (2017) Metabolism and kinetic characterization of a mixed nitrifying culture with hydroxylamine as sole substrate (In preparation)

3. C. Hoar, J.H. Ahn, S. Sathyamoorthy, Y-C Su, K. Chandran (2017) Functional Gene Expression as an Indicator of Nitrification Inhibition by Cu(II). 90th WEFTEC
4. R. Lebrero, L. Arellano-Garcia, Y-C Su, K. Chandran (2016) Metabolism and Growth of Autotrophic Ammonia Oxidizing Bacteria with Hydroxylamine as the Sole Energy and Nitrogen Source. 89th WEFTEC AEESP Session